Study for Non-uniform Aging Photovoltaic Array Performance Enhancements

A thesis submitted under the requirements of the University of Liverpool for the degree of ***Doctor of Philosophy***

By

Mohammed Alkahtani

School of Engineering University of Liverpool

May 2021

DECLARATION

I hereby declare that except where specific reference is made to others' work, the contents of this dissertation are original and have not been submitted in whole or in part for consideration for any other degree or qualification in this or any other University. This dissertation results from my own work and includes nothing which is the outcome of work done in collaboration, except where specifically indicated in the text.

Alkahtani, Mohammed

2021

ACKNOWLEDGMENTS

I want to thank my supervisors, Dr Yihua Hu and Dr Jiafeng Zhou, for their support, motivation, and guidance. Their wise advice, constructive criticism, and helpful suggestions helped me finish my PhD thesis. Above all, their energy and enthusiasm have encouraged me to produce such high-quality work for this thesis.

I owe my parents an outstanding debt of gratitude for their prayers and advice, which have helped me get through PhD study.

I want to express my sincere gratitude to my wife and children first and foremost. Her unwavering love, motivation, and guidance were undeniably the cornerstone on which I founded the last three years of my life.

Finally, I'd like to dedicate this thesis to my brother Abdullah, who passed away in March 2021. I'm hoping to express my delight to him. As a result, the least I can do for him is to thank him in my thesis for inspiring, helping, and patiently guiding me through my PhD studies over the past three years.

ABSTRACT

The use of solar energy on a large scale has been socially and politically driven by the negative impact of fossil fuels on the environment. Solar energy is advantageous because it is a renewable energy source and because the supply of sunlight is virtually boundless. On the downside, solar energy is expensive. There are issues of technical control associated with photovoltaic systems (PVs), which capture sunlight via semiconductor materials and convert it to electricity since the current and voltage dynamics of the solar cells lack linearity. Furthermore, although the solar array output is typically equivalent to the sunlight amount, the illumination of various structures (e.g. power plants, solar tents, PV arrays integrated into buildings) may occur in a non-uniform way in the majority of applications. Consequently, PV modules invariably age in a non-uniform manner. This has an adverse impact on the performance of PV plants, especially from the middle till the end of their useful life. The primary reason preventing homogeneous aging is suboptimal environmental conditions, such as temperature, dust, woodland locations, storms, structures or the shadows caused by structures.

As different PV modules in a PV array do not age homogeneously, their operating conditions are inconsistent, and the power output of PV arrays varies. The global maximum power point tracking (GMPPT) permits monitoring of the maximum power point (MPP), yet the energy potential of a non-uniform aged PV array has not been evaluated. Given these considerations, the purpose of this study is to make medium- and large-scale aging PV arrays more cost-effective to maintain and operate as well as to enhance their output power efficiency rather than substituting aged PV modules. To that end, a method of offline PV module reconfiguration was devised,

taking into account the non-uniform aging of PV arrays to attenuate the impact and preclude the necessity of additional sensors. The proposed method made provision for operational costs and electricity price in order to afford a greater economic advantage. Simulations were conducted with MATLAB and Python software, and an experimental study was performed indoors to assess the method.

Four objectives were pursued in the study. First, the method's effectiveness for non-uniformly aging 3 × 4, 5 × 8, and 7 × 8 PV arrays was investigated through repetitive module sorting in a hierarchical order. Secondly, the effectiveness of arbitrarily non-uniformly aged 5 × 5 and 7 × 20 PV arrays was evaluated by applying a gene evolution algorithm (GEA). Thirdly, empirical work was conducted with a 2 × 4 PV array to validate the proposed method. Finally, fourteen countries were chosen as a case study to implement the proposed method to enhance as much as possible the economic advantage of typical 10×10 PV arrays with an output of 18 and 43 kW, taking into account operational costs and the price of electric energy.

Key Words: Photovoltaic (PV), Rearrangement, Offline Reconfiguration, Non-Uniform Aging, Algorithm, Output Characteristics, Maintenance Cost.

LIST OF PUBLICATIONS

Journals:

1. Alkahtani, M.; Wu, Z.; Kuka, C.S.; Alahammad, M.S.; Ni, K. A Novel PV Array Reconfiguration Algorithm Approach to Optimising Power Generation across Non-uniformly Aged PV Arrays by merely Repositioning. *J.—Multidiscip*. Sci. J. 2020, 3, 32–53.

2. Alkahtani, M.; Hu, Y.; Wu, Z.; Kuka, C.S.; Alhammad, M.S.; Zhang, C. Gene Evaluation Algorithm for Reconfiguration of Medium and Large Size Photovoltaic Arrays Exhibiting Non-Uniform Aging. Energies 2020, 13, 1921.

3. M. Alkahtani, J. Zhou, Y. Hu, F. Alkasmoul, Z. H. Kiani and C. S. Kuka, "An Experimental Investigation on Output Power Enhancement with Offline Reconfiguration for Non-uniform Aging Photovoltaic Array to Maximise Economic Benefit," in IEEE Access, doi: 10.1109/ACCESS.2021.3088386.

4. M. Alkahtani et al., "Investigating Fourteen Countries to Maximum the Economy Benefit by Using Offline Reconfiguration for Medium Scale PV Array Arrangements," Energies, vol. 14, no. 1, 2021, doi: 10.3390/en14010059.

5. Wu, Z.; Zhang, C.; Alkahtani, M.; Hu, Y.; Zhang, J. Cost-Effective Offline Reconfiguration for Large-Scale Non-Uniformly Aging Photovoltaic Arrays Efficiency Enhancement. IEEE Access 2020, 8, 80572–80581.

CONTENTS

LIST OF FIGURES

Page

LIST OF TABLES

Page

Chapter 1. INTRODUCTION

1.1 Background

The increase in greenhouse gas emissions, environmental issues, and other reasons has intensified the demand for efficient renewable energy sources. At the same time, politicians have been galvanised into action by climate change movements organised in different parts of the world, and the United Nations was prompted to declare 2012 as the International Year of Sustainable Energy for All. This scheme established three aims to be attained by 2030: energy efficiency improvement, widening availability of renewable energy sources, and accessibility to cutting-edge energy services for people worldwide [1].

Through the direct conversion of sunlight into electric energy, the renewable source of energy known as photovoltaic (PV) energy can supply clean energy. This kind of energy is advantageous because, unlike wind turbines, PV cells and panels are silent and do not have any harmful effects. Additionally, PV systems can be installed on any surface where sunlight can be captured and energy produced, including rooftops, parking zones, and the vertical sides of skyscrapers. Furthermore, the technology has been embraced for residential use and has attracted investment owing to governmental subsidisation of residential PV system installation and the launch of the feed-in tariff [2].

According to preliminary data for 2021, the global PV energy production fluctuates in the range of 125 to 126 GW. This fluctuation can be attributed to the number of causes, such as the difficulty of acquiring legitimate organisational data as

the number of publicly traded companies is declining and lack of standardisation in reporting practices.

Data were derived from the stock market reports of listed companies, various market reports, and personal contacts. Figure 1.1 reveals a production of 125.6 GW, which was estimated by comparing the different sources; by contrast to 2018, this figure represents an approximately 28.95% rise [3].

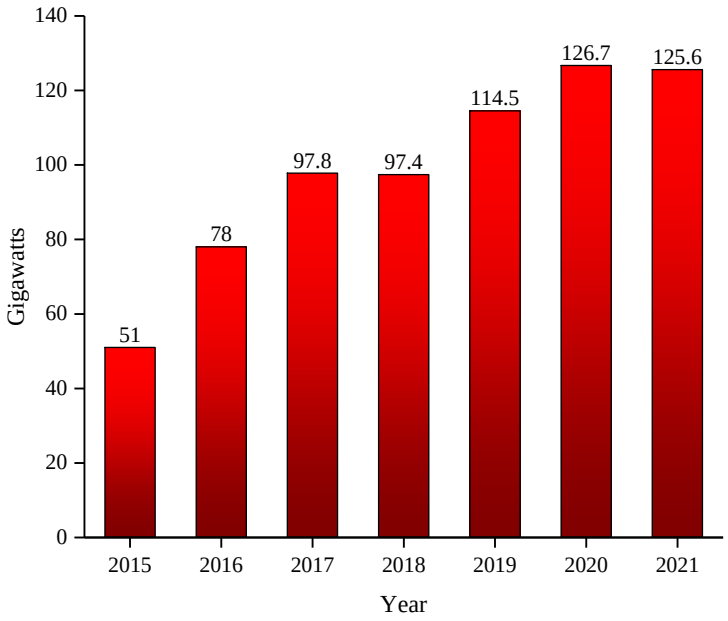

Figure 1.1: Global Cumulative PV Installation in 2021 [4, 5].

The By the end of 2020, the most PV systems were installed in Europe, Latin America, India, the Asia-Pacific region, and the US, with the addition of 19.6, 6.7, 7.5, 16.9, and 18.4 GW, respectively. However, with a capability of over 56.5 GW, the foremost country in terms of new PV system installations was China, which reflects the drive demonstrated by the Chinese government to prioritise the use of cleaner energy sources in the last three years [4, 6].

1.2 Various Solar PV System Applications

Solar cells use sunlight to produce direct current (DC), and linked solar cells make up a solar array. Solar insolation, ambient temperature, and solar array size and configuration are among the factors determining the output current of a solar array. Energy production is typically more outstanding in the case of solar panels with an expansive area and lowers in the case of solar panels with limited area.

Solar PV systems are capable of supplying DC power to load or be linked via direct current and alternating current (DC-AC) inverters to provide AC power to loads. A few PV applications are exemplified in the following part.

1.2.1.1 Utility Power Production

PV power plants of large size are capable of variable levels of energy production of up to a couple of Gigawatts, satisfying the demand of a few thousand residences as in Figure 1.2.

Figure 1.2: Solar PV power plant [7].

Solar It is possible to link solar arrays into standard modules comprising numerous PV arrays operating jointly. Subsequently, the necessary power is produced through the linkage of the modules in parallel. The straightforward installation and connection process of PV arrays make solar PV plants more advantageous than other

types of power plants. Unlike traditional plants running on fossil fuels or nuclear power, solar PV plants are constructed faster since meeting electric energy demand is more important than planning. Furthermore, the construction of PV power plants can be undertaken wherever the requirement is highest owing to the non-uniform load demand of the distributed electrical system.

Moreover, PV power plants are noiseless, do not require any fuel to operate, and are environmentally friendly. Additionally, modular PV plants permit incremental expansion with the rise in demand, in contrast to traditional power plants. Therefore, PV power plants afford many advantages for utilities when reducing fuel costs [8].

1.2.1.2 Stand-Alone Systems

Solar arrays of small size are extensively employed by numerous applications, including mobile phone chargers, calculators, a light-emitting diode (LED) lights, and traffic-warning LED lights Figure 1.3. These are capable of a power output of between a couple of microwatts to a couple of hundred watts, while the output voltage is between a couple of volts and tens of volts. Weighing just 3.66 mg/mm^2, standard solar panels can be installed on portable devices whilst still upholding weight specifications [9-11].

Figure 1.3: Small-scale stand-alone solar photovoltaic systems [10, 12, 13].

1.2.1.3 Battery Storage

Solar insolation determines the output power of solar PV systems, which therefore fluctuates over the course of the day and is not produced at all during night-time [14]. The systems are occasionally equipped with batteries to make the output power more stable. This works in the following way: the solar panels capture and convert sunlight into electric energy, which is subsequently used for charging the batteries to be used for powering devices at times when there is no sunlight.

Basic AA batteries, such as those used in flashlights, are compatible with certain solar battery chargers Figure 1.4 whereas more special batteries are needed for other chargers employed with mobile phones, solar calculators, speedometers, and LED lights. There are also chargers for batteries in laptops and other such electronic devices.

Figure 1.4: A small solar photovoltaic cell with a battery storage unit.

Solar PV systems are employed for charging large battery systems for a power output of the order of kilowatts in rural regions, mountains, and woodland. For instance, large PV systems with high battery storage capacity can power water pumps in rural regions. Overall, the intended applications of solar chargers determine the most suitable type of solar battery charger [15].

1.2.1.4 Building Integrated Photovoltaic Systems (BIPVS)

Solar PV systems with battery storage are more expensive. The direct linkage of the systems often addresses this issue to the utility grid. Power is supplied to the equipment of the grid when solar insolation is not enough, while the PV system supplements the grid during “high-demand electricity” periods. In this way, the load demand can be satisfied without expanding the primary power plant.

Traditional construction features (e.g. roof, skylights or facades in sections of the building envelope) are being more and more often substituted with PV materials Figure 1.5 , serving as the main or secondary power source. Meanwhile, retrofitting of older constructions with BIPVS modules is practiced as well. The integration of PV systems into buildings reduces the construction work, therefore decreasing costs as

fewer materials and workers are needed. Furthermore, BIPVS systems do not stand out as much compared to other solar alternatives and look better because they are integrated into the design. Consequently, such systems are enjoying tremendous growth within the PV industry [16].

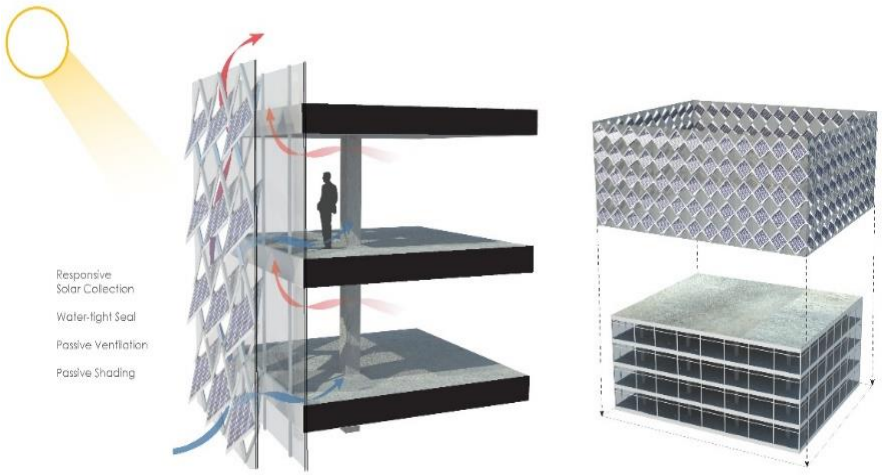

Figure 1.5: The building-integrated solar PV systems [17].

1.3 Motivations and Objectives

Solar energy has garnered enormous interest throughout the world in recent times owing to the sustainable development opportunities it affords [18, 19]. At present, the cost-effectiveness of PV panel production and ongoing innovation in power conversion technologies is making PV power devices more and more popular on the renewable energy market at a global level [20]. The appeal of PV panels stems from the fact that they are more operationally cost-effective and require less capital as energy conversion is highly efficient, and the service life is lengthy. However, a number of issues can affect PV arrays when PV systems are operational, such as short-term obstructions (e.g. dust, bird droppings) or irreversible deterioration (e.g. poorer performance, PV cell or diode breakdown) [21]. Furthermore, PV arrays do not age at

the same rate, as highlighted in a report by the National Renewable Energy Laboratory (NREL). A Gaussian distribution is reflected by the speed at which PV modules deteriorate, and in most cases, this speed is considered to range between 0.6 and 1% annually [22]. Three modules connected in series with aging to various degrees are shown in Figure 1.6 illustrates the effect of non-uniform aging PV array as service life increases.

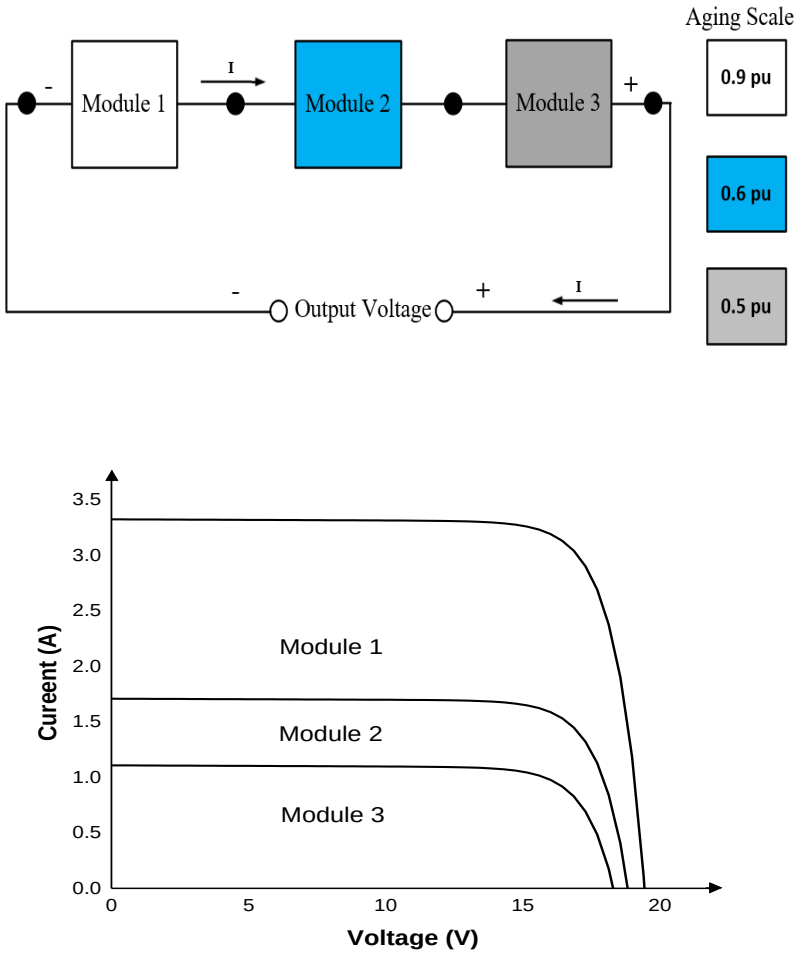

Figure 1.6: PV I-V characteristics curves for modules subject to non-uniform aging and connected in series.

PV arrays can be made to perform better based on an algorithm capable of optimising their electrical configuration to assess the energy potential within the context of PV module non-uniform aging. A novel method of reconfiguring PV arrays

is put forth in order to make maintenance more cost-effective. This method involves reorganisation of the positions instead of substituting aged PV modules to enhance the capability of PV arrays with non-uniform aging to produce power. Furthermore, the method necessitates information regarding the electrical parameters of the PV modules for the purposes of selection of the best reconfiguration topology. Moreover, the mismatch effect caused by the PV modules aging at different rates is attenuated by the algorithm through alliterative sorting of the modules in a hierarchical pattern.

1.4 Aim and Contributions

There are two ways to increase PV output power. The first is to use global maximum power point tracking (GMPPT), increasing power generation efficiency under fault conditions. Still, the ability for optimization of a whole PV array is yet to be fully established. A second approach involves reconfiguring PV arrays to increase their efficiencies under fault conditions.

This research aims to develop a reconfiguration strategy for aging PV systems so that it is possible to optimise the performance of a PV array by simply rearranging the PV module positions.

A. The research aim can be summarised as follows:

- To model the PV system, then perform simulations to validate the model's accuracy and compare it to manufactured models under varying weather conditions.
- To examine the functionality deriving a modelling and computing algorithm that simulates and analyses the possible rearrangement of aging solar PV arrays and the resulting output power.

- The experimental used a 2 × 4 PV array to assess the efficiency of different array interconnection topologies for reducing mismatch loss due to aging factors. In turn, a small PV module used eight-cell polycrystalline. Five different aging patterns were employed to effectively analyses the performance when linked in a series-parallel (S-P) topology.
- Developing a different size of PV array reconfiguration simulation to deliver the maximum output power were applied in fourteen countries to maximise economic benefit.

In this research, the methodology used is a computer simulation and analysis approach using an algorithm for optimising the configuration of a PV array within which different PV modules are subject to non-uniform aging processes. This is followed by testing to maximise the power generation across non-uniformly aged PV arrays by merely repositioning, rather than replacing, the PV modules, thereby keeping maintenance costs to a minimum. Therefore, each of the analysis has been performed to assess the efficacy of the suggested approach for a variety of dimensions of randomly non-uniformly aged PV arrays by using both MATLAB/Python. In addition, the offline reconfigurations method was also applied to the experimental laboratory work to ensure its effectiveness.

1.5 Thesis Outline

The thesis is divided into seven sections. The research background and primary objectives are introduced in the first section. The second section is concerned with a review of the literature pertaining to solar concentrated PV technology, with particular emphasis on types of cells, methods of increasing performance, simulation and

analysis of solar PV current and voltage, causes of PV module aging, possible issues, and strategies of detection. Topologies of PV arrays and the reason for choosing a (S-P) configuration are addressed as well. The proposed algorithm for improving power generation by reconfiguring PV arrays based only on the rearrangement of PV modules with non-uniform aging is presented in the third section. Also ,the algorithm of gene evaluation is validated in third section using 5×5 and 7×20 PV arrays. A computer-based creation of a PV array model is used to measure the maximum power output of the chosen PV configurations before and after repositioning. The efficiency of a 2×4 PV array with non-uniform aging is evaluated in the fourth section through an indoor empirical study. To that end, a GEA for offline reconfiguration is suggested to rearrange rather than substitute aged PV modules to increase the output power of PV arrays with non-uniform aging. In the fifth section, a number of fourteen countries are chosen as a case study to implement and assess through modelling and simulation the proposed method to enhance as much as possible the economic advantage of typical 10×10 PV arrays with the output of 18 and 43 kW, taking into account labour costs and the price of electric energy. Concluding remarks and recommendations for further study are outlined in the sixth section.

Chapter 2. LITERATURE REVIEW OF PV RECONFIGURATION STRATEGY

2.1 Introduction

The present section comprehensively reviews the literature related to solar energy technologies and the impact of unfavourable environmental factors (e.g. temperature, dust, bird droppings, hotspots, storms) on PV systems. Initially, the basic concepts pertaining to PV technology and the influence of environmental conditions on PV systems are addressed. Different types of PV technologies and simulation studies on concentrated PV systems with various reconfiguration methods are reviewed as well.

This section affords an overview of PV history in terms of how the technology was first created and how it has developed. The PV silicon crystalline structure is illustrated, and analysis and mathematical modelling of PV cells are presented. The primary ways in which PV modules deteriorate and the various existing issues and detection strategies are presented. Maximum power point tracker (MPPT) is defined, and its role and related algorithms are explained. All the chief methodologies are delineated with associated flowcharts or diagrams. The key aspects of MPPT algorithms are summarised in a comparative table. The reason for (S-P) configuration choice is also provided.

Empirical work on wet-cell batteries led Alexandre-Edmond to discover in 1839 the influence of the PV effect, resulting in light-based production of electric energy. The next important discovery was made in 1873 by Willoughby Smith, who recognised that selenium had photoconductive capability [23]. Three years later, that

capability was empirically investigated by William Adams and Richard Day, proving that the light effect in solid selenium permitted current production [24]. The work laid the foundations for PV cell development.

The PV cell prototype was created by Charles Frittes in 1883 through the compression of a selenium film of minimal thickness between two layers of distinct materials. Gold was the material for the superior layer, being capable of gathering the free electrons resulting from the light impact on selenium. It undertook the conversion of light to electricity at an efficiency below 2%, thereby generating electric energy [23].

Advances in crystal manufacturing methods allowed Pearson, Chapin, and Fuller to create the first modern silicon cell in 1954, demonstrating around 6% efficiency [25]. In 1955, the first PV product became commercially available, although its price was extremely high at 1000 $/W, hindering its use as a viable alternative source of electric energy [26]. Nevertheless, in 1959, the aerospace industry embraced the technology and incorporated it in the Vanguard 1 Satellite, functioning effectively for a period of eight years. This prompted a broader use of PV technology, which has come to be the foremost power source for numerous satellites. The PV arrays integrated by national aeronautics and space administration (NASA) in its Nimbus spaceship in 1964 had a production capacity of 470 W, while those integrated into the Orbiting Astronomical Observatory in 1966 had a capacity of 1 kW. The extensive aerospatial applications of PV technology has stimulated its ongoing development and efficiency refinement. For such applications, costs can be disregarded, but other factors (e.g. weight, materials, temperature, efficiency) cannot [27].

During the 1970s, there was a significant decrease of around 80% in the cost of PV technology from 67 to 13.3 $/W, leading to a rise in the use of such technology in a wide range of applications, such as offshore signal lights, railroad crossings, and highway signs. A laboratory specifically focusing on PV technology was first created by the University of Delaware in the US. In 1973, this university successfully deployed PV technology to supply electric energy to a residential unit, and the connection to the grid permitted the sale of surplus energy [26].

The PV technology advanced at a growing pace in the US. 1-MW production capacity was first achieved by the Atlantic Richfield Company (ARCO) Solar in 1980, while production in the range of MW became established with the creation of a PV plant capable of generating 6 MW in 1983, while the global production reached 21 MW in the same year. In 1985, the silicon PV cell was successfully made 20% efficient [26].

A variety of initiatives were launched during the 1990s to promote the use of PV technology as the primary source of electric energy, such as the "100,000 roofs" PV programme in Germany and the Million Solar Roofs in the US. At the same time, the existing PV technology became more efficient, with PV types of gallium indium phosphide and gallium arsenide reaching 30% and CdTe thin-film reaching 16% [26]. As a result, the use of PV technology intensified significantly, with a production of up to 177 GW. Table 2.1 summarises the history of PV technology development.

Table 2.1: This historical review is summarised in the PV evolution timeline.

Year	*PVs Science Discovery*	*Summarised*
1839	Edmond Becquerel	The first person to notice the impact of photovoltaic
1873	Willoughby Smith	Identified the selenium ability of photo conductivity
1876	William Adams and Richard	The start point for the current PV cell after successfully experiments the possibility of

		generating current in the solid selenium under the effect of light
1883	Charles Frittes	Build the first base on the electrical power producer by a thin-layer stack of selenium between two gold layers and produce electricity from light with 2% efficiency.
1954	Pearson, Chapin and Fuller	The first modern silicon cell was invented with a 6% efficiency.
1959	Vanguard	The first satellite to be powered by solar energy and survive for eight years.
1973	University of Delaware	The first home powered by solar energy is constructed.
1980	ARCO Solar	For the first time, 1 MW of PV is generated.
1983	ARCO Solar	6 MW plants new era.
1985	University of New South Wales	Silicone PVs effectiveness has risen to 20%.
1990	"Encouragements"	For instance, the 100,000 roofing program in Germany and the Million solar roof in the USA are funded by established initiatives to enable people to use PV as their main energy source.
1994	"Information"	Efficiency of PV is raised to 30%.
1999	"Information"	Total photovoltaic energy installed globally amounts to 1 GW.
2013	"Information"	138.9 GW of total worldwide PV installed.

2.2 Types of Photovoltaics Module Crystalline

The crystalline structure of first-generation PV technology integrated silicon to produce the combined solar cells and create PV modules. This technology is still being refined to make it more efficient and increase its capacity. The main types of PV panels with a silicon crystalline structure are presented in Figure 2.1 and addressed individually in the next part.

(a) (b) (c)

Figure 2.1: (a) Monocrystalline, (b) polycrystalline and (c) thin-film are the three primary kinds of solar panels [28].

2.2.1.1 Monocrystalline Photovoltaic

With a market share of around 80%, the mono-crystalline type of PV cell has the highest prevalence. It will probably only be superseded by PV technology of greater efficiency and cost-effectiveness that is yet to be innovated. Crystalline silicon p-n junctions underpin the structure of this PV cell type. Mono-crystalline silicon is produced by applying the Czochralski technique to cultivate a crystal ingot [29]. The silicon material restricts endeavours to increase efficiency due to the decline in the quantity of photon-generated energy at elevated wavelengths. Furthermore, thermal dissipation stems from radiation with longer wavelengths, making the cell less efficient by heating it up. Under STC, the highest efficiency attained by the monocrystalline silicon PV cell was about 23%, with an absolute maximum of 24.7%. Self-losses arise from the joint effect of solar cell resistance, solar radiation reflection, and metal contacts present on the superior part.

The produced silicon ingot has a diameter of 10-15 cm. It is cut into wafers with a thickness of 0.3 mm, yielding a solar cell displaying a current of around 35 mA/cm2 and 0.55-V voltage at complete illumination. Under STC, a capacity of up to

30% can be attained for a few other semiconductor materials with various wavelengths. Nevertheless, modules are never as efficient as the cell itself. In recent times, a full panel efficiency of 27.6% was claimed by Sunpower [30], which NREL measurements indicate to be a record efficiency [31]. It is anticipated that this panel will possess improved service life and match other sources in terms of cost. There are numerous shared traits between the solar silicon processing technology and the microelectronics industry. Laboratory cells can perform better due to the advantages garnered from the significant advances in the technologies for processing silicon wafers employed in microelectronic applications. This can have positive implications for the technology.

2.2.1.2 Polycrystalline Photovoltaic

Novel crystallisation methods have been devised as part of endeavours to diminish the costs of PV technology and enhance its production throughput. At a silicon price of 340 $/kg, poly-crystalline PV technology was most prominent in the PV industry. Owing to the reduced costs of manufacture, the decrease in the cost of silicon to 50 $/kg has not diminished the appeal of this technology, despite the fact that the cells have an efficiency that is 13-16% lower compared to mono-crystalline cells. The defects in metal contamination and crystal structure can be minimised through the conversion of crystalline PV cell generation from mono- to multi-silicon [32]. The production of poly-crystalline cells starts with silicon being melted and solidified into orient crystals in a fixed direction, resulting in a multi-crystalline silicon ingot of rectangular shape. This ingot is subsequently cut into blocks and then into wafers of minimal thickness. Cultivation of poly-crystalline silicon ribbons of wafer thinness can eliminate the need for the latter procedure. Evergreen Solar designed this technology [33].

2.2.1.3 Thin-film Technology

Thin-film technology differs from crystalline silicon cells in that it has the potential to make PV arrays more cost-effective by reducing the costs of material and manufacture whilst maintaining cell life expectancy and sustainability.

To produce thin-film panels, sputtering tools are employed to deposit layers of the minimal thickness of specific materials on glass or stainless steel (SS) substrates. This differs from the production of crystalline PV cells, whereby modules are developed by inserting semiconductor materials between glass panels. Thin-film panel production is more advantageous because the deposited layers are much thinner than the crystalline wafers (<10μm vs several hundred μ) and PV molecules demonstrating flexibility can be attained owing to the potential films placed on SS sheets. This ensures high throughput deposition and reduces material costs, thus making production more cost-effective. However, thin-film PV modules are less efficient than crystalline ones because the significantly reduced thickness of the layers limits the area of PV material that can assimilate sunlight. Nevertheless, efficiency has been substantially improved due to the possibility of depositing a wide range of materials and alloys. Additionally, thin-film PV modules have managed to secure 15-20% of the market because they are versatile and resistant to temperature.

The types of thin-film cells that are particularly prominent on the market are amorphous silicon cell with a structure comprising multiple junctions, thin poly-crystalline silicon on inexpensive substrate, copper indium diselenide/cadmium sulphide hetero-junction cell, and the cadmium telluride/cadmium sulphide hetero-junction cell.

- Amorphous silicon
- Amorphous-Si, double or triple junctions

- Tandem amorphous-Si and multi-crystalline-Si
- Cadmium telluride or cadmium sulphide/cadmium telluride

2.3 Characteristics of PV Output and Modules

2.3.1.1 Characteristics of Single PV Output

The traits of PV output are typically represented via I-V and P-V curves [34, 35]. These traits are usually defined by five major parameters; namely, open-circuit voltage V_{oc}, short-circuit currents I_{sc}, the voltage at the MPP V_{mp}, current at the MPP I_{mpp} and power at the MPP P_{mpp}, as shown in Figure 1.6.

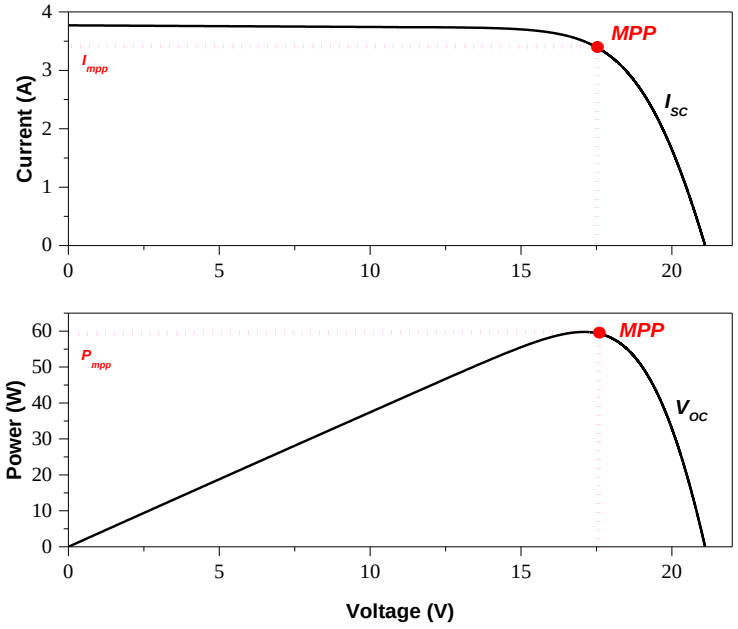

Figure 2.2: The main parameters for the PV cell output characteristics.

The parameters are specified in the PV manufacturing datasheet under standard test condition (STC), with solar irradiance of 1000 W/m2 and cell temperature of 25°C. Table 2.2 lists the Solarex (MSX60) electrical properties selected for the purposes of the present study.

Table 2.2: The disclaimers of the Solarex MSX60 photovoltaic module.

PV panel parameters	*Values*	*Values*
Open-circuit voltage	V_{OC}	21.1 V
Short-circuit current	I_{SC}	3.8 A
Maximum power	P_{mpp}	60 W
Maximum power current	I_{mp}	3.5 A
Maximum power voltage	V_{mpp}	17.1 V
Cell temperature	$°C$	25 °C

2.3.1.2 Characteristics of a Multi Sub-String PV Array

An array comprises multiple devices with joint operation. At the same time, topology is created by linking several sub-strings through two methods, namely, in series (one current branch and the voltages add) or in parallel (one terminal voltage and the currents add).

a) Linked Sub-strings in Parallel

Similar to other sources of electric energy, in parallel connection of solar devices means that the highest amount of current supplied by the terminals represents the total of the currents of the separate devices (Equation 2.1). The voltage of the shared terminals determines how much the sub-strings contribute to this current. In this manner, a terminal voltage that every sub-string can produce is maintained because the contribution of stronger sub-strings is greater compared to that of weaker sub-strings. Consequently, sub-strings connected in parallel all possess a comparable VMAX, so they can all function close to their MPP at the same time. Furthermore, the circuit is naturally resilient to power loss due to environmental conditions, causing the PV modules to age [21].

Progressive sweeping of the operating voltage, such as from 0V to V_{oc}, is necessary for composite curve detection from parallel devices. The equivalent currents

from every sub-string have to be summed up, yielding a graph that looks like one sub-string of high power Figure 2.4.

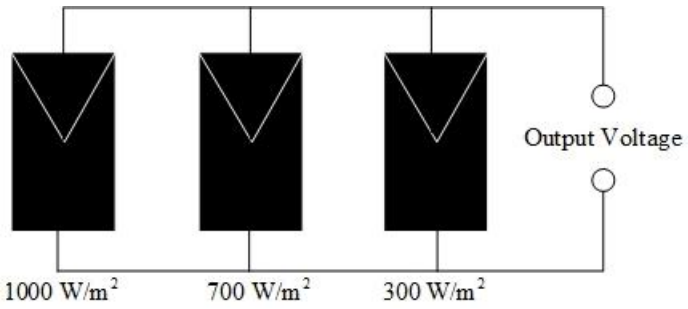

Figure 2.3: The three parallel sub-strings connection of PV modules.

The three parallel sub-strings are capable of simultaneous operation close to their MPPs, creating what is referred to as a tier, as shown in Figure 2.3.

$$Current_{out} = \sum_{i=1}^{n} Current_i \tag{2.1}$$

$$Voltage_{out} = Voltage_1 = Voltage_2 = \cdots = Voltage_n \tag{2.2}$$

$$Power_{out} = Voltage_{out} \times \sum_{i=1}^{n} Current_i \tag{2.3}$$

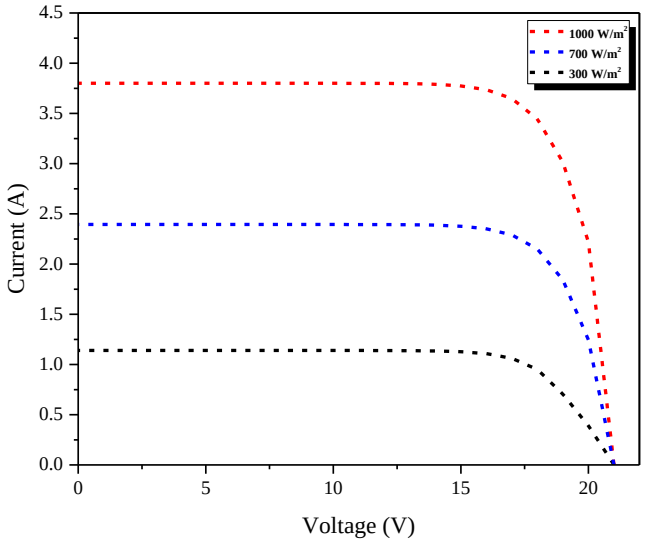

Figure 2.4: The predicted I-V curve from the three sub-string parallel connection.

b) Series Connected Sub-Strings

Unlike sub-strings connected in parallel, sub-strings connected in series exhibit interference in the current flows of one another Figure 2.5. Nevertheless, the integration of a bypass diode in every sub-string can ensure that each of them can likely pass the same current and prevent the weakest link effect. However, another problem stems from the use of such a diode, namely, several local maxima can be displayed by the PV curve, resulting in issues with MPPT at a later point. In spite of this, advances have undoubtedly been made given the notable increase in power production and the safe operation of series string in the context of aging processes. Progressive sweeping of the operating current, such as from 0 to I_{sc}, is necessary to attain a composite curve of devices with in-series connection, with the addition of the equivalent voltages [36].

$$Voltage_{out} = \sum_{i=1}^{n} Voltage_i \tag{2.4}$$

$$Power_{out} = Current_{out} \times Voltage_{out} \tag{2.5}$$

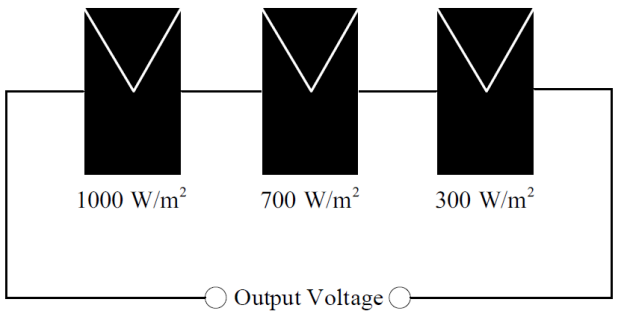

Figure 2.5: The three sub-strings series.

Noted in Figure 2.5 they all must move the same current, which means there are dependencies between all of them.

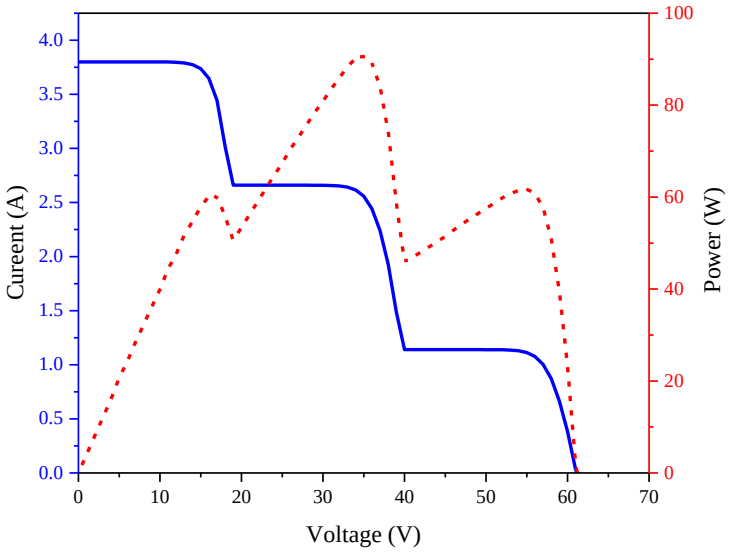

Figure 2.6: The three serial cells, composite I-V and P-V curves with bypass diodes under different irradiances. Due to the bypass diodes turning on, several peaks appear in the P-V curve.

2.3.1.3 PV Cell/ PV Array Equivalents Circuit Modelling

2.3.1.4 PV Cell Module

The entire I-V curve associated with a cell, module or array is represented as a continuous function for a specific set of functioning circuit variables by equivalent circuit models. The equivalent single diode circuit related to a PV cell is shown in Figure 2.7 [37, 38].

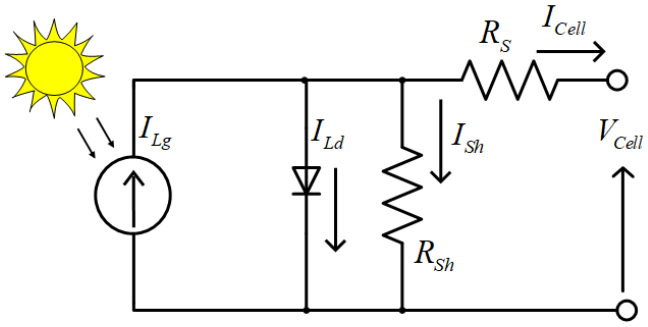

Figure 2.7: The equivalent of a single diode circuit of PV cell.

The equation for the equivalent circuit of the PV cell is formulated by using Kirchhoff's law for current I_{Cell}.

$$I_{Cell} = I_{Lg} - I_{Ld} - I_{Sh} \tag{2.6}$$

Where, I_{Lg} is the light-generated current in the cell, I_{Ld} is loss diode-current and I_{Sh} is the shunt-leakage current. In a single diode module, I_{Ld} modelled using the Shockley equation for an ideal diode.

$$I_{Ld} = I_S \left[\exp\left(\frac{(V_{Cell} + I_{Cell} \bullet R_S)\, q}{n \bullet V_T} \right) - 1 \right] \tag{2.7}$$

Where the diode ideality factor between 1 and 2 for a single-junction cell is n, I_S is the reverse saturation current of the diode, V_{Cell} is the output voltage of the cell and V_T is the voltage thermal can be expressed as:

$$V_T = \frac{k \bullet T_C}{q} \tag{2.8}$$

Where the temperature of the p-n junction is T_C, K is Boltzmann constant 1.38×10^{-23} J/K and q is the elementary charge 1.6×10^{-19}.

Here, R_S is the series resistance and R_{Sh} the shunt is current can be expressed as:

$$I_{Sh} = \frac{(V_{Cell} + I_{Cell} \bullet R_S) q}{R_{Sh}} \tag{2.9}$$

Then, the final single diode model can be expressed from the above equations results as:

$$I_{Ld} = I_{Lg} - I_S \left[\exp\left(\frac{(V_{Cell} + I_{Cell} \bullet R_S)\, q}{n \bullet V_T} \right) - 1 \right] - \left(\frac{V_{Cell} + I_{Cell} \bullet R_S}{R_{Sh}} \right) \tag{2.10}$$

2.3.1.5 PV Array Module

A PV array is made of a group of several PV modules connected in series and with parallel circuits to generate the required current and voltage. The corresponding circuit pertaining to a PV module with a configuration of N_P parallel and N_S series is illustrated in Figure 2.8 [39].

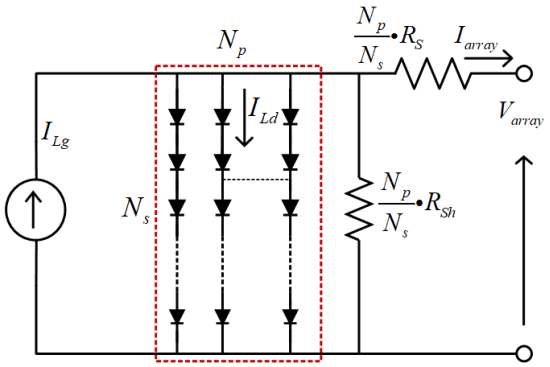

Figure 2.8: Uniform operation of the modules.

Therefore, for the PV array, as shown in Figure 2.8, the output current equation as given below:

$$I_{array} = N_p I_{Lg} - N_p I_{Ld} \bullet I_S \left[\exp\left(\frac{\left(\frac{V_{array}}{N_s} + \frac{I_{array} \bullet R_S}{N_p} \right) q}{n N_s \bullet V_T} \right) - 1 \right] - \left(\frac{\frac{V_{array}}{N_s} + \frac{I_{array} \bullet R_S}{N_p}}{N_s \bullet R_{Sh}} \right)$$

(2.11)

Form Figure 2.8, the bandgap voltage and the current for a PV array with N_S cells in series and N_P strings in parallel are respectively denoted by V_{Array} and I_{Array}, while the diode current is denoted by the reverse saturation I_S and the diode factor and voltage thermal are respectively denoted by *n* and V_T (Equation 2.7).

A Numerous PV cells with in-series connection make up a PV module, which in turn usually comprises 36 PV cells within the series connection. The resistance in the direction of the current flow supplied by the solar cells and the resistance supplied by

the leakage current are respectively given by R_S and R_{Sh} [40]. Photoelectric current represents a feature of short-circuit current, and its expression takes the following form.

$$I_{Lg} = I_{SCm}(1+\alpha(T-T_m))\left(\frac{G}{G_m}\right)\left(\frac{R_S+R_{Sh}}{R_{Sh}}\right) \tag{2.12}$$

Where is the short circuit-current of the modules I_{SCm} at standard insolation G_m (1000 W/m^2) and standard temperature T_m ($25\,°C$) and α is the module's temperature coefficient for the current. As seen in Equation 2.7, the short current-circuit can be defined by the next equation [41].

$$I_{SCm} = \frac{I_{Lg}}{\left(1+\frac{R_S}{R_{Sh}}\right)} \tag{2.13}$$

In addition, Equation can explain the open-circuit voltage (2.9).

$$V_{OC} \approx \left(\frac{nV_T}{q}\right) In\left(\frac{I_{Lg}}{I_{Ld}}\right) \tag{2.14}$$

Last, Equation (2.10) for calculating the solar cell power.

$$P = V \times I = V \times \left(I_{Lg} - I_{Ldo} - \frac{V_{Ldo}}{R_{Sh}}\right) \tag{2.15}$$

2.4 Aging on PV Modules

The light reaching the modules and the status of cells and connections underpin the primary ways in which PV modules undergo deterioration. Soiling, shade, and snow deposition are the major factors associated with the light reaching the modules, while breakdown, patches of delamination, and cracks determine the status of cells and connections.

2.4.1.1 The Non-Uniform Aging Phenomenon

Usually, a PV generator comprises multiple strings of PV modules arranged in an array. The voltage needed for the grid inverter determines the number of series-connected (S-P) modules allocated to each string. The grid power supply determines the number of parallel-connected strings. **Error! Reference source not found.** d isplays a representative string PV array structure. The voltage through the strings and across the array in this arrangement on the right is the same (V_T), and the current through the array (I_{ARRAY}) is the aggregate of the currents through the individual strings [41].

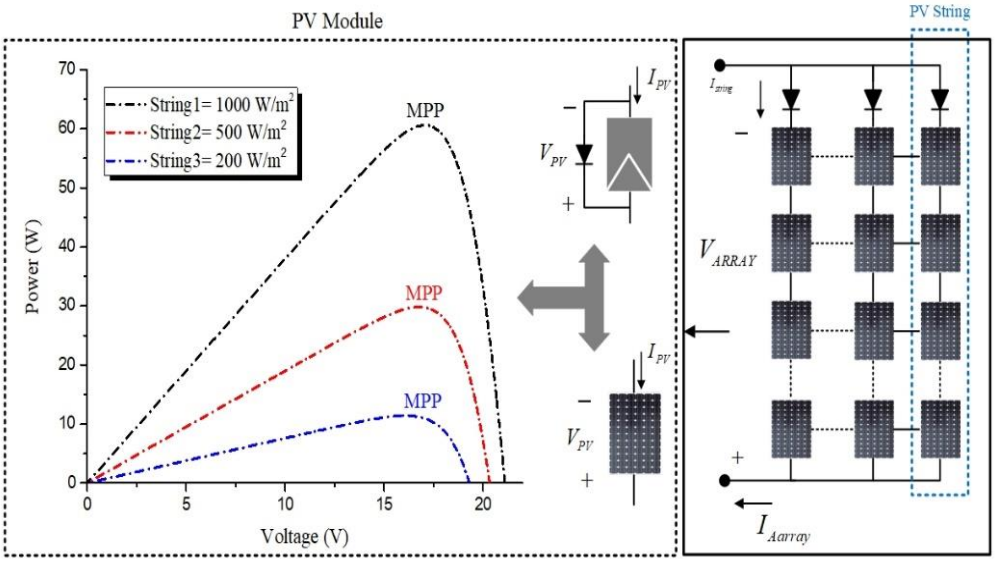

Figure 2.9: The PV multi-string equivalent [41].

Error! Reference source not found. shows the interior layout of a typical PV m odule, which consists of several series-connected cells. The installation also includes an anti-parallel bypass diode which avoids potential negative variations across the photovoltaic module, which would otherwise result in waste power. Also non-linear features of the Solarex (MSX60) standard module, which has variable output PPV power depending upon the applied VPV voltage and the irradiance *S*. Under each condition of radiation, the module's output power reaches its peak at a certain point,

called MPPT [223]. Owing to irradiance's variable existence, these are also continually traced in commercial models by the online maximum power-point tracking algorithms (MPPT) [41].

In a short circuit situation, where VPV is equal to zero voltage, peak PV current is reached, as shown in the expression and **Error! Reference source not found.**. E quation (2.5) in chapter 2 also, states that the photo-induced current powers the PV module, and therefore the current value is always lower than that of I_{SC}. The efficient irradiance obtained by the PV module is nevertheless dependent on the I_{SC}. Thus, if aging is seen through a string of PV modules, the irradiation received, hence the I_{SC} is different. Although the modules in a PV string have been arranged into series with an identical current, a discrepancy in the I_{SC} values will enable a diode to bypass the additional current path.

In **Error! Reference source not found.**, an example of this is depicted. A s tring of a pair of PV modules is shown in the diagram, one of which is completely exposed to irradiance and the other is partially shielded, resulting in a smaller I_{SC}. In this case, the current must be less than the photo-induced current in the string through the upper module. There are two possible operating situations, however. First, the corresponding G_2 diode is activated by a lower current in G_1 ($I_T < I_{SC1}$) than in the string ($I_T > I_{SC2}$), opening a route for the extra current (I_D $G_2 = I_T$-I_{SC2}) and causing a negligible voltage across the lower module so that no power is produced. Second, the corresponding G_1 diode is deactivated by a higher current in G_2 than in the string ($I_T < I_{SC1}$), and power is produced. The point of activation of the bypass diode is referred to as the inflexion point, and the mismatch phenomenon is referred to as the dual-state characteristic overall.

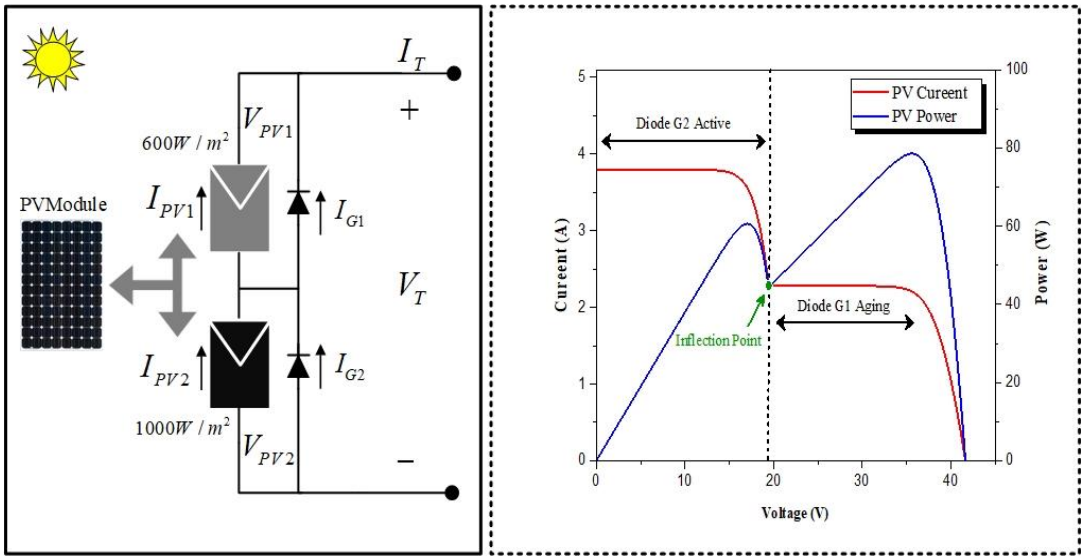

Figure 2.10: Outputs from PV strings under mismatched situations [41].

The key indication of an aging PV string affected by the mismatch phenomenon is that in the power-voltage (*P-V*) curve, as shown in **Error! Reference s ource not found.**, the activated bypass diodes cause several local maximum power points (LMPP) to appear. The simulated irradiance values are 1000 W/m^2 at G_2 and 600 W/m^2 at G_1, while more severe results of more substantial irradiance inequalities have been observed. A considerably more significant number of LMPP can also appear in larger PV arrays in the *P-V* curve, as shown in **Error! Reference source not found.**. I n this case, the number of LMPPs for n strings, each consisting of m modules, is *n x m* [224].

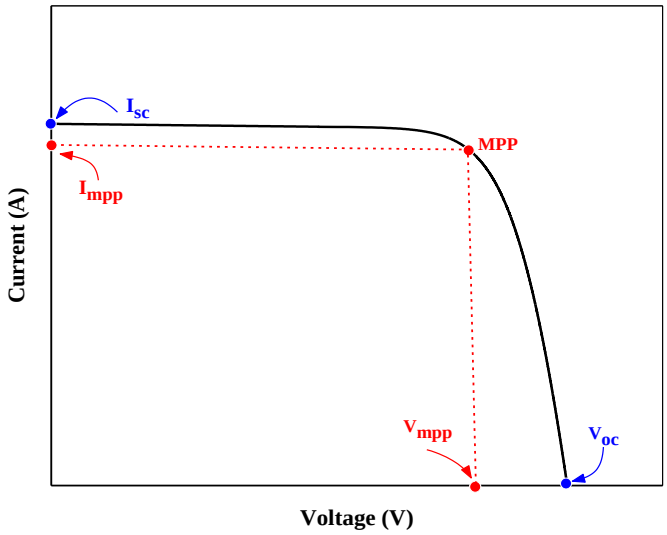

Figure 2.11: I–V current against voltage curve at standard test conditions (STC) for good PV single -diode characteristics [41].

2.4.1.2 Soiling

When the surface of PV modules is covered with dust, dirt, pollen, and other materials, the phenomenon is known as soiling. This is highly significant for solar energy, particularly in equatorial regions of a desert environment, which is why dust tends to be investigated more than other types of deposits. However, it does not have a long-term impact because soiling is a solvable problem in most cases. Dust-related factors such as density, content, size distribution, aggregation, removal, and environmental parameters determine the nature of soiling [42]. Furthermore, three major types of factors causing dust to accumulate have been delineated, namely, environmental conditions (e.g. wind, temperature, humidity, pollution), dust characteristics (e.g. sand, clay, bacteria, carbon), and installation features (e.g. material, orientation, situation, the character of the area) [43].

The place where the installation is situated determines the properties and effects of dust. One study conducted a comparative analysis of the content and effects of dust from sites in Mumbai and Jodhpur, India, through artificial soiling tests in the laboratory [44]. Results revealed that the dust samples differed significantly in size

and content, with 5 g/m2 of dust associated with more substantial losses in Mumbai than Jodhpur samples (18% vs 10% of losses). In a different study, clean and dusty panels were contrasted for laboratory and outdoor conditions. It was found that the open-circuit voltage losses of the dusty panel did not differ markedly from those of the clean panel under comparable conditions. Nevertheless, indoor testing yielded 45-55% power losses, while outdoor testing yielded power losses of just 6-8% [45]. Similarly, in [46] dust samples from various desert areas throughout the world were compared. Additional studies on the characteristics of dust have been conducted by [47-49].

Measurements of soiling-related power losses have been carried out under laboratory conditions, with controlled irradiation and rate of soiling, and outdoors. The materials and dust deposition determine the outcomes of such measurements. For instance, in [50], under indoor conditions, 2 g/m2 of dust on glass covers caused linear modifications on losses up to 20%. Under outdoor conditions, power losses exceeding 18% for one month were reported by an Iraqi study [51], average annual losses of 11.9% on horizontal surfaces were documented in another study [52], losses of up to 7.2% in dry periods were obtained by a study in California [53]. and peaks of over 11% of losses were found in California as well [54]. Furthermore, in [55]. , it was noted that efficiency declined by 0.2% per day in dry climates, amounting to 1.5-6.2% per year, according to the plant site. A different study reported that the soiling rates varied from 0.5 to 5% monthly [56]. In [57] , 10 mg/m2 of soiling was associated with a 0.1% rate of transmittance loss.

To sum up, the majority of PV installations, especially in desert environments, are susceptible to the effects of soiling, which impacts the system intensity rather than the voltage. The dust characteristics have been prioritised overpower losses in existing studies, and significant discrepancies have been observed between tests conducted

indoors and outdoors. In general, soiling effects are transient and can be straightforwardly addressed by cleaning surfaces adequately.

2.4.1.3 Snow and ice deposition

Snow and ice are problematic in cold climates propitious to their formation. They can block sunlight either partially or completely, diminish efficiency, cause cracks and delamination, or generate mechanical loads. On the upside, snow and ice can cool modules [58], but on the downside, light cannot reach the modules, and moisture may seep in. The impact of snow and ice and prevention methods have been extensively studied, with power losses, image processing or temperature markers being typically the basis for measuring snow depositions [59].

Regarding Studies on various climates and determinants (e.g. climate, adhesion, angle) were reviewed in [60] to gain insight into power losses. The foremost short- and long-term forecasting and modelling, and alleviation strategies (e.g. coatings, heating) were reviewed. In [61], it was observed that power losses were intermittent and associated solely with periods of low temperatures, such as October-April in the US, when blocked panels lost 30-35% energy per year, whereas unblocked panels lost 5-15% energy per year. In [62] , solar panels with various inclination angles were created, and the method of image processing was applied to determine the annual energy losses caused by snow. According to the findings, losses were not significantly affected by the inclination angle and crystalline material losses slightly exceeding amorphous material losses in the range between 3% for 10° angle and 0.5% for 60° angle.

To achieve more effective operation and maintenance, a range of parameters, including air temperature, angle of inclination, irradiance, and material, have been considered in the modelling of snow deposition impact. In [63], measurement of snow-

related losses was based on different sensors and a system for evaluating the monitoring and maintenance of modules were devised. In [64], modelling and comparison of losses between clean and obstructed modules relied on several parameters, such as temperature, humidity, and snowfall, resulting in the formulation of a framework for the forecast of snow deposition and losses over a period of a few years.

Snow slide and melting have been modelled in some studies through the methods of image processing, heat transmission, and fluid dynamics [65] and [66].

Research is scarcer on the effect of ice, even though the conditions of its formation are identical to those of snow [67]. In [68], a general discussion of the impact of ice on renewable energy sources was extended, highlighting that ice adhering to PV panels in great proportion led to less energy being generated. In [69], ice adhesion and sliding on PV modules were examined in the context of snow deposition and solar irradiation.

To summarise, snow deposition occurs intermittently during periods of low temperatures, greatly obstructing sunlight and causing ice to deposit and moisture seepage. Consequently, the impacted modules lose substantial amounts of power. Variables related to the environment and panels underpin the modelling of snow deposition. The effect of fluid dynamics and heat transmission is considered in the modelling of snow slide and melting, although insufficient research has been conducted in this regard. The available research tends to prioritise sliding and melting over engendered losses.

2.4.1.4 Hot spots

The phenomenon of hot spots is reflected in a rise in the temperature of PV cells due to modules being partly shaded or flawed inter-cell links. Consequently, energy is dissipated as heat rather than electricity [70].

In a study conducted in Spain, potential hot spots in two solar plants in the middle of the country were detected through a range of approaches [71]. Visual observation revealed that certain cells had cracks and bubbles, whereas the situation of the hot spots was obtained via thermography (Figure 2.12). Also, a different study proved the efficiency of using uncrewed aerial vehicles (UAVs) affixed with a thermal camera [72]. This was confirmed by other studies conducted in various settings, such as a solar farm [73] and test sites [74] and [75]. The PV panel deterioration and decline in PV plant performance induced by hot spots are illustrated in Figure 2.12 [71]. Hot spots arise due to a range of reasons, including shading, bypass diode malfunction, and incompatibility amongst electrical features [76, 77].

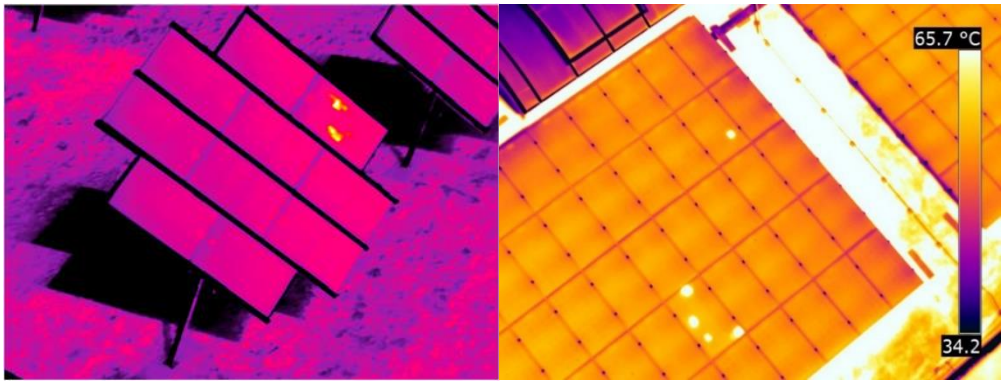

Figure 2.12: Hot spots in a PV module [71].

In [78] the contribution of impurities to hot spot formation was investigated by conducting tests under conditions without light, revealing three zones, namely, hot spot centre, outside hot spot, and non-hot spot. Thermography and microscopy were deployed to examine those zones, indicating that zones with a high density of

impurities were directly associated with hot spot heating, while oxygen, carbon, iron, and platinum dominated the composition of the impurities. Building on this work, a different study devised a model for PV cell process control [79], which involved coercing the cells to function on reverse conditions through voltage application to them, with the subsequent creation of cell thermography within an interval of less than half a second. The process control compared reverse power and temperature, accepting or dismissing cells according to their correlation. In this way, end-product quality could be increased without major investment.

Software-based hot spot simulation and modelling were undertaken in numerous studies. [80], heat dissipation was modelled under a range of shading circumstances. [81], the accuracy of thermal distribution calculation was increased by considering the multiple layers of a solar cell in modelling its thermal attributes. The inverse proportionality of hot spot size and the temperature was thus determined. In [82], modelling of how hot spots behaved was performed. The results achieved in outdoor settings were confirmed via a high-speed thermal camera, PV modules with known hot spots, and a meteorological station for determining environmental conditions. It was found that hot spot temperature was lowered by wind speed, opaque and semi-transparent modules behaved similarly, and hot spot temperature and number were negatively correlated.

Hot spot investigation has also been conducted based on electrical stimulation and testing. For instance, a temperature-reliant electrical model was created in [83], while a number of measurements were applied for hot spot identification according to electrical attributes in [84]. The correlation between hot spots and shading was examined as well [85] and [86].

In short, a range of factors contributes to the formation of the flaws known as hot spots, which cause the impacted cells and modules to heat up and lose power. Thermography is typically adopted to identify hot spots, while their investigation is aided by electrical modelling and software-based simulations.

The received light and the status of cells and connectors have been proposed to be the main determinants of PV system deterioration. The received light is associated with both short- and long-term effects; the former arises from soiling and snow deposition, which block light and cause power losses in distinct ways, while the latter (e.g. corrosion, delamination, deterioration) arise under outdoor conditions and are permanent and interconnected. Meanwhile, the status of cells and connectors are associated with the formation of cracks and hot spots. The occurrence and implications of such flaws can be alleviated or prevented via appropriate maintenance.

2.4.1.5 Outdoor exposure

PV modules suffer both short- and long-term effects due to outdoor conditions and sunlight exposure, which are closely connected to one another so that their actions are typically explained jointly. Moisture seepage and overall deterioration of the modules lead to corrosion and delamination, which are the major flaws associated with protracted exposure.

2.4.1.6 Corrosion

Organic PVs display greater susceptibility to corrosion, although the properties of crystalline and thin-film modules are affected by this phenomenon as well. The correlation between corrosion and various parameters (e.g. stability, climate, temperature) can be assessed through different methods. [87], the primary approaches and specifications for determining PV module corrosion and deterioration at various light, temperature, and irradiation levels were outlined. [88], a range of modules was

examined to establish how stable they were following 10000 hours of testing in several countries and terms of outdoor parameters. The modules were maintained stable in the long run through adequate preparation and encapsulation.

2.4.1.7 Delamination

When the encapsulant and the photosensitive components of cells no longer adhere to one another, delamination takes place (Figure 2.13). In turn, this can contribute to a decline in performance by promoting moisture seepage and corrosion. Areas with metal (e.g. gridlines, bus bars) are particularly prone to delamination. The effect is permanent and makes it more likely for modules to deteriorate in the long run. Delamination and interface adhesion can be measured in various ways. One suggested approach involves measuring the adhesion energy and chemical analysis of a developed standardised PV module. [89] Meanwhile, delamination in glass substrates could be examined through the application of an electric current for up to a quarter of an hour and effect measurement following the reduction in the temperature of the specimen [90]. Furthermore, one study suggested two distinct tests for PV modules and adhesive materials to determine the per surface energy necessary for the division of two adhesive sheets [91].

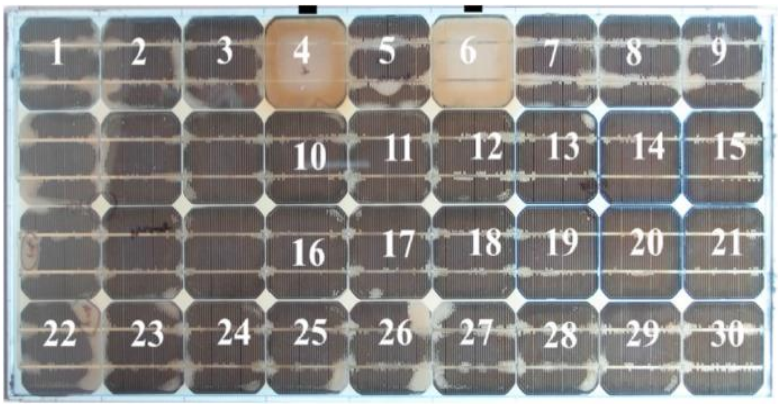

Figure 2.13: Degradation of a PV module that is 25 years old (Aging).

In [92], PV module packaging materials were examined in detail, and their reaction to adhesion tests was inspected under a range of settings. The manner in which adhesion evolved and moisture was transported were analysed as well. The samples subjected to testing were classified according to how their performed in terms of adhesion, glass cleaning, and shear strength. It was found that, compared to products available on the market, the suggested method yielded superior outcomes. Still, mixed packaging could permit water to seep in and toxic substances to seep out. Furthermore, the temperature of 85°C and moisture of 85% were excessive for testing, whereas the temperature of 60°C and moisture of 70% were insufficient. Therefore, further research is needed to establish optimal conditions.

Modules aged 25 years were used in [93] to investigate the long-term action of delamination and discolouration within a coastal area (Figure 2.13). Although there was power loss of nearly 18%, the modules did not exhibit any dielectric breakdowns. The primary flaws were identified through a specially devised visual test, which revealed that the modules had obviously degenerated, while the affected cells showed poorer electrical attributes and the areas where the cells came into contact with metal displayed corrosion. Another study examined discolouration as well, with

categorisation of determinants and detection of its impact on modules after protracted exposure based on non-destructive tests [94].

A study conducted in South Africa investigated how a PV module responded to delamination and moisture seepage [95]. Physical deterioration was apparent and fluctuated according to distance to the frame, and moisture could seep in due to the delamination. Furthermore, performance declined by over 16%, and the temperature was not homogeneous across cells. However, performance increased during periods with high temperatures and no humidity as moisture seeped out.

The effect of 'snail trails' is associated with moisture seepage that arises under circumstances of reaction between local PV cell zones and moisture, resulting in a chemical reaction with the silver, sulphur, and phosphorus contained [96]. The flaw is straightforward to identify because it engenders electroluminescence losses. Additionally, the flaw has been reported to elicit losses in performance of about 9% as well, although the impacted cells do not heat [97].

2.4.1.8 Deterioration

Studies conducted on overall module degeneration have focused primarily on causes and long-term effects. Concerning causes, one study provided an overview of the various determinants of degeneration, along with the elements it impacted and its implications [98]. Meanwhile, a different study explored how a module degenerated electrically and physically under outdoor conditions [95]. Yet another study examined PV modules with exposure to the environment of the Sahara in terms of degeneration, soiling, delamination, and corrosion [99]. With respect to long-term effects, irreversible damage and power losses have been distinguished as the main effects. Different studies analysed these effects in different regions and after different intervals

of time, such as after five years in Madrid [100], after four years in Thailand [101], and after 28 years in western India [102].

In summary, exposure to outdoor conditions causes permanent effects and typically impacts how PV modules behave in the long run. There are close connections between the flaws discussed in this part; for instance, moisture seepage engenders corrosion and delamination, which result in long-term module degeneration. The module power profile and production reflect these effects.

2.4.1.9 Cracks

Cracks can form throughout the use life of PV modules. For example, during the basic process of manufacture, they can arise during packaging and transport due to incorrect handling and vibration (Figure 2.14 and Figure 2.15), during the process of installation or during post-installation due to hard objects crashing into the module [103, 104].

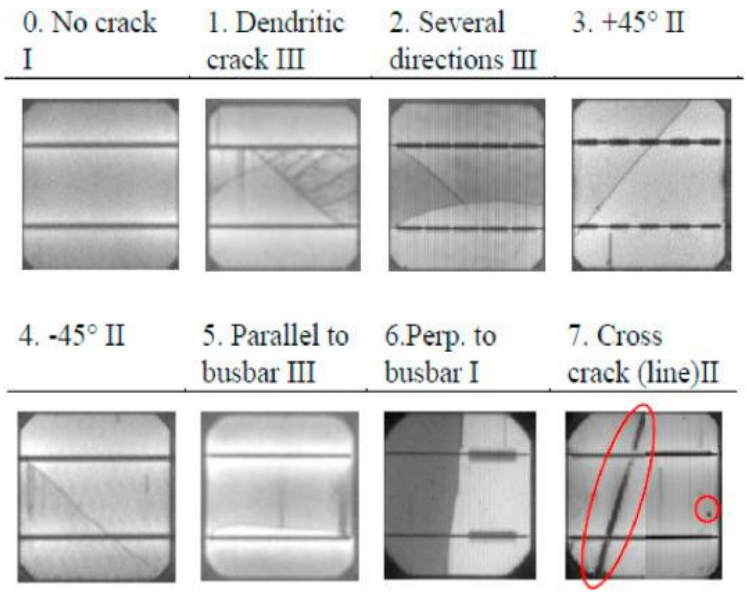

Figure 2.14: Classification of crack fractures.

Figure 2.15: Back view of the PV module and defective cells distribution shown in the back view [104].

A crack formation can occur during PV module transportation, and during mechanical tests, a crack formation can occur due to module vibration and resonance modes. Comparison of how cracks were statistically distributed revealed that around 70% of cracks were cracking with parallel and 45° orientation. Cracks were attributed primarily to mechanical loads during transportation since the modules displayed identical distribution regardless of the manufacturer [105].

The manner in which cracks were distributed following mechanical load tests was examined in [106], with emphasis on the impact of uniform static mechanical loads, such as snow or wind, on the occurrence of cracks. The way in which cracks were distributed and modules were orientated was established via post-test electroluminescence measurement. Half of the cracks were found to be parallel to the busbar, while about 15% of the cracks were diagonal, dendritic, and multi-directional cracks. In a different study, the performance of PV modules and crack formation were investigated in relation to dynamic loads (e.g. vibrations, wind), indicating that cracks were most pronounced at 16 Hz and the highest amplitude was 7 mm at 20 Hz [107].

In [108], a PV cell study was undertaken to determine how electrical resistance varied under cyclic bending loads. The crack formation could be seen and heard during the initial bending cycle, with force decreasing and system resistance increasing. Resistance was incremental in the posterior processes with declining value every time. In [109], various loads were used to assess the electroluminescence of modules and determine how it evolved. Pre-test cracks caused by manufacturing-related soldering or lamination were retained. Crack size and number increased exponentially during the empirical work, as confirmed by both tests.

Cracks have been identified via image processing based on a range of approaches taking into account the electroluminescence of PV cells. For instance, micro-cracks with logical gate enhancement were analysed through a three-dimensional model in [110], while an algorithm underpinned by Gaussian pyramid and wavelet modulus was employed for the same purpose in [111]. Furthermore, in [112], crack size and direction were examined in relation to performance, whereas in [113], micro-cracks and related effects were explored on the basis of electric modelling electroluminescence measurements.

To summarise, mechanical loads are the foremost cause of crack formation, which in turn leads mainly to electroluminescence alterations and power decline. The majority of existing studies are concerned with how cracks are distributed and how properties evolve, relying on modifications in electroluminescence for investigative purposes.

2.5 The Numerous Faults and Detection Methods

It is essential to assess PV system performance precisely and consistently to enable the industry to develop sustainably. Performance planning is a foremost marker of product quality from the manufacturers' perspective, whilst at the same time, it is a major indicator of possible issues within research studies.

The scheme known as Active Operation and Maintenance (O&M) was introduced to enable PV system production to attain its target performance level so that the systems could be perceived more trustworthy by consumers. Nevertheless, costs related to operation and maintenance are significant [114], and they can be diminished through O&M standard measures and especially PV monitoring systems [115, 116].

The purpose of PV system monitoring is to establish correspondences between the plant output and the forecasted output as well as to issue reports to consumers. Electrical and environmental sensors, alongside data collection systems with adapted communication protocols and data analysis algorithms, constitute the primary components of such systems.

There is an increasing number of studies dedicated to systems of PV plant monitoring, with the majority of them focusing on a particular facet of monitoring (e.g. sensors, data acquisition). However, there is only a handful of cutting-edge studies

[117-120], and all of them address a specific issue. In [117, 118], the significant features of specific commercial products are investigated. In [118, 119], the focus is on tools for measuring data, systems of collecting and storing data, strategies for transferring data, and applications intended for system control. Furthermore, one study outlines a few aspects that can serve as the basis for developing algorithms of PV module diagnosis and prognosis [117]. Methods for analysing PV system data are recommended in [119], while relevant guidance, techniques, and analytical PV system monitoring models are put forth [121].

Table 2.3 lists the latest methods and algorithms of diagnosis for PV plant monitoring, failure forecasting, and enhancement of PV system performance.

Table 2.3: Diagnostic techniques and algorithms to monitor photovoltaic plants.

Diagnostic Techniques and Algorithms Methods	***References***
Electrical Circuit Simulation of PV Generator	1. Modelling and fault diagnosis of a photovoltaic system [122]. 2. Automatic failure detection in photovoltaic systems [123]. 3. Use of PV circuit simulation for fault detection in PV array fields [124].
Electrical Signal	1. Fault detection method for grid-connected photovoltaic plants [125]. 2. Automatic supervision and fault detection of PV systems based on power losses analysis [126]. 3. Automatic failure detection in photovoltaic systems [127]. 4. Monitoring, modelling and simulation of PV systems using LABVIEW [128]. 5. Real-Time Fault Detection in Photovoltaic Systems [129]. 6. An efficient fault diagnosis method for PV systems based on operating voltage-window [130]. 7. Experimental studies of fault location in PV module strings [131]. 8. Mismatch Based Diagnosis of PV Fields Relying on Monitored String Currents [132]. 9. Automatic fault diagnosis in PV systems with distributed MPPT [75].
Time Domain Reflectometry	1. Monitoring, modelling and simulation of PV systems using LABVIEW [128].

	2. Diagnosis photovoltaic failure by simple function method to acquire I–V curve of photovoltaic modules string [133].
Maximum Power Point Tracking (MPPT)	1. Automatic failure detection in photovoltaic systems [123]. 2. Use of PV circuit simulation for fault detection in PV array fields [124]. 3. Analysis and Classification of Maximum Power Point Tracking (MPPT) Techniques [134].
Measured and Modelled PV System Outputs	1. Fault detection method for grid connected photovoltaic plants [125]. 2. Automatic supervision and fault detection of PV systems based on power losses analysis [126]. 3. Automatic fault detection in grid connected PV systems [127]. 4. Monitoring, modelling and simulation of PV systems using LABVIEW [128]. 5. Photovoltaic Array Condition Monitoring Based on Online Regression of Performance [135]. 6. Simple diagnostic approach for determining of faulted PV modules in string based PV arrays [136].
Artificial Intelligence	1. An intelligent fault detection method of a photovoltaic module array using wireless sensor networks [137].
Particularly Neural Network	1. Automatic fault detection and diagnosis for photovoltaic systems using combined artificial neural network and analytical based methods [138]. 2. Modelling and Health Monitoring of DC Side of Photovoltaic Array [139]. 3. Photovoltaic prognostics and heath management using learning algorithms [140].
Bayesian Belief Network	1. Intelligent fault detection and diagnostics in solar plants [141].
Fuzzy Logic	1. Research on Fault Detection of PV Array Based on Data Fusion and Fuzzy Mathematics [142]. 2. An intelligent system for detecting faults in photovoltaic fields [143].
Learning Method	1. Diagnostic technology and an expert system for photovoltaic systems using the learning method [144].
Extension Theory	1. Two-Stage Fault Diagnosis Method Based on the Extension Theory for PV Power Systems [145].
Satellite Observations	1. Monitoring and remote failure detection of grid-connected PV systems based on satellite observations [146]. 2. Intelligent performance check of PV system operation based on satellite data [147].

2.6 Maximum Power Point Algorithms

The PV operating point can fluctuate in the range between zero and open-circuit voltage, according to the I-V curve. The solar energy is not entirely supplied by the system to the load all the time because the operating point changes with a load rather than remaining fixed at the MPP. Nevertheless, the issue can be easily addressed by having an excess number of PV modules in the system. On the downside, such a solution will make the system costlier and more energy will be lost [148, 149]. MPPT is an innovative power electronic device that has been developed to compute the maximum operating point and thus tackle the issue. By linking to an MPPT controller, a PV system can search for the MPP and take advantage of the PV array so that it is uninterruptedly operational at the actual MPP [149].

There is a range of MPPT algorithms available for PV systems, with two major classes being distinguished, namely, traditional and stochastic methods. Traditional methods effectively identify the MPP when solar irradiance is homogeneous, but their performance suffers under constantly fluctuating environmental conditions and partial shade. Stochastic methods were introduced to overcome such limitations, being capable of determining the MPP irrespective of environmental circumstances. The selection of a method for finding the actual MPP must take into account the suitability of that method alongside costs and convergence speed. Table 2.4 outlines the existing MPPT algorithms.

Table 2.4: Under uniform and partial shading conditions, MPPT algorithms differ from each other.

MPPT Algorithms	
Partial shading condition	***Uniform irradiance condition***
Fuzzy Logic Controller (FLC)	Perturb and Observation (P&O)
Artificial Neural Network (ANN)	Hill Climbing (HC)
Differential Evolution (DE)	Incremental Conductance

Genetic Algorithm (GA)	Fractional V_{oc}
Particle Swarm Optimization (PSO)	Fractional I_{sc}
	Ripple Correlation Control (RCC)
	Current Sweep (CS)
	DC link capacitor droop control
	Load Current or Load Coltage Maximization

2.6.1.1 MPPT Algorithms Based on Stochastic

2.6.1.2 Fuzzy Logic Controller (FLC)

A fuzzy logic controller (FLC) can be achieved by implementing expert knowledge alongside the notion of fuzzy logic. It is advantageous because a precise model is possible to attain without technical know-how, and its design is uncomplicated. Therefore, it can be used for MPP search under different environmental conditions. Furthermore, the FLC employs terms like "many", "low", "medium", "often", and "few" to overcome the lack of accuracy and information granularity [67].

System stabilisation in the ideal voltage attained by the Distributed Fuzzy Control (DFC) is the purpose of the FLC. The input and output of the FLC are respectively, the variations between the output voltage of the PV array (V_{pv}) and ideal voltage (V_{mpp}) ($E = V_{pv} - V_{mpp}$), and the alteration of duty cycle D. The chosen FLC model is Madman's model [34]. In relation to membership functions underpinned by the rule of five, they are given by the five fuzzy sets into which the discourse universe is separated. Negative Big (NB), Negative Small (NS), Zero (ZO), Positive Small (PS), and Positive Big (PB) are the five linguistic variables. Table 2.5 lists the five rules.

Table 2.5: The Fuzzy rule is used in the proposed method of fuzzy logic control.

E	**NS**	**NB**	**PS**	**ZO**	**PB**
ΔD	*NS*	*NB*	*PS*	*ZO*	*PB*

The work point is nearer the MPP, and the nearer E is to zero. Therefore, several premises are applied to formulate the membership functions for E (Figure 2.16):

- The "MPP zone (ZO)" will be taken as V_{mpp}-V_{pv} discrepancy < 5 V, while the choice of the triangle (MF) is justified by its straightness and lack of complexity;
- "Near to the MPP zone (NS) or (PS)" will be taken as the V_{mpp}-V_{pv} discrepancy < 10 V;
- The "far from MPP zone" will be taken as V_{mpp}-V_{pv} discrepancy > 10 V, with conversion of the (MF) to trapezoidal (MF) for (NB) or (PB) state saturation;
- Figure 2.16 illustrates the membership functions associated with E and ΔD [150].

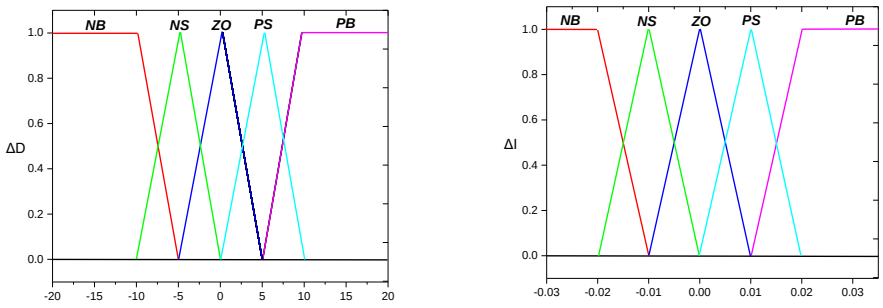

Figure 2.16: Membership function of input and output.

2.6.1.3 Artificial Neural Network (ANN)

Non-linear tasks can be more effectively undertaken based on artificial neural network (ANN), which is why this method is growing in popularity in different disciplines. Underpinned by the learning process, ANN does not require reprogramming and comprises three layers, namely, input, hidden, and output layers. Its modelling is based on weights that link neural networks and possess their own

strength. For example, wij is obtained when i and j are linked (Figure 2.17). The totality of the inputs is compiled and altered according to the weights.

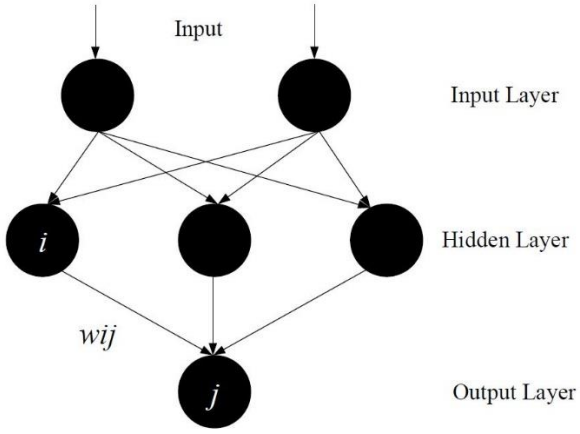

Figure 2.17: The three layers of ANN structure [151].

Input acquisition, data processing, and output production are the three processes integrated within the ANN framework. The design determines how many nodes and parameters ANN has. PV array inputs (e.g. temperature, solar irradiance rate, short-circuit current or open-circuit voltage) can be used to set the input variables. Meanwhile, the ANN output can serve as the basis for a power converter through duty-cycle signal adjustment or input provision to a different controller to enable operation of the PV array at or close to the MPP. The way in which the algorithm performs in concealed layers and neural network training are the determinants for achieving reliable operational outcomes [151, 152].

For aged systems, ANN has the capability of estimating the universal MPP voltage and power through observation of the P-V curve under different conditions of shading on the PV array [152]. The maximum power can be tracked based on the MPPT controller error input yielded by the discrepancy between the estimated and real voltage from the PV array.

Feed-forward neural networks (Figure 2.18a) and recurrent neural networks (Figure 2.18b) are the two topologies associated with the ANN connection. The former is characterised by exclusive input-output data [153] and the possibility of extending data processing to several layers without feedback links. Furthermore, the link is linear from the inputs to the outputs of units in the same or preceding layers. On the other hand, dynamic network properties influence recurrent neural networks, and these networks encompass feedback denoting short-term memory. Moreover, during the relaxation process underwent by the activation values, neural network conversion into a stable state leaves activations unaffected[152].

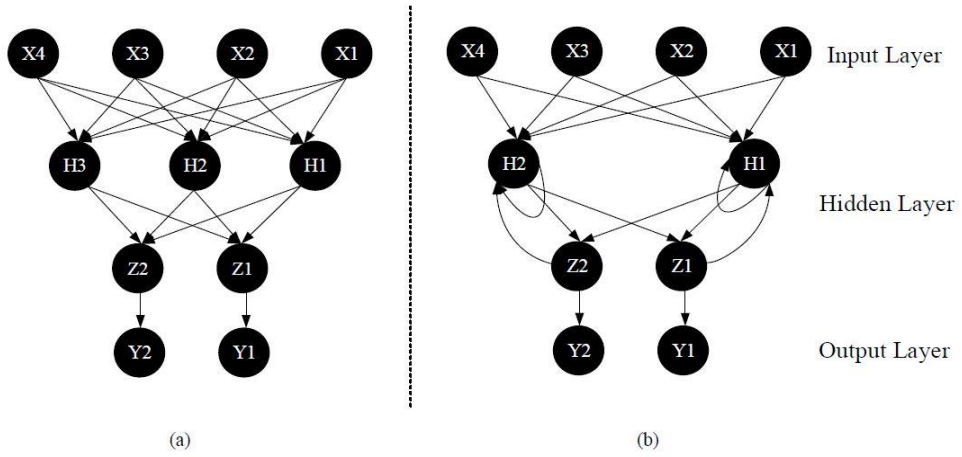

Figure 2.18: Where feed-forward (a) and Recurrent (b) neural network with four inputs and two outputs.

It has been suggested that ANN should be employed alongside fuzzy logic and polar information controller to determine the maximum power to improve the MPPT for the PV system under circumstances of partial shade [154]. Identification of the ideal PV voltage requires training of three layers feed-forward of ANN under several aging PV arrays. Comparative analysis of the proposed approach with the P&O for a number of shade patterns within a given temporal interval has revealed that the former can perform tracking twice as efficiently as the latter.

2.6.1.4 Differential Evolution (DE)

The evolutionary algorithm called differential evolution (DE) [155] constitutes a branch of genetic algorithms (GAs) that are stochastic-based algorithms for the identification of optimisation. Consequently, the tasks involved in GAs (i.e. initialisation, mutation, crossover, evaluation, and selection) are probably identical in DE. Furthermore, DE includes search variable vectors within an NP population, making it similar to other algorithms.

2.6.1.5 Initialization

The initial parameters, population, and maximum generation are established through DE optimisation. The selection of the initial vector is made arbitrarily to encompass the whole search space [91]. The parameter has to be in a particular spectrum for the search to produce effective results. At first, the execution of the DE algorithm is followed by the formation of the *jth* parameter. Initiation of the parameter is done at a point within the set spectrum with a superior limit x_j^L and an inferior limit x_j^U. The *jth* parameter in the *ith* population subsequently is:

$$x_{i,j}(0) = rand(0,1) + x_j^L. \quad \mathrm{x}_j^U - x_j^L \tag{2.16}$$

where rand (0, 1) is uniformly distributed random between 0 and 1.

2.6.1.6 Mutation

Individuals constitute a target vector for every generation. Meanwhile, a mutant vector $V_i(t)$. is obtained through the mutation of every individual. The arbitrary selection of three additional parameter vectors, r_1, r_2 and $, r_3$ from the existing population, is performed to generate $V_i(t)$ for the *ith* population. The discrepancy of any two of the three vectors is scaled by a scalar number *F* and added to the third one

derived from $V_i(t)$, thereby yielding a novel *jth* parameter in the population. The latter takes the following form:

$$v_{i,j}(t+1) = x_{r1,j}(t) + F.(x_{r2,j}(t) - x_{r3,j}(t))\cdots \quad (2.17)$$

2.6.1.7 Crossover

Crossover involves an expansion of the parent for the future generation. A trial vector will emerge from the third individual when the target vector is combined with a mutant vector in the process of crossover. The exponential and binomial methods are the two distinct crossover approaches associated with the DE [92].

Exponential crossover involves arbitrary selection of integer n from amongst the number of [0, $D-1$], which becomes the point of initiation of the target vector. Furthermore, the additional integer L is selected from an [1, D] interval and denotes a few elements. Based on the selection of n and L, the trial vector:

$$u_{i,j}(t) = \left[u_{i,1}(t), u_{i,2}(t), \cdots u_{i,D}(t)\right] \quad (2.18)$$

Is formed by

$$u_{i,j}(t) = u_{i,j}(t) \quad \text{for } j = (n)D, (n+1)D, \cdots, (n-L+1)D = x_{i,j}(t) \quad (2.19)$$

A modulo function with modulus D is defined by the angular bracket () D. Consequently, for any $m > 0$, $(L>m) = (CR)^{m-1}$. The DE parameter is regulated by the crossover constant CR.

When a number selected arbitrarily between 0 and 1 is within the CR value, then binomial crossover is accomplished on the D variables. This has the following expression:

$$u_{i,j}(t) = u_{i,j}(t) \quad \text{if } rand(0,1) \prec CR, = x_{i,j}(t) \tag{2.20}$$

2.6.1.8 Evaluation and Selection

A selection operator comes into play owing to the importance of preventing fluctuation in population size over future generations. In the context of the selection operation, the parent target vector will be substituted with the trial vector for the subsequent generation if the latter can identify a better fitness value than the former. A local search for the optimal individual involves one-to-one competition, but a global search involves identifying the optimal individual amongst the population. The implementation of DE to determine the best value is illustrated by the flow chart in Figure 2.19.

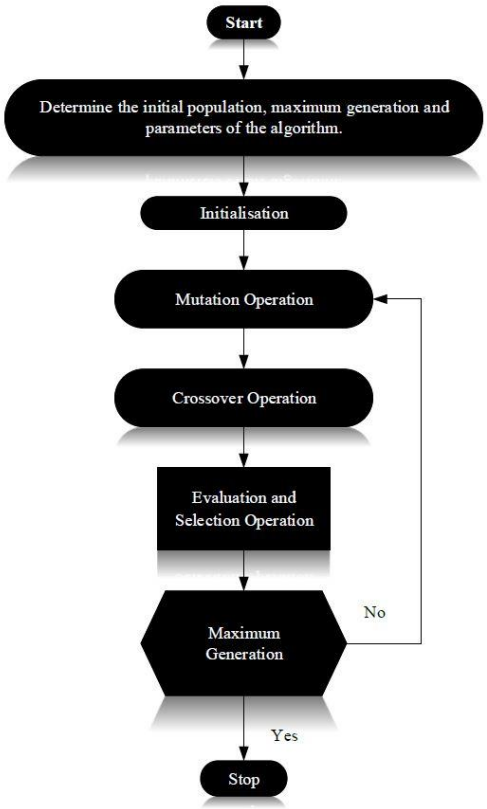

Figure 2.19: A chart in order to explain the process of differential evolution MPPT algorithm [152].

In [156], DE was employed to apply the MPPT algorithm under conditions of partial shade. DE demonstrates extremely rapid convergence and determines the MPP

with no fluctuation even under circumstances of partial shading by contrast to P&O, the main MPPT algorithm. Furthermore, unlike the P&O, DE is capable of tracking the MPP under environmental conditions that change fast.

2.6.1.9 Genetic Algorithm (GA)

In [157] a GA was adopted to implement an MPPT controller under partial shade conditions. As a heuristic search method rooted in natural evolution, GA is suitable for addressing the optimisation issue. It has been suggested as an approach for managing obstacles in global MPP tracking under shading conditions.

Selection, crossover, and mutation are the main operations drawing on natural evolution principles [158]. Selection involves a stochastic selection of a chromosome from the population of a present generation to be included in the population of the future generation, depending on fitness. In the case under consideration, the fitness value corresponds to the power level. Subsequently, in the crossover process, a new chromosome is generated through the integration of two chromosomes.

The purpose of mutation is to ensure that the future generation is as genetically diverse as the current one and seeks to attain a degree of stochastic variation of GA to speed up convergence. Figure 2.20 delineates the stages of GA application.

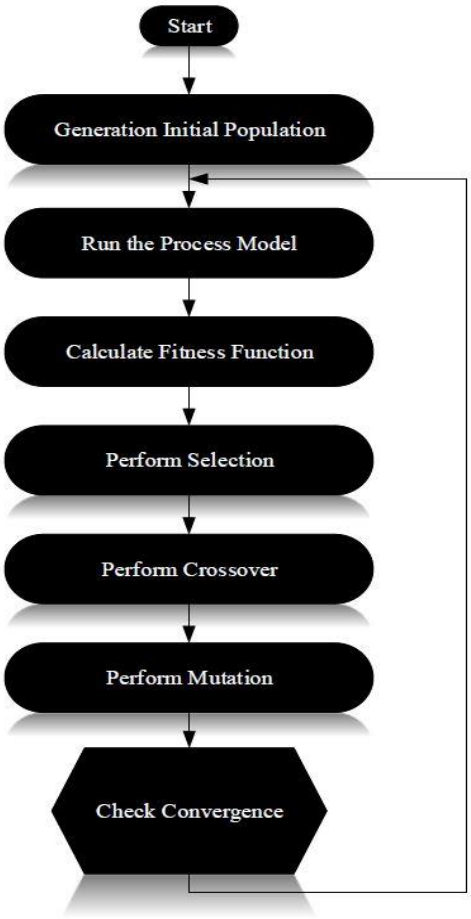

Figure 2.20: A chart in order to explain the process of the GA implementation steps [157].

2.6.1.10 Particle Swarm Optimization (PSO)

The Drawing inspiration from behaviours in the natural world, J. Keneddy introduced the particle swarm optimisation (PSO) algorithm in 1995. The underlying principle is that the problem of optimisation can be solved by mimicking the adaptational movements exhibited by birds, fish, and other organisms to compete and cooperate [159, 160].

A set of particles move within a search space to identify the optimal solution, with the movement being modulated according to the best-found solution during the search for novel solutions. The particle position must follow the ideal particle position

or the ideal position of an adjacent particle in order to determine the optimal solution Figure 2.21.

The PSO is regulated by position update and velocity update, which are expressed as follows:

Updating the velocity is given by

$$v_i^{k+1} = c_1 r_1 (Pbest_i - x_i^k) + wV_i^k + c_2 r_2 (Gbest_i - x_i^k) \quad (2.21)$$

While the update to the location is expressed by

$$x_i^{k+1} = V_i^{k+1} + x_i^k \quad (2.22)$$

Where:

- V_i^{k+1} Particle velocity update.
- V_i^k Current particle velocity.
- w Inertia weight.
- c_1 Influence of individual learning rate.
- c_2 Influence of individual learning rate.
- $Pbest_i$ The optimal location that the particle has found.
- $Gbest_i$ The swarm's best solution discovered.
- c_1 and r_2 Two uniformly distributed random values to add randomness to the movement of the particle.
- x_i^k The current position of the particle.
- x_i^{k+1} Updating particle position.

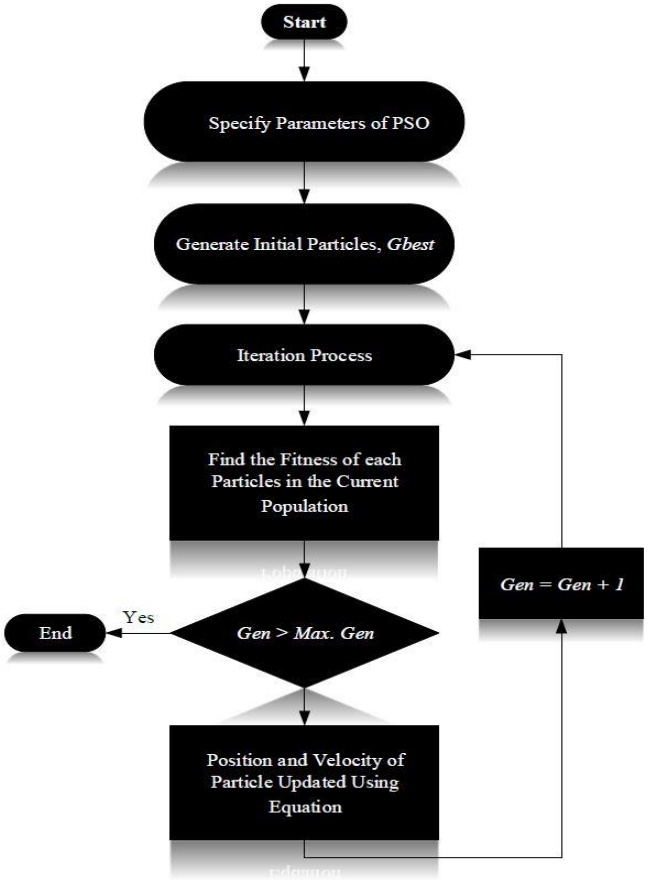

Figure 2.21: The particle swarm optimization flow chart for MPPT.

Parameter adjustment is challenging in this approach, prompting the introduction of the parameters applied in 2.11 and 2.12 for enhanced optimization [161].

2.6.1.11 MPPT Conventional Algorithms

2.6.1.12 Perturb and Observation (P&O)

The Perturb and Observation (P&O) algorithm are straightforward to apply, so it is so popular. The first step in the process is determining the PV power by sensing the current PV voltage and current values. A slight increase causes a perturbation in the PV array output voltage, determining power alteration ΔP. The perturbation advances the operating voltage in the direction of the MPP for a positive ΔP, and the perturbation size (C) is subsequently produced in an identical direction. Conversely, if ΔP is negative, system operation is remote from the ideal point, and the operating

points have to be brought back to the MPP by diminishing the perturbation size [162-164]. Figure 2.22 illustrates the flow chart associated with the P&O MPPT algorithm.

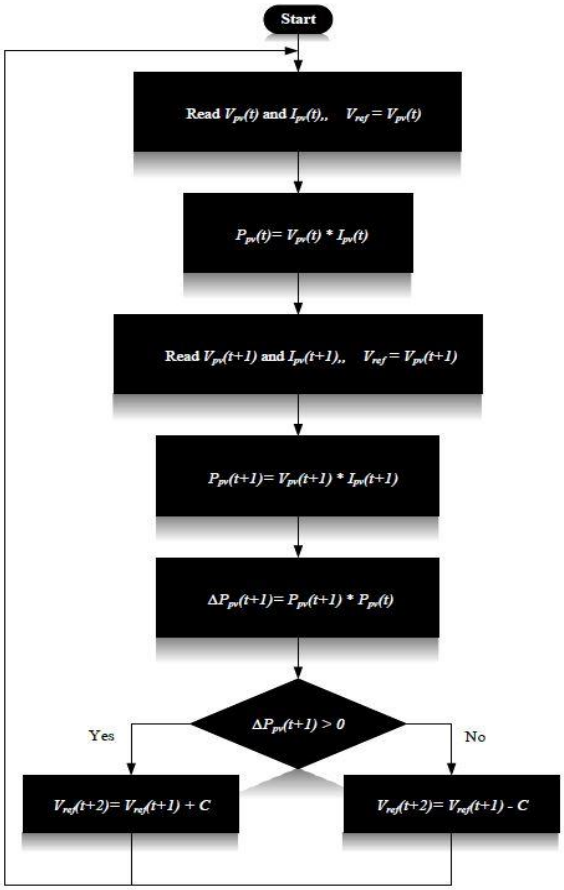

Figure 2.22: The flow chart of perturb and observe MPPT algorithm.

The operating point moves in the direction of the MPP when the rise in instantaneous PV power is linear with the rise in operating voltage, as can be deduced from the flow chart. Hence, the perturbation size becomes positive or stays the same. On the other hand, the operating point becomes distanced from the MPP when the decrease in instantaneous PV power is linear with the decrease in operating voltage, with a reversal in perturbation size to return the operating point to the actual MPP. However, this algorithm presents the limitation that fast changes in environmental conditions make tracking less efficient. The MPPT is incapable of identifying the real maximum point, fluctuating around the MPP constantly and altering the perturbation

sign following ΔP calculation. Furthermore, the real MPP cannot be identified by the P&O when solar irradiance is inconstant [163].

2.6.1.13 Incremental Conductance (INC)

The two foremost weaknesses of the P&O have been detailed in [165]. One weakness is that slight power variability around the MPP is constant owing to the fact that the degree of perturbation does not change at a steady-state, contributing to certain power losses. The other weakness is that there is a high probability of operating point divergence from the real MPP when environmental conditions change quickly. It has been suggested that these weaknesses can be addressed via the INC approach [165].

The INC relies on the fact that at MPP the derivative of (dP/dV) is zero. It is possible to express it as:

$$dP/dV = d(IV)/dV = I + V\, dI/dV = 0 \tag{2.23}$$

It is possible to write Equation (1) as:

$$-I/V = dI/dV \cong \Delta I/\Delta V \tag{2.24}$$

Where ΔV and ΔI are the PV voltage and current increments. It is possible to obtain the working theory of INC from the P-V curve, as shown in Figure 2.23.

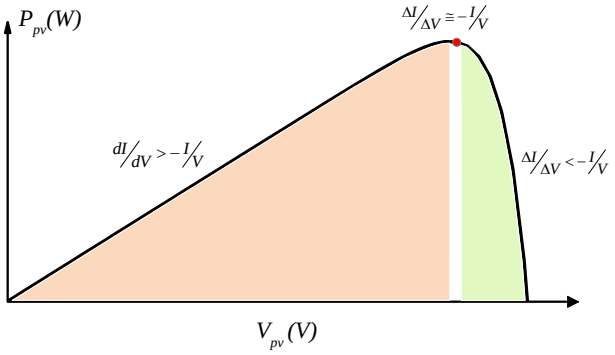

Figure 2.23: The P–V curves for the basis of the INC algorithm.

And can be written in the following as:

Left to MPP is $$dI/dV > -I/V \quad (2.25)$$

Right to MPP is $$dI/dV < -I/V \quad (2.26)$$

At MPP is $$dI/dV = -I/V \quad (2.27)$$

Establishing a gradual correspondence between instance conductance and the behavioural derivative ratio is the key principle underpinning the INC method [165]. Figure 2.24 illustrates the basic flow chart of the INC algorithm based on the rules from Equations 2.15 and 2.17.

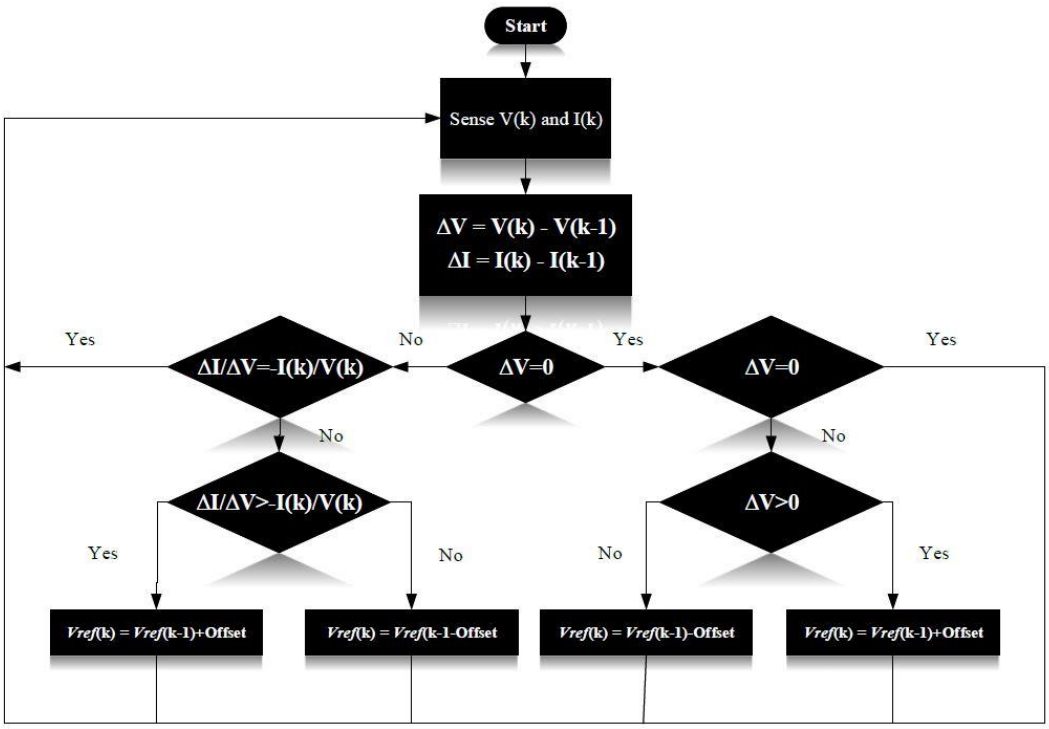

Figure 2.24: The flowchart of the INC method.

What makes the INC method advantageous is that it enables improved performance under environmental conditions changing quickly and reduced fluctuation around MPP. Nevertheless, the method does not differ much from the P&O regarding efficiency to attain MPP [166]. On the downside, the INC method cannot track the global MPP when there is partial shade, and the complexity of its control circuitry increases system costs.

2.6.1.14 Hill climbing

From the perspective of controlling the PV voltage to follow the ideal setting point (VMPP), the hill-climbing (HC) algorithm is closely similar to the P&O. For MPP detection, the HC algorithm concentrates on duty cycle perturbation of the power converter. It constantly tracks and updates the ideal point until the identification of the MPP ($dP/dV = 0$) is achieved. Furthermore, the algorithm continuously references the present value of the PV power *P(k)* against the valued obtained earlier, *P(k-1)*.

Controller sensing of the PV voltage and PV current restarts if the value is unchanged, whereas slope complementing occurs if *P(k)* exceeds *P(k-1)*. Furthermore, there is continuous change in the power converter switching duty cycle until the operating power fluctuates around the MPP [152, 160, 167].

On the upside, the HC algorithm is easy to implement, but on the downside, it is incapable of MPP tracking when environmental conditions change fast. Mitigating this weakness has been the focus of many studies. In [168] , a modified adaptive HC MPPT approach was proposed, encompassing both an automatic parameter for system tuning and control mode switching to enable algorithm implementation under different environmental conditions. Meanwhile, in [169], a digital HC approach integrated with bidirectional current mode power cell for space application was developed, revealing the MPPT had great potential for extracting the highest amount of power from PV arrays. Figure 2.25 illustrates the flow chart associated with the HC algorithm.

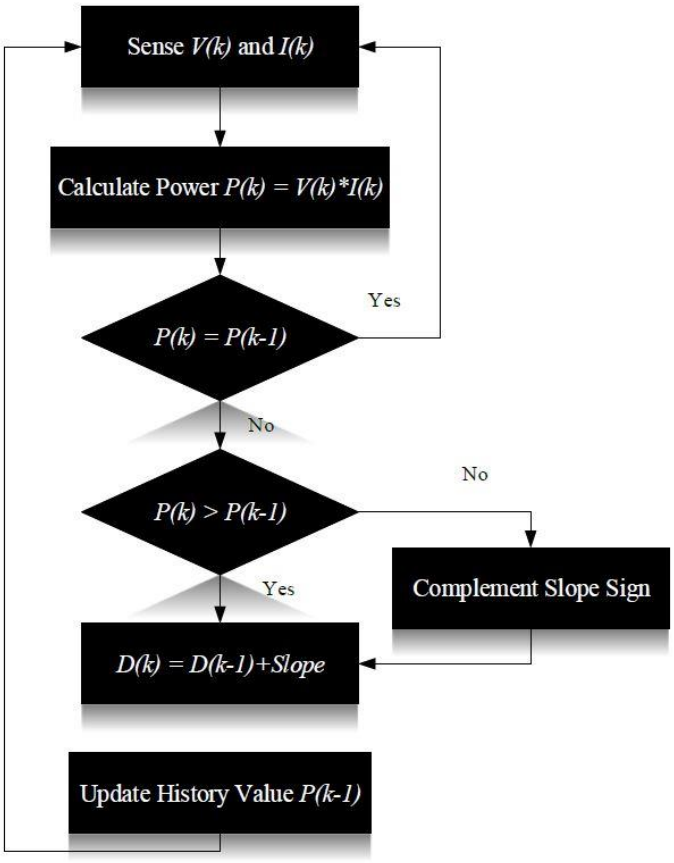

Figure 2.25: The Hill Climbing MPPT Algorithm flowchart.

2.6.1.15 Open-Circuit Voltage and Short-Circuit Current

The A streamlined method for offline (stand-alone) application was proposed in [151], namely, the open-circuit voltage V_{OC} MPPT algorithm. It is based on a more or less linear correlation between V_{OC} and the maximum output voltage (VMPP) of a PV array under fluctuating environmental conditions. This correlation is expressed as:

$$V_{MPP} \approx kV_{OC} \tag{2.28}$$

In the above, the constant k fluctuates in the range 0.7-0.8, according to the features of PV cells. The *k* value is assessed under variable environmental conditions, after which V_{MPP} and V_{OC} are used for its empirical computation.

The PV array load is shed to enable V_{OC} measurement, enabling estimation of V_{MPP}. This algorithm is straightforward to apply, but on the downside, the PV array functioning at the MPP is not very accurate because Equation 2.28 is merely an estimation. Another limitation is that the regular load shedding may disrupt the circuit operation.

Functioning similarly to the open-circuit voltage method, the short-circuit current method is a streamlined offline approach as well [151]. The equation below reflects the nearly linear correlation between the short-circuit current I_{SC} and the current at the MPP, I_{MPP}:

$$I_{MPP} \approx kI_{SC} \tag{2.29}$$

In the above, the constant (k) typically has a value between 0.8 and 0.9. Load shedding is necessary for I_{SC} measurement, as in the case of the V_{OC} approach. Subsequently, it is possible to determine I_{MPP}. Although it has greater precision than the V_{OC} approach, the short-circuit method is expensive to implement.

2.6.1.16 Ripple Correlation Control (RCC)

PV array voltage and current are subject to a ripple effect as the power converter switching action induces power ripple output. The MPP can be tracked based on the ripple effect. The time-varying power $\dot{P}$ has a value of zero at the MPP, so it is applied together with the time-varying current $\dot{I}$ or voltage V to determine the maximum power [170-172]. This is achieved through the equations:

$$d(t) = -k_2 \int \frac{\dot{P}}{\dot{I}} dt \qquad \text{or} \qquad d(t) = -k_2 \int \dot{P} V dt \tag{2.30}$$

In [173] the effect of output power decrease in the PV system was avoided by incorporating an MPPT control in a passive ripple cancelling circuit (PRCC) to extract

the greatest amount of power. By contrast to a non-RCC standard system, the suggested approach was 7% more efficient at 97.8%. In a different study, an MPPT of high speed and accuracy was created based on digital dithering [174], which was 2% more efficient compared to P&O without dithering at 99.8%. In [175], MPP identification was achieved through current-based ripple orientation with ongoing phase difference detection. MPPT based on current ripple searches for the power point by relying on hysteresis contour occurrence, with the MPP being attained through phase difference identification. Unlike the traditional RCC approach, this method possesses a rapid convergence time of around 100 ms [170]. Efficiency exceeding 99% and convergence time within 0.1 s were achieved through application of MPP tracking with extremum-seeking (ES) controller and inverter ripple as current and power input via high pass filters.

In [176] the suggested approach took advantage of RCC application in discrete-time domain, thus simplifying it to a basic sampling problem for MPPT, with 98.3% tracking precision and 1-kHz update rate. In another study, MPPT was managed under fast changes in environmental conditions by applying RCC and model reference adaptive control [177]. Meanwhile, the MPPT strategy adopted in within a PV system involved integration of RCC and extremum seeking control. Performance at both transient and steady state can be effectively enhanced via the two control methods on their own, so their joint use achieved even greater efficiency of up to 99.4%.

2.6.1.17 Different MPPT Techniques Comparison

The selection of optimal MPPT must take into account how complex its design is in order for the PV system to capture maximal solar energy, the precision of the calculation estimation of the algorithm regarding the detection of the real MPP or local peaks is critical to MPPT efficiency and complexity. Furthermore, users' capability to

manage the MPPT influences its application, with some users being able to manage analogue circuits and other digital circuits. However, software and computer programming are necessary for most stochastic-based MPPT algorithms due to the digital nature of their implementation.

The occurrence of partial shading is likely due to the lack of predictability of solar irradiance. As a result, several peaks may form on the P-V curve, directly impacting how efficiently the PV system can perform tracking. Whereas traditional MPPT algorithms cannot track the real MPP, stochastic-based MPPT algorithms can track the global peak across a number of local peaks. From this perspective, the greatest efficiency is demonstrated by the PSO and DE. Still, an extra driver is needed by the ANN and FLC algorithms so that the highest amount of power can be derived from the system by the controller.

For certain applications, particularly commercialisation, the matter of cost must be taken into account. The number of system sensors, design sophistication, and the nature of the system (i.e. analogue or digital) is among the determinants of MPPT cost. Compared to voltage sensors, current sensors are significantly more expensive, which is why the cost of the system depends on how many and what kind of sensors are used. Furthermore, the cost of implementation hinges on the hardware employed for MPPT control as well, and the capital cost of the system depends on the type of algorithm selected. Additionally, digital circuits rely on computer programming, so they are costlier than analogue circuits.

For an MPPT algorithm to be considered effective, it has to display sufficient sensitivity to fluctuations in environmental conditions. It has to be capable of rapid reaction and tracking of the MPP of a given PV system, regardless of conditions, such

as homogeneous solar irradiance or partial shading. The capability of automatic updating of PV system optimum power in response to modifications in solar irradiance and ambient temperature is demonstrated by the PSO and DE algorithms. Thus, a highly sensitive MPPT algorithm ought to rapidly accomplish convergence to the specified operating voltage and current, independent of how progressively or abruptly environmental conditions change. Convergence to the real MPP is achieved faster by stochastic methods than traditional MPPT methods. Furthermore, tracking can be undertaken by stochastic methods with little or insignificant fluctuation. Thus, to prevent energy losses, the convergence speed and tracking efficiency of the MPPT algorithm must be taken into account in the context of PV system design. An overview of the MPPT algorithms for PV systems discussed above is provided in Table 2.6 and Table 2.7.

Table 2.6: Characteristics of a stochastic algorithm and artificial intelligence focused on MPPT techniques.

Criteria	*PSO*	*ELC*	*DE*	*GA*	*ANN*
PV array dependent	×	×	×	×	×
Convergence speed	FAST	MODERATE/LOW	FAST	FAST	MODERATE/LOW
Periodic tuning	×	√	×	×	√
Voltage and/or current sensing	√	√	√	√	√
Complexity	SIMPLE	COMPLICATED	SIMPLE	SIMPLE	COMPLICATED
Analog/digital	DIGITAL	DIGITAL	DIGITAL	DIGITAL	DIGITAL
Ability to track true maxima	√	Poor performance in tracking	√	√	Poor performance in tracking

Initial parameter requirement	√	√	√	√	√
Sensitivity	HIGH	MODERATE	HIGH	MODERATE	MODERATE

Table 2.7: The attributes of standard MPPT techniques.

Criteria	*P&O*	*HC*	*RCC*	*Voc*	*Isc*	*INC*
PV array dependent	×	×	×	√	√	√
Convergence speed	VARIES	VARIES	FAST	MEDIUM	MEDIUM	VARIES
Periodic tuning	×	×	×	√	√	×
Sensed parameters	Voltage and Current	Voltage and Current	√	Voltage	Current	Voltage and Current
Complexity	LOW	LOW	LOW	LOW	MEDIUM	MEDIUM
Analog/digital	BOTH	BOTH	ANALOG	BOTH	BOTH	DIGITAL
Ability to track true maxima	√	√	√	×	×	√
Sensitivity	MODERATE	MODERATE	MODERATE	LOW	LOW	MODERATE

2.7 Array Topologies

In general, a PV system is made of a multitude of cells clustered into a module. In turn, a PV panel is created from clustering of modules, and a PV array consists of a set of PV panels [178]. In series or parallel are the two possible types of connections that can exist between those components, and they are geared towards maximising PV system output power. A graphic representation of this is provided in Figure 2.26.

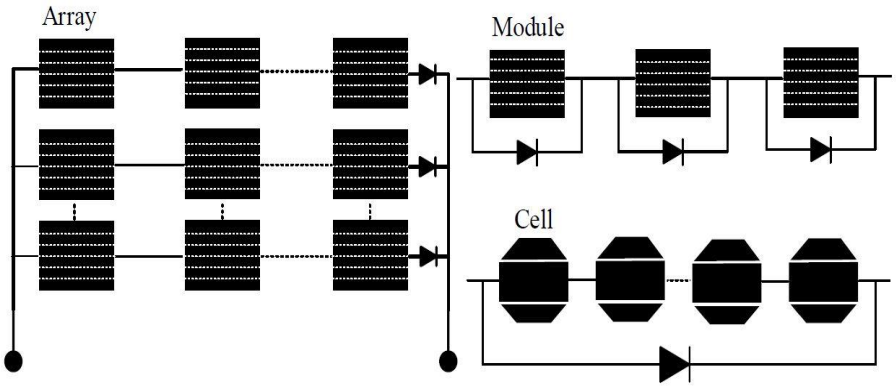

Figure 2.26: The definition of PV array, panel, and module.

The empirical work conducted in [179] demonstrated that implementing appropriate PV module configurations according to a given setting was important for achieving enhanced power production at PV module output. Open-circuit voltage and short-circuit current are respectively increased by in series and parallel connection of the PV modules. Therefore, different configurations are adopted in PV systems to attain voltage and current target levels [180]. Furthermore, ties linked amongst the PV module strings (Figure 2.27), Total Cross Tied (TCT), Bridge-Link Interconnection (BLI), and Honey-Comb (HC) are often referred to as cross-tie configurations. Table 2.3 provides an overview of the weaknesses and strengths of the different configurations in Table 2.8.

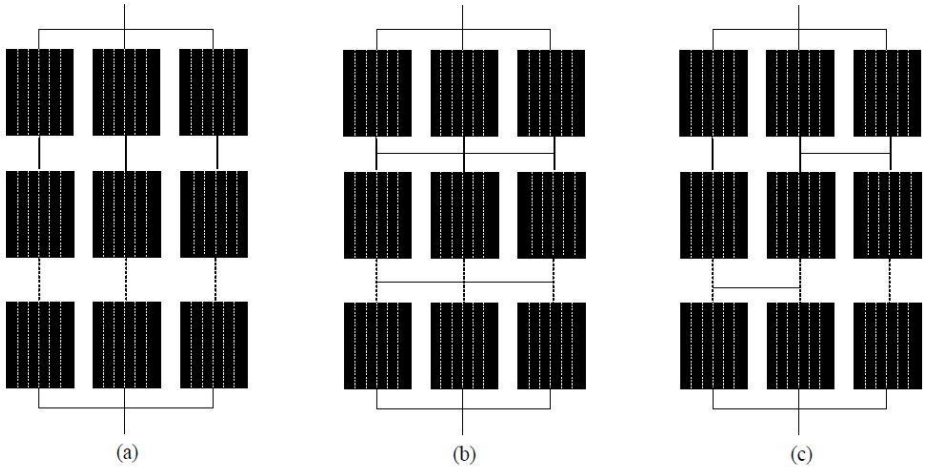

Figure 2.27: Different connection patterns from modules in the array. (a) Series-Parallel (SP), (b) Total Cross Tied (TCT) and (c) Bridge-Link Interconnection (BLI).

Table 2.8: Summary of advantages and restrictions of different configurations.

Configurations	*Restrictions*	*Advantages*
Simple-Series (SS)	• Current is too low • Voltage is too high • Very low maximum output during partial shading • Very prone to mismatch losses	• Simple to connect • Quite vulnerable to issues with aging • Minimum amount of cables
Parallel (P)	• Voltage is too low • Current is too high • Not usually used in the PV application	• Simple to connect • High power output and low mismatch loss • Normally, the power peak is just one
Series-Parallel (SP)	• More impact multi-peak • In most cases, low maximum power compared to cross binding configurations	• One of the most common PV modules configurations • Performs better than TCT when shaded row-wise • Aware of issues with aging
Bridge-Linked-Interconnection (BLI)	• Extreme redundancy • High wiring loss • In partial shading, lower maximum power than TCT	• Responds and adapts well to random patterns of shading • Has high maximum power during the condition of unshaded • Slightly longer service life than TCT • Higher maximum power when unshaded than TCT
Total-Cross-Tied (TCT)	• Extreme redundancy • High wiring loss • A lot of ties. • Needs an unrealistic number of switches and sensors	• Point of smooth inflexion • Multi-peak effect less • In the majority of situations, high maximum power

	• Low output in the reverse situation	• The broad lifetime of operations • Efficient fault tolerance
Honey-Comb (HC)	• High wiring loss • Extreme redundancy • In most cases, the maximum power is slightly lower than (TCT)	• A smooth point of inflexion • Less multi-peak effect • Better performance than TCT when an array is organized asymmetrically • Better than TCT results during row-wise shading

2.7.1.1 Simple-Series Connection (SS)

The basic configuration without any cross ties amongst neighbouring columns is connected to PV modules in a series string, with the output taken over the two ends. This kind of connection is advantageous because it is simple, so it does not need a significant amount of wiring, thereby curtailing wire losses [181]. By contrast to wire losses, the mismatch losses taking place during partial shade conditions can be substantial in the SP configuration. Compared to SS, cross-ties configurations provided a different current flow path under shading conditions, so they perform better [182]. The simulations conducted in [183] revealed that SS demonstrated the poorest performance regarding power loss and power output under the majority of partial shade conditions. Additionally, the SS configuration was associated with a suboptimal current level but a high level of voltage. Meanwhile, in [184], it was observed that the SS configuration displayed extreme sensitivity to aging-related decrease in power generation, but the in-parallel configuration can overcome this issue.

2.7.1.2 Parallel Connection (P)

Among the most basic PV module configurations, the P configuration involves the parallel connection between the PV modules, with a single module per string and the output being taken parallel over the entirety of linked modules. In this configuration, PV modules are not significantly impacted by partial shading [185]. Furthermore, one study has reported that, regardless of partial shading conditions, the

P configuration generated maximum power at MPP [183]. Moreover, the power loss is measured based on the MPP discrepancy under conditions without shade and with partial shade. Therefore, the P configuration is associated with minimal relative power loss. In the context of partial shading, a single power peak is exhibited by the P-V curve of PV modules with P configuration. This is conducive to MPPT and makes PV modules easy to operate at the MPP. On the downside, the high current and low voltage associated with the P configuration are impractical for PV module application. Furthermore, the shading pattern is not the same in SS and P configurations in [186], it was found that, concerning the output power, the performance of the P configuration was superior to that of the SS configuration. Still, the extremely high current in the output that was displayed by the P configuration required changes and a different configuration. Thus, to overcome the limitations of the SS and P configurations, the series-parallel (SP) configuration was developed.

2.7.1.3 Series-Parallel Connection (SP)

PV modules often display an SP configuration, being linked to one another in a series string to attain the target voltage level, and, in turn, the strings connected in series adopt a parallel configuration to attain the target level of current. The output is measured parallel over the PV module strings. In terms of output performance, the SP configuration is typically considered less efficient than the cross-ties configuration [187]. To give an example, one study investigated the TCT mathematical model and revealed that SP was associated with greater losses due to partial shading than TCT [188]. The performance of TCT may be better than that of SP in the majority of instances, yet in terms of row-wise shading pattern, SP performance can surpass TCT performance [189]. Moreover, SP exhibits higher power output, and the P-V curve shows just one power peak during row-wise shading.

The SP performance is usually poorer than that of other configurations due to the fact that SP possesses more series string, so it presents greater proclivity towards mismatch losses [190]. In [191] , an examination was conducted of two SP connected arrays of PV modules with identical array size yet a distinct number of rows and columns. It was found that greater wiring loss caused the MPP associated with the 3×4 configuration to be slightly lower than the MPP associated with the 6×2 configuration. However, under partial shading conditions, the 3×4 configuration demonstrated better efficiency, maximum power peak, fill factor, and a number of power peaks than the 6×2 configuration. Thus, it was deduced that the ideal situation was having a lower number of modules with SS configuration and a higher number of modules with P configuration. Therefore, the achievement of output power is not favoured by a series string in SP of excessive length.

2.7.1.4 Bridge-Linked-Interconnection (BLI)

An array of 4×3 PV modules with the configuration of bridge-linked-interconnection (BLI) is shown in Figure 2.27. The connection of every four modules to one another resembles a rectifier bridge, with SS configuration for the initial two modules and P configuration for the last two modules. Compared to TCT, BLI has a service life that is a bit longer and is not as prone to electrical mismatch loss [192, 193]. One study demonstrated that, by contrast to SP and TCT, BLI was associated with the highest MPP under conditions without shade [194].

However, analysis of the maximum power output in the context of the ladder and column-wise shading pattern revealed that BLI had only the second-best performance compared to SP and TCT [195]. , being intermediate between the other two configurations [190]. More specifically, under conditions of row-wise shading, SP performance may be higher than that of TCT, whereas TCT performance is superior

in the majority of other circumstances. Meanwhile, under conditions of partial shade, BLI performance is average amongst SP and TCT.

2.7.1.5 Total-Cross-Tied Connection (TCT)

A 4×3 array with PV modules in total-cross-tied (TCT) connection is illustrated in Figure 2.27. The formation of the TCT configuration involves SP linkage of the entirety of nodes of the rows, given rising to asymmetrical connection resembling a matrix. The sum of the current at different junctions and voltage at all nodes is the same. One study proposed that the bypass diode is more unlikely to be switched on. The higher the number of interconnections in the configuration is [190] , leading to fewer mismatch losses and minimising the multi-peak effect.

A feature of the TCT is the interlinking between all modules in every string. By contrast, the BLI configuration is associated with fewer cable losses and faster wiring during implementation because its wiring is half that of TCT. In turn, the reduced cable losses enable BLI to outperform TCT by a bit in output power under conditions without shade. However, in the majority of circumstances with partial shading, TCT has a higher performance than BLI. Furthermore, by comparison to the SP configuration, TCT possesses a greater number of parallel circuits, and its cross-ties afford an almost twofold increase in PV module use life [192]. Shadow effects and manufacturer's tolerances in the properties of cells make TCT more permissive to flaws compared to BLI [196]. On the other hand, the latter has better resistance to electrical mismatch loss [193]. Furthermore, as reported in [197], in the TCT configuration, PV module features display several power peaks under row-wise shading and mainly just one peak under column-wise shading. Hence, under row-wise shading, SP performance may surpass TCT performance. Nevertheless, the higher number of cross-ties in TCT maximising the use of arrays explains why this

configuration achieves superior performance in the majority of cases [182]. Additionally, under partial shading, the MPP voltage interval fluctuates to a lesser degree in TCT. Dc-dc or dc-ac power converters have an MPPT window restricted to a particular range, which explains the high importance of the voltage fluctuation interval [198].

Page limitations prevent the referencing of further comparable studies but lower importance. PV modules are increasingly configured as TCT since this helps to counteract the effect of partial shading. However, this configuration has become highly complex due to its numerous cross-ties. The non-linear features make the mathematical solution of the system more time-consuming and computationally burdensome [199]. Furthermore, there is evidence that an unfeasible number of switches and sensors would be necessary to dynamically reconfigure TCT via power electronics, despite the potential for attaining exceptional output performance [200]. Despite this, research findings, such as those of [187], support the implementation of TCT under real-world environmental conditions with complicated and variable shading pattern because the configuration can effectively adjust to arbitrary patterns of shading as far as output performance is concerned.

2.7.1.6 Honey-Comb Connection (HC)

As a modified form of the 4×3 BLI configuration (Figure 2.27), the HC configuration is considered to merge the advantages of BLI and TCT [201]. Under the circumstances with asymmetrical array layout and connection or when more columns are getting the same amount of sunlight than rows, HC may have superior performance to TCT [202]. Nevertheless, due to its greater number of internal links that afford more current paths and hinder a decrease in current in the branches, the TCT configuration continues to have a better performance than HC in the majority of instances. Therefore,

both the total current output and the output power are higher. It can be thus said that, in terms of performance, HC sits between BLI and TCT. Additional simulation-based research has to be conducted to gain more insight into the HC configuration as, so far, it has not been extensively studied.

2.8 The Motives for Using (SP) Reconfiguration

TCT and SP module interconnections have been the basis of most proposals for interconnection topologies that have been extended [203]. PV power plants often adopt an SP configuration, which is underpinned by strings of interconnected PV modules. This setting enables the provision of the voltage needed by the inverter, which has a P configuration to increase the total current as much as possible. As regards the TCT configuration, the PV modules are connected in parallel at first, which allows summation of currents and constancy of voltages. Meanwhile, an in-series configuration is displayed by a few module rows. The power produced by the TCT and SP configurations is nearly the same when conditions do not fluctuate, whereas TCT usually demonstrates a better energy performance than SP when conditions fluctuate [204].

The required number of sensors and switches and the level of complexity of the algorithms applied for reconfiguration underscore an important aspect that has to be taken into account in relation to PV structures amenable to reconfiguration (section 2.5). An unfeasible number of switches and sensors is necessary for the majority of TCT-based reconfiguration approaches, which is a particularly notable matter [203]. To give an example, a switching matrix with Number of Photovoltaic Modules (NPV2) double-pole switches and NPV single-pole switches, with N denoting the PV module number, was devised in [204]. This type of switching matrix is compatible with all

configurations between the two limits of a configuration with parallel connection of all modules (each module per single row) and a configuration with series connection of all modules (one module per every row). Hence, 600 switches would be required for a system with 24 PV modules. In a different instance, 1152 switches (2 · NPV2) were needed for the switch structure formulated in [205], and control algorithms of fair complexity are essential for most TCT-based methods of reconfiguration.

The purpose of algorithms is to determine the point for turning switches on or off, but their efficiency may depend on an inordinately dense computation process [203]. In [204], another study addressed the possibility of occurrence of a number of overall configurations of *(NPV * NPV)!/(NPV!)NPV* and, based on earlier expression results in an overflow derived from MATLAB, it was concluded that NPV had to be equal to 24. Practically, however, the control of TCT arrays available on the market is not straightforward, effective, and efficient. The examination of the existing evidence in the present work has led to the conclusion that the only system available on the market for PV array reconfiguration based on SP topology is ENDANA (Bitron) [200]. The reconfiguration of 24 PV modules can be achieved by the basic ENDANA system in two strings. A number of PV modules showing significant signs of aging can be eliminated following assessment of the P-V curve for each PV module and reconfiguration of the links between the modules into two substrings.

Taking into account the previously highlighted considerations, the SP topology is explored in the present work since it allows retrofitting on most current PV fields, in theory. It must also be emphasised that the investigation of PV units is the basis for analysing TCT reconfiguration in the majority of cases. PV cell strings can be employed for a simple representation of the PV units. Furthermore, it is unnecessary to consider the possible occurrence of several maxima in the P-V characteristics of a

number of strings of this type. Under aging phenomenon, a specific bypass diode is used to protect each cell string in PV modules available on the market. Such an approach often gives rise to a number of MPPs. However, the multi-modal nature of P-V curves has been disregarded in the majority of studies focusing on TCT-related reconfiguration algorithms.

Investigation of short-circuit currents constitutes a major research priority as well. Under these circumstances, the present work draws on knowledge of the complete I-V feature of each PV module in order to evaluate a reconfiguration algorithm for PV modules available on the market with SP connection. By adopting such an approach, it is possible to effectively manage the multiple MPPs that unavoidably emerge in the P-V features of a number of PV modules.

A comparative analysis between SP and other configurations (see Section 2.8) in terms of performance is not the goal of this work. Instead, the work is concerned with devising a method of SP reconfiguration compatible with PV systems displaying flaws or aging, relocating the PV modules in order to enhance the maximum power output of the PV array. More to the point, the formulated algorithm has to rapidly identify the best configuration and achieve its implementation in polynomial time.

2.9 Challenges

PV cells and modules can deteriorate through a range of processes. Although they are manufactured from different materials and in different ways, PV cells and modules generate energy in a similar manner. To capture energy, PV modules necessitate an expansive surface, which is why ample attention is paid to the matters of soiling and snow deposition. The latter is a particularly serious mechanism of deterioration in regions with low temperatures because it generates mechanical loads

on PV panels that can lead to crack formation and moisture seepage, which in turn give rise to corrosion and damage. Meanwhile, crack formation induced by mechanical loads within PV cells can cause hot spots and severe power losses by disrupting connections. Corrosion can have a massive impact on PV materials of an organic nature, but the problem has not been extensively researched, so it remains inconclusive. Further knowledge is needed about the effect of PV material type on potential defects and about the correlation between PV content and deterioration mechanisms.

It is worth investigating and taking preventive measures against transient deterioration processes (e.g. sudden cracks, periodic soiling and snow aggregation) to mitigate long-term deterioration and corrosion into which those processes usually degenerate. Hence, it is necessary to explore the environmental factors impacting PV modules regarding how they occur and how they can be avoided. It is essential to prolong system use life and make it more profitable.

A range of methods is available for detecting, preventing, and tackling processes of PV energy deterioration. Condition Monitoring System (CMS) and non-destructive testing permit the identification of the majority of such processes [206, 207]. Since system thermal fluctuations are a frequent corollary of faults, thermography is among the foremost mitigation methods. It enables solar plants to be rapidly and automatically investigated when deployed alongside UAVs and image processing. Defect type and the site can be derived from I-V and P-V curves as well, while maintenance can be made less time-consuming and more cost-effective by using methods of data processing.

Due to unfavourable environmental conditions (e.g. temperature, dust, snow, hot spots, storms), PV modules inevitably age non-uniformly. As a result, PV plants

start performing at lower efficiency, especially during the middle and later period of their useful life. Therefore, the present work aims to make the maintenance of PV power plants, regardless of size, more cost-effective by enhancing PV power efficiency.

Chapter 3. PV ARRAY RECONFIGURATION SORTS CALCULATIONS REPETITIVELY AND HIERARCHICALLY ALSO ALGORITHM APPROACH TO OPTIMISING POWER GENERATION ACROSS NON-UNIFORMLY AGED PV ARRAYS BY MERELY REPOSITIONING.

The content of this chapter has been published in the following papers:

1. Alkahtani, M.; Wu, Z.; Kuka, C.S.; Alahammad, M.S.; Ni, K. A Novel PV Array Reconfiguration Algorithm Approach to Optimising Power Generation across Non-uniformly Aged PV Arrays by merely Repositioning. *J.—Multidiscip*. Sci. J. 2020, 3, 32–53.
2. Alkahtani, M.; Hu, Y.; Wu, Z.; Kuka, C.S.; Alhammad, M.S.; Zhang, C. Gene Evaluation Algorithm for Reconfiguration of Medium and Large Size Photovoltaic Arrays Exhibiting Non-Uniform Aging. Energies 2020, 13, 1921.

3.1 Introduction

The new emphasis on clean energy has led to a growing interest in photovoltaic (PV) power production. To afford competitiveness to this new method of generating power, it must be made more energy-efficient and cost-effective. With numerous applications in producing and transporting power and in mobile appliances, PV systems are embraced evermore. It is anticipated that, by 2020, renewable sources will satisfy 20% of European energy demand [208, 209]. In this context, PV plant-related financial and maintenance issues call for more efficient solar energy conversion and prolonging the useful life of PV arrays [210].

The multitude of options requiring consideration to establish the best solution is the main obstacle that must be overcome for PV array rearrangement. Researchers have proposed different approaches in this regard. One approach proven to be suitable for sorting methods is determining PV array rearrangement based on a genetic algorithm (GA) [211]. Meanwhile, other rearrangement approaches are geared towards enhancing power yield in settings with shade [212]. However, by prioritising the methods of array construction, [212] failed to implement real-time executable control algorithms, which resulted in an unfeasible number of sensors and switches requiring complicated control algorithms to detect on/off switch turning. Unlike the approach put forward in [212], a lower number of voltage or current sensors and switches are necessary for adaptive PV array rearrangement. In [213], an offline rearrangement approach was devised to make aged PV systems more energy efficient by inspecting the possible options for PV module rearrangement based on identifying the maximum power point. Meanwhile, in [208], the ideal arrangement for balancing and attenuating the switches' aging process in the switching matrix was assessed based on the Munkres algorithm [214, 215]. Issues related to restructuring modules in PV arrays of different sizes can be managed via additional approaches proven to be efficient. However, these are computationally too complex and time-consuming because they involve searching every possible manner, in which restructuring can be achieved [216].

In order to achieve quick calculation with low computing resources, this chapter proposed theoretically that sorts calculations PV modules repetitively and hierarchically and practical that optimise problems based on a gene evaluation algorithm for medium and large PV arrays exhibiting non-uniform aging. Therefore, the strategy offers the minimum swapping/replacing times to maximize the output

power and improve electric revenue by reducing maintenance costs. However, solar power plants can achieve better financial increments within a decade.

3.2 The Non-Uniformly Aged Cell Terminal

The short-circuit current fluctuates more widely compared to the open-circuit voltage caused by the *p-n* junction features of the PV cell as the latter ages according to the author [217]. This work evaluates the PV module aging status based on the short-circuit current, while maintaining the open-circuit voltage unchanged for different aging conditions. In the case of *m* PV modules with in-series connection making up a PV array, their output currents will be the same, while the total module voltages will be added up to obtain the output voltage [218].

$$I_{total(string)} = I_{module(1)} = I_{module(2)} = I_{module(3)} = \cdots = I_{module(m)} \tag{3.1}$$

$$V_{total(string)} = \sum_{\tau}^{m} = 1\left[V_{module(1)} + V_{module(2)} + V_{module(3)} + V_{module(m)}\right] \tag{3.2}$$

The modules must be the same for equation (3.1) and equation (3.2) to be applicable. As shown in Figure 3.1, in the best scenario, the behaviour of the modules does not differ, and the voltage is continuously at 63 V in the case of three modules. Likewise, the short-circuit current going through PV modules with in-series linking is always at 3.55 A, because the modules are similar (Figure 3.1).

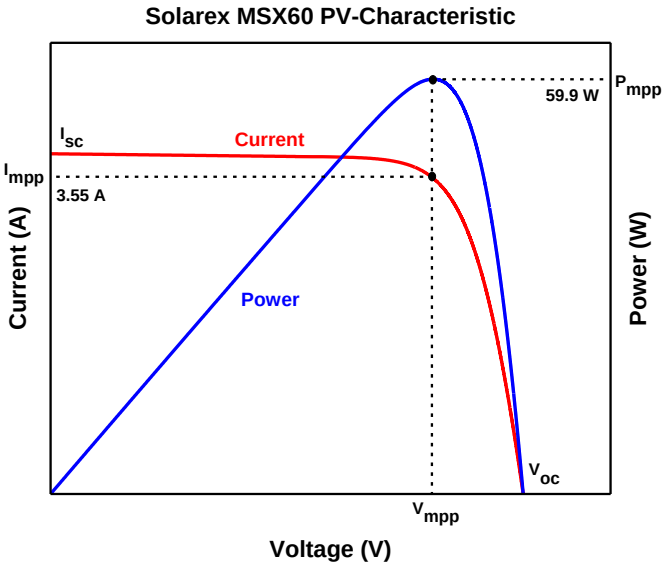

Figure 3.1: Simulation responses: I-V curve and P-V curve (at standard test conditions) for good quality modules of Solarex MSX60 connected in series.

Due to the non-uniform aging conditions, multiple PV power output steps and peaks observed in

Figure 3.2 divides PV array operation into three different operational levels, where each peak relates to a particular level. Level 1 indicates a phase where module 1 is active, while the currents across modules 2 and 3 are being bypassed through the diodes. At Level 1, the current ranges between 0 A and 3.45 A, and the corresponding voltage is 0–22 V. Similarly, level 2 corresponds to the phase where module 1 and module 2 are active, while module 3 is being bypassed.

The current for the un-bypassed series-connection is determined by the current of the most aged PV module (in this case, module 2). The level 2 current ranges between 0 A and 2.30 A, with a corresponding voltage of 0–42 V. Level 3 represents the stage where modules are active, i.e. none are bypassed. Again here, the current for the un-bypassed series connection is determined by the current of the most aged PV module (i.e. module 3). The current at level 3 ranges between 0 A and 1.5 A, with a

corresponding voltage of 0–82 V. Moreover, there are many maximum power points expressed by the knee points for the various levels in the characteristic I–V curve. These knee points are correlated with particular currents and voltages that are utilised to derive the maximum power points at various locations on the P–V curve. The knee point at Level 1 arrives at 16.79 V and 3.45 A (54.42 W); the knee point at Level 2 is at 35.69 V, and 2.30 A (65.45 W); whilst the knee point at Level 3 is at 54.9 V and 1.5 A (60.61 W), as depicted in Figure 3.2. The knee point at Level 2 indicates the global maximum power point (GMPP). The knee point at Level 1 tasks at 16.79 V and 3.45 A (54.42 W); The knee point at Level 2 tasks at 35.69 V and 2.30 A (65.45 W); whilst

the knee point at Level 3 tasks at 54.9 V and 1.5 A (60.61 W), as depicted in Figure 3.2 The knee point at Level 2 indicates the global maximum power point (GMPP).

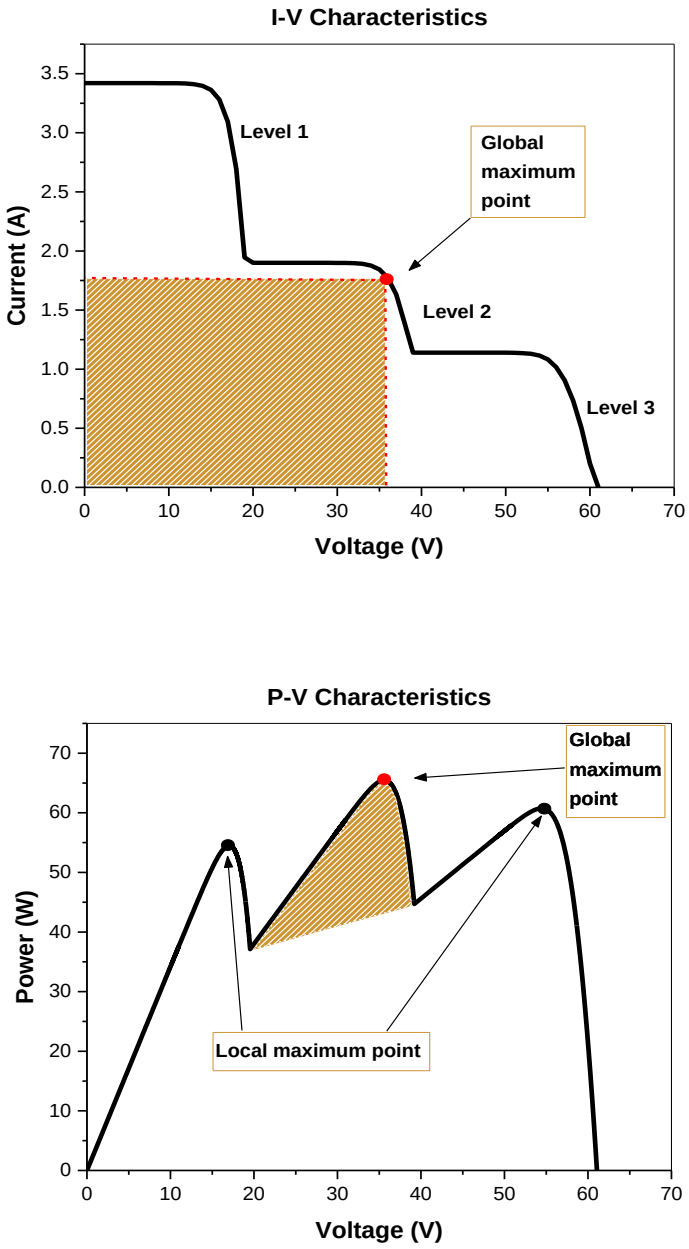

Figure 3.2: Series-connection of PV modules.

3.3 PV Array Reconfiguration Scheme

In an $N \times M$ PV array, N and M respectively denote the strings with in-parallel linking and the PV modules with in-series linking as shown in Figure 3.3. The number

of active modules for a string voltage is given by the voltage at which the PV array GMPP is found in the P-V curve. Therefore, by adding up all the string currents and multiplying that figure by the string voltage of the active modules, the PV array maximum power can be obtained.

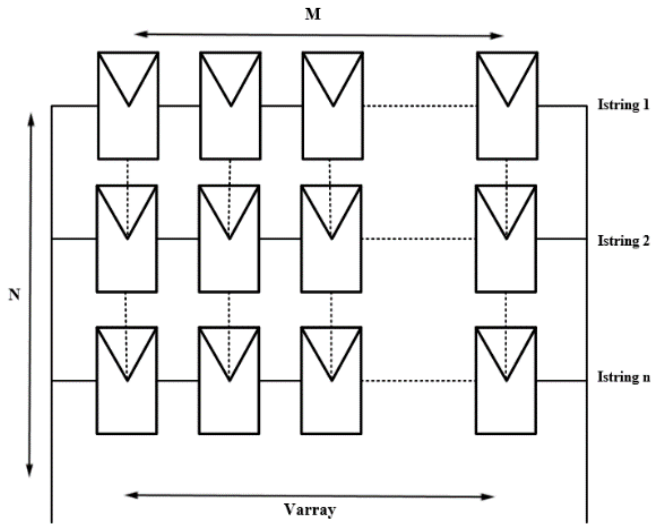

Figure 3.3: A series-parallel (SP) PV array involving N×M (number of parallel-connected strings × number of series-connected PV modules).

A PV array comprising 12 aged modules connected in a 4×3 PV array SP configuration (as depicted in Figure 3.4 will be utilised to demonstrate this concept.

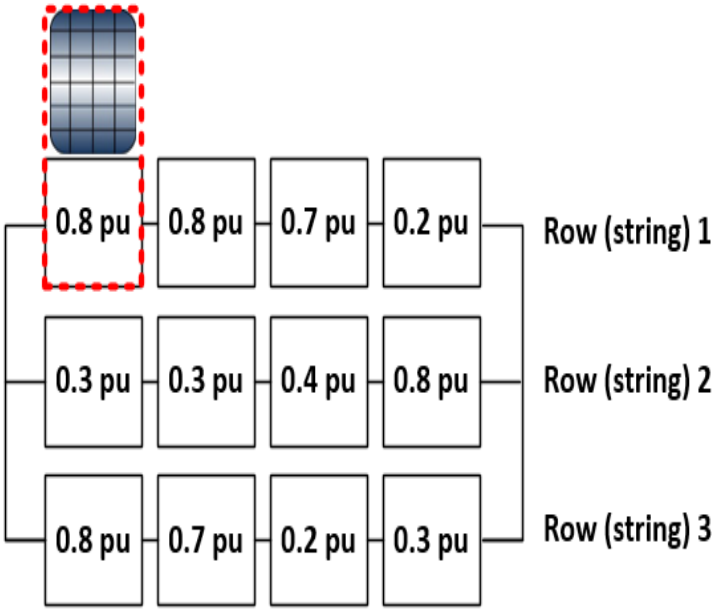

Figure 3.4: A 4 × 3 PV array SP configuration with non-uniform aging.

3.4 Sorts Calculations PV modules Repetitively and Hierarchically

By applying the rearrangement algorithm to then *N-M* PV array, the totality of potential rearrangements is:

$$\left(N(M)/M\right)\left(N(M-M)/M\right)\left(N(M-2)/M\right)\ldots\left(2(M)/M\right)\left(M/M\right)/N\iota \qquad (3.3)$$

Every potential combination of repositioned PV module must be determined, and the maximum power must be computed for the above array. To attain the best arrangement in several repetitive steps, the suggested sorts calculations PV modules repetitively and hierarchically, with the employed variation parameter being the aging scale or coefficient because of its direct correlation to the short-circuit current of every separate PV module. Five modules representing different levels of solar irradiance:

- Module 1: solar irradiance 200 W/m^2 and temperature $25^{\circ}C$
- Module 2: solar irradiance 400 W/m^2 and temperature $25^{\circ}C$
- Module 3: solar irradiance 600 W/m^2 and temperature $25^{\circ}C$
- Module 4: solar irradiance 800 W/m^2 and temperature $25^{\circ}C$
- Module 5: solar irradiance 1000 W/m^2 and temperature $25^{\circ}C$

In a suitable module, the STC specifies the short-circuit current to be 1 per unit (pu), which corresponds *1000* W/m^2. The various aging factors (AF) associated with the PV modules are indicated by the digits in the array, is directly correlated with their separate short-circuit current. For instance, the optimisation issue is addressed in the present work based on a genetic algorithm, which is applied to a 4×3 PV array arrangement as seen in Figure 3.4. The AFs take the form of (pu) value of the health condition of separate PV modules and represent the working box variables. The rules suggested for this work are listed below.

- The first rule specifies that equivalence exists between string one working box, string two working box and string n working box. Means that both string two and string n will have three working boxes if the string is associated with three working boxes.
- The second rule specifies that, in a string, the minimal number represents the working box output. Its means that the output is the lowest among all values from high to low.
- $P_{string(n)} = \sum AF$ = Summation of aging factors in a series of connected modules.

A. Pre-arrangement can be mathematically characterised within five steps.

Step 1: Initialize the summation of AFs for each string Pre-arrangement, as follows:

0.8 pu	0.8 pu	0.7 pu	0.2 pu
0.3 pu	0.3 pu	0.4 pu	0.8 pu
0.8 pu	0.7 pu	0.2 pu	0.3 pu

Sum:

$$P_{string1} = 0.8 + 0.8 + 0.7 + 0.2 = 2.5$$
$$P_{string2} = 0.3 + 0.3 + 0.4 + 0.8 = 1.8 \quad (3.4)$$
$$P_{string3} = 0.8 + 0.7 + 0.2 + 0.3 = 2$$

Step 2: Arrange the working boxes of $P_{4(total)}$ Pre-arrangement in descending order, in the case study.
Select the lowest number of $P_{4\ string\ n}$:

0.8 pu	0.8 pu	0.7 pu	0.2 pu
0.3 pu	0.3 pu	0.4 pu	0.8 pu
0.8 pu	0.7 pu	0.2 pu	0.3 pu

$$P_{string1} = 0.2 \times 4 = 0.8$$
$$P_{string2} = 0.3 \times 4 = 1.2 \quad (3.5)$$
$$P_{string3} = 0.2 \times 4 = 0.8$$

Sum:

$$P_{4(total)} = P_{string1} + P_{string2} + P_{string3} = 2.8 \quad (3.6)$$

Step 3: Arrange the working boxes of $P_{3(total)}$ Pre-arrangement in descending order, in the case study.

Select the lowest number of $P_{3\ string\ n}$:

0.8 pu	0.8 pu	0.7 pu	0.2 pu
0. 3 pu	0.3 pu	0.4 pu	0.8 pu
0.8 pu	0.7 pu	0.2 pu	0.3 pu

$$P_{string1} = 0.7 \times 3 = 2.1$$
$$P_{string2} = 0.3 \times 3 = 0.9 \quad (3.7)$$
$$P_{string3} = 0.2 \times 3 = 0.6$$

Sum:

$$P_{3(total)} = P_{string1} + P_{string2} + P_{string3} = 3.6 \tag{3.8}$$

Step 4: Arrange the working boxes of $P_{2(total)}$ Pre-arrangement in descending order.

Select the lowest number of $P_{2\ string\ n}$:

0. 8 pu	0.8 pu	0.7 pu	0.2 pu
0.3 pu	0.3 pu	0.4 pu	0.8 pu
0.8 pu	0.7 pu	0.2 pu	0.3 pu

$$\begin{aligned} P_{string1} &= 0.8 \times 2 = 1.6 \\ P_{string2} &= 0.4 \times 2 = 0.8 \\ P_{string3} &= 0.7 \times 2 = 1.4 \end{aligned} \tag{3.9}$$

Sum:

$$P_{1(total)} = P_{string1} + P_{string2} + P_{string3} = 3.8 \tag{3.10}$$

Step 5: Arrange the working boxes of $P_{1(total)}$ Pre-arrangement in descending order.

Select the lowest number of $P_{1\ string\ n}$:

0. 8 pu	0.8 pu	0.7 pu	0.2 pu
0.3 pu	0.3 pu	0.4 pu	0.8 pu
0.8 pu	0.7 pu	0.2 pu	0.3 pu

$$\begin{aligned} P_{string1} &= 0.8 \\ P_{string2} &= 0.8 \\ P_{string3} &= 0.8 \end{aligned} \tag{3.11}$$

$$P_{1(total)} = P_{string1} + P_{string2} + P_{string3} = 2.4 \tag{3.12}$$

B. The potential PV array arrangements from initial to final string must be identified sequentially. As shown by the equation below, the PV array takes the form of a matrix to facilitate the running of the MATLAB program.

$$N \times M = \begin{bmatrix} 0.8 & 0.8 & 0.7 & 0.2 \\ 0.3 & 0.3 & 0.4 & 0.8 \\ 0.8 & 0.7 & 0.2 & 0.3 \end{bmatrix} \tag{3.13}$$

Figure 3.5 illustrates the flowchart associated $N \times M$ with the rearrangement algorithm for the PV array. The suggested algorithm geared towards mitigating the impact of mismatch losses between the PV modules in a given string by relocating separate PV modules in every string according to their AFs. Due to the direct correlation between aging and the short-circuit current, AFs are the only short-circuit current data needed

by the algorithm. To attain the best arrangement, the algorithm run until every criterion is satisfied in Figure 3.5.

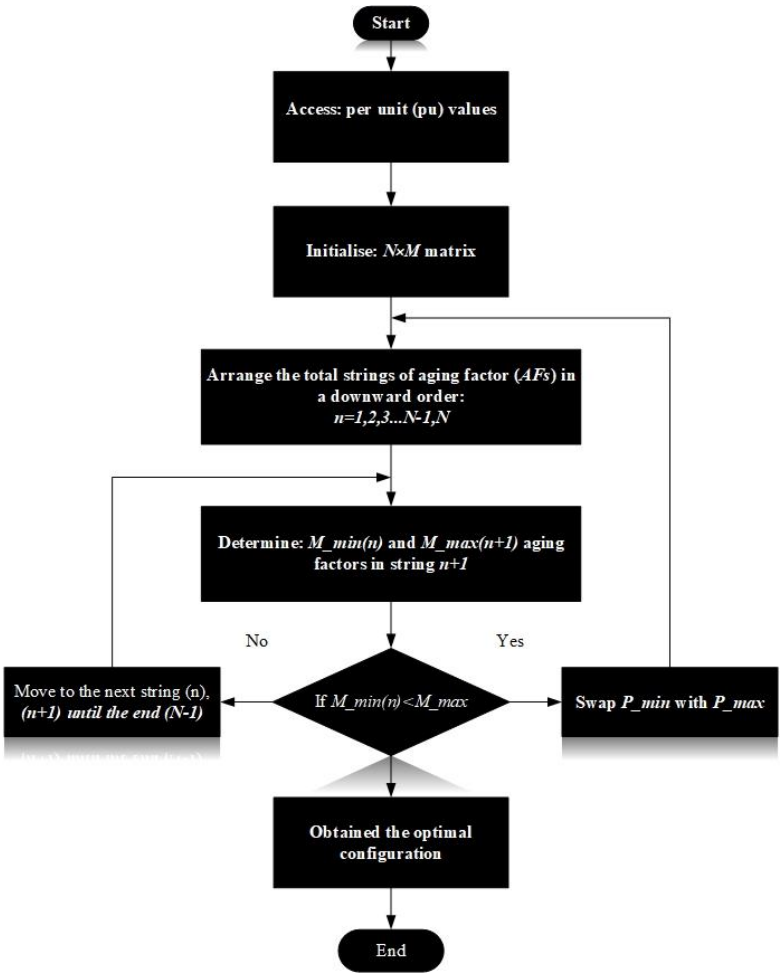

Figure 3.5: Flowchart of PV reconfiguration algorithm process.

Before presenting the five steps of the suggested algorithm, several parameters need to be described to elucidate the rearrangement approach from the previous flowchart.

$n = 1, 2, 3 \ldots N-1, N$, where the number of strings in the PV array called *N*.

- $\sum AF =$ Summation of aging factors in a series of connected modules.
- $M_{string(\min)n}$ = Minimum *AFs* in a series connection for a string (*n*).
- $M_{string(\max)n}$ = Maximum *AFs* in a series connection for a string (*n+1*).
- $P_{string(\min)}$ = Position of PV module with a minimum *AFs* in a series of connected modules.

- $P_{string(\max)n+1}$ = Position of PV module with a maximum *AFs* in a series of connected modules.

Step 1: Initialize the summation of $P_{string(n)} \approx AFs$ for each string and arrange the total string level $P_{string(n)}$ in descending order, in the case study**.**

$$\begin{aligned} P_{string1} &= 0.8+0.8+0.7+0.2 = 2.5 \\ P_{string2} &= 0.3+0.3+0.4+0.8 = 1.8 \\ P_{string3} &= 0.8+0.7+0.2+0.3 = 2 \end{aligned} \tag{3.14}$$

Step 2: Arrange the total string level *AFs* in a downward order in the case study.
Step 3: Determine $M_{\min(n)}$ and $M_{\max(n+1)}$ for $n=1$

0.8 pu	0.8 pu	0.7 pu	0.2 pu
0.3 pu	0.3 pu	0.4 pu	0.8 pu
0.8 pu	0.7 pu	0.2 pu	0.3 pu

Now, if $M_{min\ A} < M_{max\ B}$, then swap P_{min} with P_{max} , repeat steps 1,2 and 3.

where Swap$_1$ is:

0.8 pu	0.8 pu	0.7 pu	0.8 pu
0.3 pu	0.3 pu	0.4 pu	0.2 pu
0.8 pu	0.7 pu	0.2 pu	0.3 pu

Then $P_{string\ (n)}$ become:

$$\begin{aligned} P_{string1} &= 0.8+0.8+0.7+0.8 = 3.1 \\ P_{string2} &= 0.3+0.3+0.4+0.2 = 1.2 \\ P_{string3} &= 0.8+0.7+0.2+0.3 = 2 \end{aligned} \tag{3.15}$$

For Swap$_2$:

0.8 pu	0.8 pu	0.7 pu	0. 8 pu
0.8 pu	0.7 pu	0.2 pu	0.3 pu
0.3 pu	0.3 pu	0.4 pu	0.2 pu

Moreover, $P_{string\ (n)}$ become:

$$P_{string1} = 0.8 + 0.8 + 0.7 + 0.8 = 3.1$$
$$P_{string2} = 0.8 + 0.7 + 0.2 + 0.3 = 2 \quad (3.16)$$
$$P_{string3} = 0.3 + 0.3 + 0.4 + 0.2 = 1.2$$

Step 4: Repeat steps 1, 2 and 3 tills $M_{\min(n)} \geq M_{\max(n+1)}$.

For Swap$_3$

0.8 pu	0.8 pu	0. 7 pu	0.8 pu
0. 8 pu	0.7 pu	0.2 pu	0.3 pu
0.3 pu	0.3 pu	0.4 pu	0.2 pu

Then, the sum of $P_{string(n)}$ from Swap$_3$ are:

$$P_{string1} = 0.8 + 0.8 + 0.7 + 0.8 = 3.1$$
$$P_{string2} = 0.8 + 0.7 + 0.2 + 0.3 = 2 \quad (3.17)$$
$$P_{string3} = 0.3 + 0.3 + 0.4 + 0.2 = 1.2$$

Moreover, Swap$_4$ are:

0.8 pu	0.8 pu	0. 8 pu	0.8 pu
0.7 pu	0.7 pu	0.2 pu	0.3 pu
0.3 pu	0.3 pu	0.4 pu	0.2 pu

Then, the sum of $P_{string(n)}$ from Swap$_4$ are:

$$\begin{aligned} P_{string1} &= 0.8+0.8+0.8+0.8=3.2 \\ P_{string2} &= 0.7+0.7+0.2+0.3=1.9 \\ P_{string3} &= 0.3+0.3+0.4+0.2=1.2 \end{aligned} \tag{3.18}$$

Step 5: Find $M_{\min(n)}$ and $M_{\max(n+1)}$ for $n=2$, swap the corresponding $P_{\min}$ with and $P_{\max}$ repeat steps 1 and 2 until the end (N – 1).

For Swap$_5$:

0.8 pu	0.8 pu	0.8 pu	0.8 pu
0.7 pu	0.7 pu	0.2 pu	0.3 pu
0.3 pu	0.3 pu	0.4 pu	0.2 pu

Then, the final step, the sum of $P_{string(n)}$ in Swap$_5$ are:

$$\begin{aligned} P_{string1} &= 0.8+0.8+0.8+0.8=3.2 \\ P_{string2} &= 0.7+0.7+0.2+0.3=1.9 \\ P_{string3} &= 0.3+0.3+0.4+0.2=1.2 \end{aligned} \tag{3.19}$$

Finally, for Swap$_6$:

0.8 pu	0.8 pu	0.8 pu	0.8 pu
0.7 pu	0.7 pu	0.4 pu	0.3 pu
0.3 pu	0.3 pu	0.2 pu	0.2 pu

Then, the final step, the sum of $P_{string(n)}$ in Swap$_6$ are:

$$\begin{aligned} P_{string1} &= 0.8+0.8+0.8+0.8=3.2 \\ P_{string2} &= 0.7+0.7+0.4+0.3=2.1 \\ P_{string3} &= 0.3+0.3+0.2+0.2=1 \end{aligned} \tag{3.20}$$

According to the final step, the best arrangement exhibited by the PV array on Swap$_6$. Nevertheless, a comparison conducted between every arrangement arriving at every step and the initial arrangement Figure 3.4. Under non-uniform aging conditions, the ideal arrangement was obtained solely through five repetitive steps for a 4×3 PV

array. In the case of a large PV array, execution modelling based on a MATLAB program command as seen below, with the configuration for the best power yield being represented by the enhanced form. Hence, the ideal arrangement for a 4×3 PV array is the PV array Post-arrangement. The PV arrays of Pre-Post arrangements are compared in Table 3.1.

Table 3.1: PV Array Pre-Post rearrangements.

Pre-arrangement			
0.8 pu	0.8 pu	0.7 pu	0.2 pu
0.3 pu	0.3 pu	0.4 pu	0.2 pu
0.8 pu	0.7 pu	0.2 pu	0.3 pu
Post-arrangement			
0.8 pu	0.8 pu	0.8 pu	0.8 pu
0.7 pu	0.7 pu	0.4 pu	0.3 pu
0.3 pu	0.3 pu	0.2 pu	0.2 pu

In Table 3.2, the maximum power and voltage at MPP are set out for all arrangements and the string currents in every case. It is obvious that, from the first to the fifth step, there is a 22.4% rise in the overall output power and the voltage at MPP is greater than the output current. To minimise multiple peaks caused by incompatibility effects (non-uniform aging), the proposed algorithm increases the currents in every string as much as possible through the integration of the PV modules showing similar electrical features.

Table 3.2: Electrical parameters obtained for different reconfiguration.

Steps	V_{mmp} *(V)*	P_{mmp} *(W)*	*Current* I_1 *(A)*	*Current* I_2 *(A)*	*Current* I_3 *(A)*
1	53	254.3	2.531	1.141	1.143
2	70	286.9	2.587	0.759	0.751
3	70	287.1	2.586	0.758	0.751
4	69	297.7	2.798	0.761	0.756
5	68	320.8	2.844	1.142	0.728

3.4.1.1 Simulation Results

PV arrays of different dimensions (e.g. 4 × 3, 8 × 5 and 8 × 7) were assessed to prove that the suggested algorithm was valid. A MATLAB-developed PV array model was used to compute the maximum power outputs from the PV structures pre-arrangement as well as post-arrangement. The computations were conducted with an

Intel® Core™ computer with i3-3220 CPU, 30.30 GHz and 8 GB (RAM), with tabulation of the equivalent computing times for the different PV array dimensions indicated above.

3.4.1.2 Case study on 3 × 4 PV array

Figure 3.4 shows the MATLAB-based validation of the results. Under STC, the maximum short-circuits current in a suitable module established at 1 (pu), which is equivalent to 1000 W/m^2 irradiance at a module temperature of 25°C.

Table 3.1 shows the PV configuration following a rearrangement using the proposed algorithm. Using the PV array data presented in Table 3.2, I-V and P-V curves were then plotted as depicted in Figure 3.6. In Figure 3.6 highlights that the maximum output power pre-arrangement, is 247.4 W, with a PV array output voltage of 51V and a GMPP current of 4.8 A, respectively. The maximum output power post-arrangement is 320.8 W, with a PV array output voltage of 68 V and GMPP current of 4.68 A, respectively. The total power output increases by 29.7% as presented in Figure 3.6 when using the proposed algorithm. The computational time for these rearrangements (as presented in Table 3.3) for an aged 4 × 3 PV array took 0.02 seconds.

Table 3.3: PV array 4 × 3 parameters of Pre-Post arrangements.

PV Array 3 × 4 parameters				
Parameters	*Pre-arrangement*	*Post-arrangement*	*Power Improvement*	*Computing time (s)*
Current I_{mpp}	4.8 A	4.68 A		
Voltage V_{mpp}	51 V	68 V	29.7 %	0.02
Power W_L	247.4 W	320.8 W		

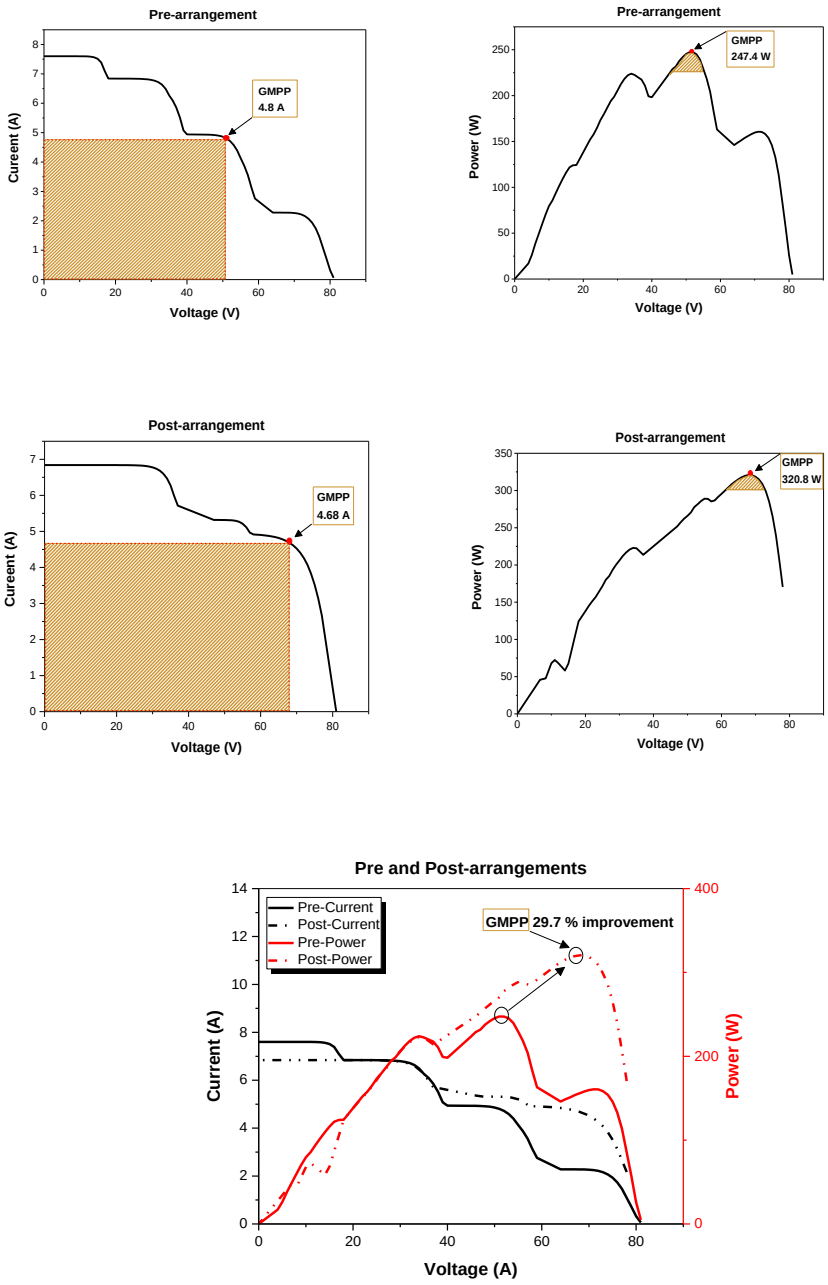

Figure 3.6: The output of the Array (pre-post rearrangements) for case 1.

3.4.1.3 Case study on 5 × 8 PV array

The PV array of dimensions 5×8 consisted of eight strings and five modules with in-parallel and in-series linking, respectively. For the purpose of developing an 5×8 matrix, simulating non-uniform aging PV array pre-arrangement and determine the best PV structure post-arrangement for this particular case, MATLAB (R2018a) employed for arbitrary production of the AFs in the range 0.9-0.6 (pu) in Table 3.4.

The ability of the suggested algorithm to yield the ideal arrangement was confirmed by simulating both PV structures. Figure 3.7 illustrates that the maximum power output pre-arrangement is 1722 W, with a PV array output voltage of 143 V and a GMPP current of 11.9 A, respectively. The maximum power output post-arrangement is 1885 W, with a PV array output voltage of 138 V and a GMPP current of 13.6 A, respectively. The computational time for the proposed algorithm to identify the rearrangements of an aged 8 × 5 PV array as presented in Table 3.5 took 0.25 seconds.

Table 3.4: PV array configuration for case 2.

Pre-rearrangement							
0.9 pu	0.8 pu	0.9 pu	0.9 pu	0.8 pu	0.9 pu	0.9 pu	0.7 pu
0.8 pu	0.9 pu	0.7 pu	0.8 pu	0.9 pu	0.9 pu	0.9 pu	0.8 pu
0.7 pu	0.9 pu	0.8 pu	0.9 pu	0.8 pu	0.7 pu	0.6 pu	0.7 pu
0.8 pu	0.8 pu	0.9 pu	0.7 pu	0.7 pu	0.6 pu	0.7 pu	0.6 pu
0.9 pu	0.7 pu	0.8 pu	0.9 pu	0.9 pu	0.8 pu	0.8 pu	0.6 pu
Post-rearrangement							
0.9 pu	0.9 pu	0.9 pu	0.9 pu	0.9 pu	0.9 pu	0.9 pu	0.9 pu
0.9 pu	0.9 pu	0.9 pu	0.9 pu	0.9 pu	0.9 pu	0.9 pu	0.8 pu
0.8 pu	0.8 pu	0.8 pu	0.8 pu	0.8 pu	0.8 pu	0.8 pu	0.8 pu
0.8 pu	0.8 pu	0.7 pu	0.7 pu	0.7 pu	0.7 pu	0.7 pu	0.7 pu
0.6 pu	0.7 pu	0.7 pu	0.6 pu	0.6 pu	0.7 pu	0.7 pu	0.6 pu

Table 3.5: PV array 5×8 parameters Pre- and Post-arrangement.

PV Array 5 × 8 parameters				
Parameters	*Pre-arrangement*	*Post-arrangement*	*Power Improvement*	*Computing time (s)*
Current I_{mpp}	11.9 A	13.6 A		
Voltage V_{mpp}	143 V	138 V	9.47 %	0.25
Power W_L	1722 W	1885 W		

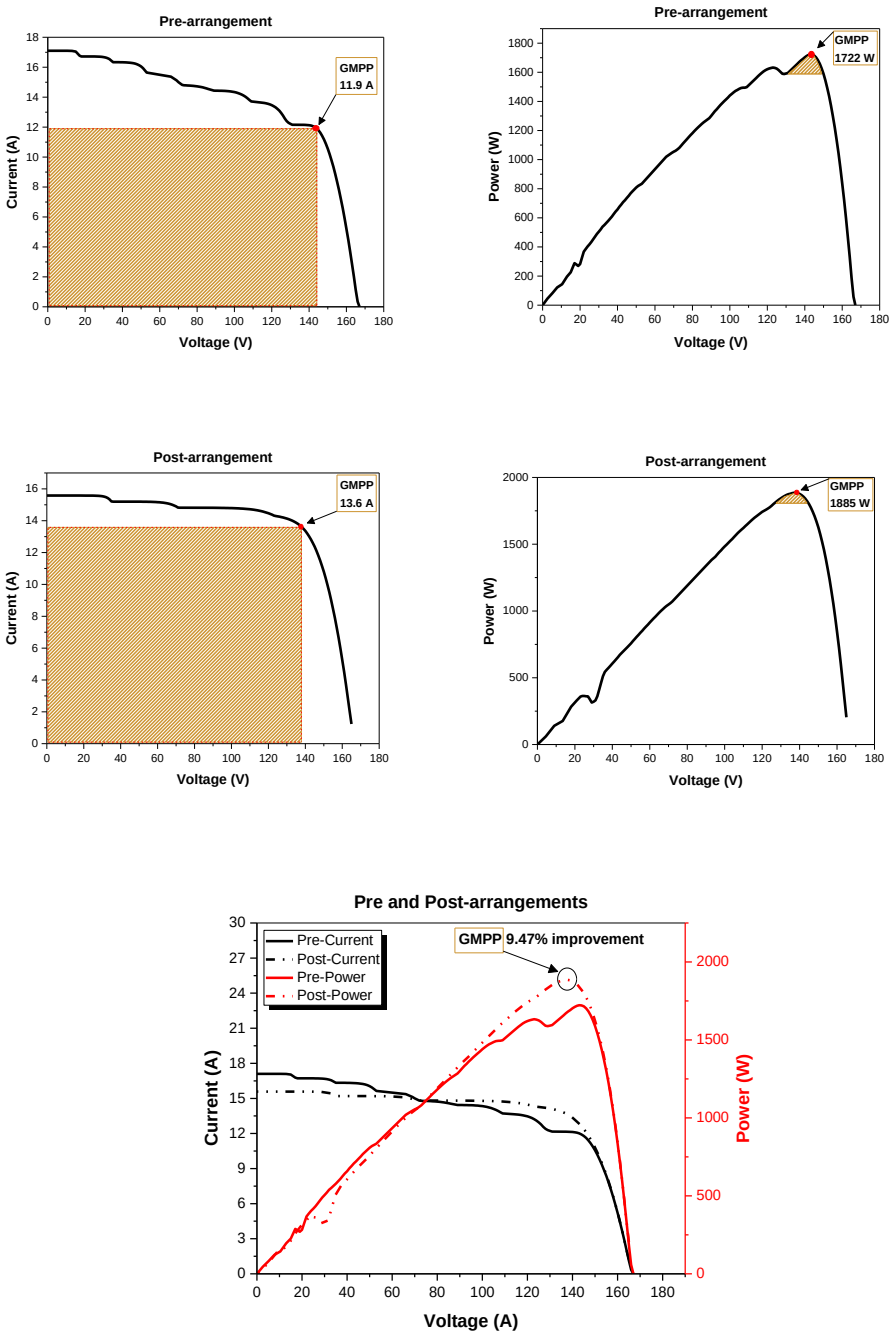

Figure 3.7: The output of the Array (pre-post rearrangements) for case 2.

3.4.1.4 Case study on 7 × 8 PV array

In this case, an 7 × 8 PV array, comprising eight series-connected strings and seven parallel-connected modules, The aging factors, ranging from 0.9 pu to 0.4 pu as shown in Table 3.6, were randomly generated, as in case 1 and 2. Figure 3.8 illustrates that the total output power increases by 32.5% when the proposed algorithm used. The

computational time for the proposed algorithm to identify the rearrangements as presented in Table 3.7 took time 5.64 seconds.

Table 3.6: PV array configuration for case 3.

Pre-rearrangement							
0.4 pu	0.6 pu	0.4 pu	0.6 pu	0.9 pu	0.6 pu	0.8 pu	0.5 pu
0.8 pu	0.4 pu	0.9 pu	0.9 pu	0.8 pu	0.5 pu	0.6 pu	0.6 pu
0.6 pu	0.8 pu	0.7 pu	0.5 pu	0.6 pu	0.8 pu	0.5 pu	0.8 pu
0.6 pu	0.8 pu	0.7 pu	0.5 pu	0.6 pu	0.8 pu	0.6 pu	0.4 pu
0.4 pu	0.4 pu	0.9 pu	0.4 pu	0.6 pu	0.6 pu	0.5 pu	0.4 pu
0.7 pu	0.8 pu	0.9 pu	0.5 pu	0.5 pu	0.7 pu	0.4 pu	0.5 pu
0.5 pu	0.7 pu	0.4 pu	0.9 pu	0.9 pu	0.6 pu	0.9 pu	0.7 pu
Post-rearrangement							
0.9 pu	0.9 pu	0.9 pu	0.9 pu	0.9 pu	0.9 pu	0.9 pu	0.9 pu
0.8 pu	0.8 pu	0.8 pu	0.8 pu	0.8 pu	0.8 pu	0.8 pu	0.8 pu
0.7 pu	0.7 pu	0.7 pu	0.7 pu	0.6 pu	0.6 pu	0.7 pu	0.6 pu
0.6 pu	0.6 pu	0.6 pu	0.6 pu	0.6 pu	0.6 pu	0.6 pu	0.6 pu
0.5 pu	0.5 pu	0.5 pu	0.5 pu	0.5 pu	0.5 pu	0.5 pu	0.5 pu
0.5 pu	0.5 pu	0.4 pu	0.5 pu	0.5 pu	0.4 pu	0.4 pu	0.5 pu
0.4 pu	0.4 pu	0.4 pu	0.4 pu	0.4 pu	0.4 pu	0.4 pu	0.4 pu

Table 3.7: PV array 8 × 7 parameters Pre and Post-arrangement.

PV Array 7 × 8 parameters				
Parameters	*Pre-arrangement*	*Post-arrangement*	*Power Improvement*	*Computing time (s)*
Current I_{mpp}	12.17 A	15 A		
Voltage V_{mpp}	127 V	136 V	32.5 %	5.64
Power W_L	1550 W	2053 W		

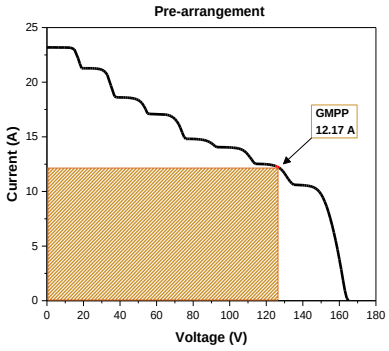

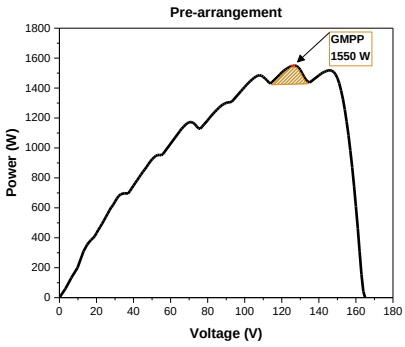

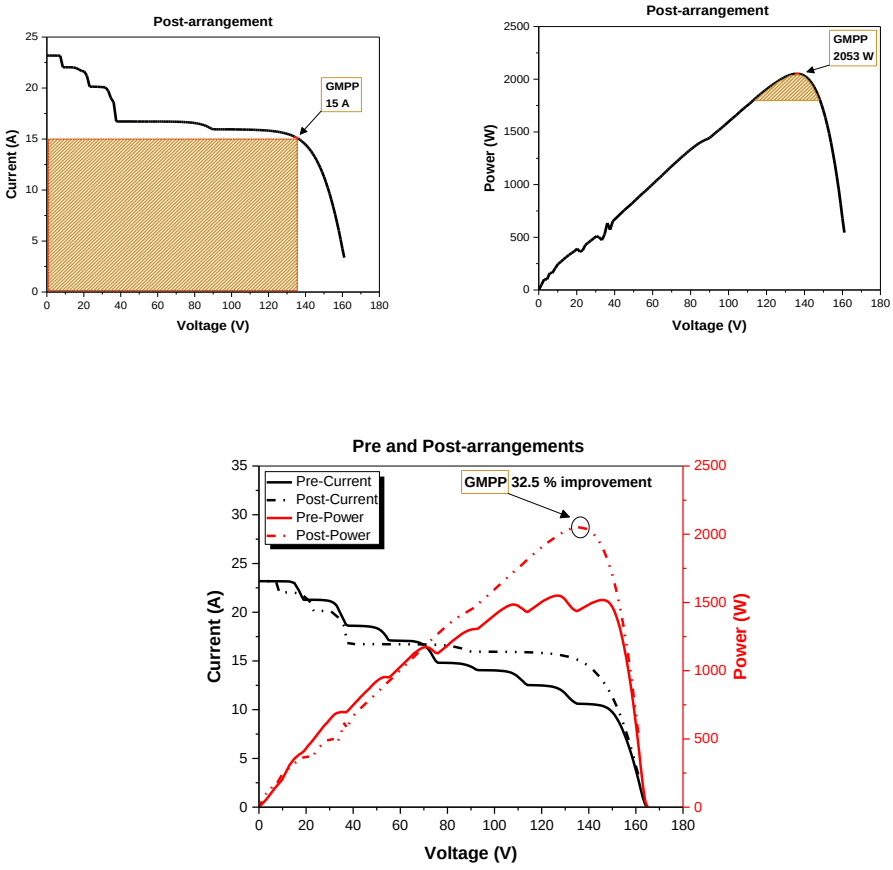

Figure 3.8: The output of a PV array (pre-post rearrangements) for case3.

3.4.1.5 Discussion

The applicability of the suggested algorithm to different PV array dimensions and its ability to enhance maximum power output for every dimension considered is proven by the results obtained. By repositioning individual PV modules in every string based on their suitable AFs, the algorithm can also attenuate the bypass diodes' effect, thus reducing the implications of incompatibility losses across PV modules in a string. On the downside, attention was not paid to voltage drawbacks, although these have been addressed in [210]. PV modules are sorted by the suggested algorithm hierarchically and repetitively. The post-arrangement minimisation of the impact of incompatibility among PV modules is indicated by the output resulting in P-V curves for the three scenarios investigated Figure 3.9. The algorithm's capability to speedily generate results stems from the fact that it does not need to access all potential

configurations for a given PV array. For example, the ideal PV module configuration was determined by the algorithm in the first scenario based solely on five steps. The potential 2,627,625 arrangements did not have to examine in their entirety. Table 3.3, Table 3.5 and Table 3.7 respectively show the computational times for each scenario. Thus, it is apparent that the ideal module arrangement can be identified quickly by the suggested algorithm and subsequently applied rapidly in real-time. Moreover, the algorithm is useful because it only repositions the damaged PV modules, while the others are left unchanged; thereby reducing the number of relays necessary for switching purposes. Makes the algorithm more cost-effective and less time-consuming than other strategies [210, 216, 218, 219]. Because of the electric switches to achieve online reconfiguration that would need many switches and many cables, the high cost makes this kind of solution unaffordable in a real application.

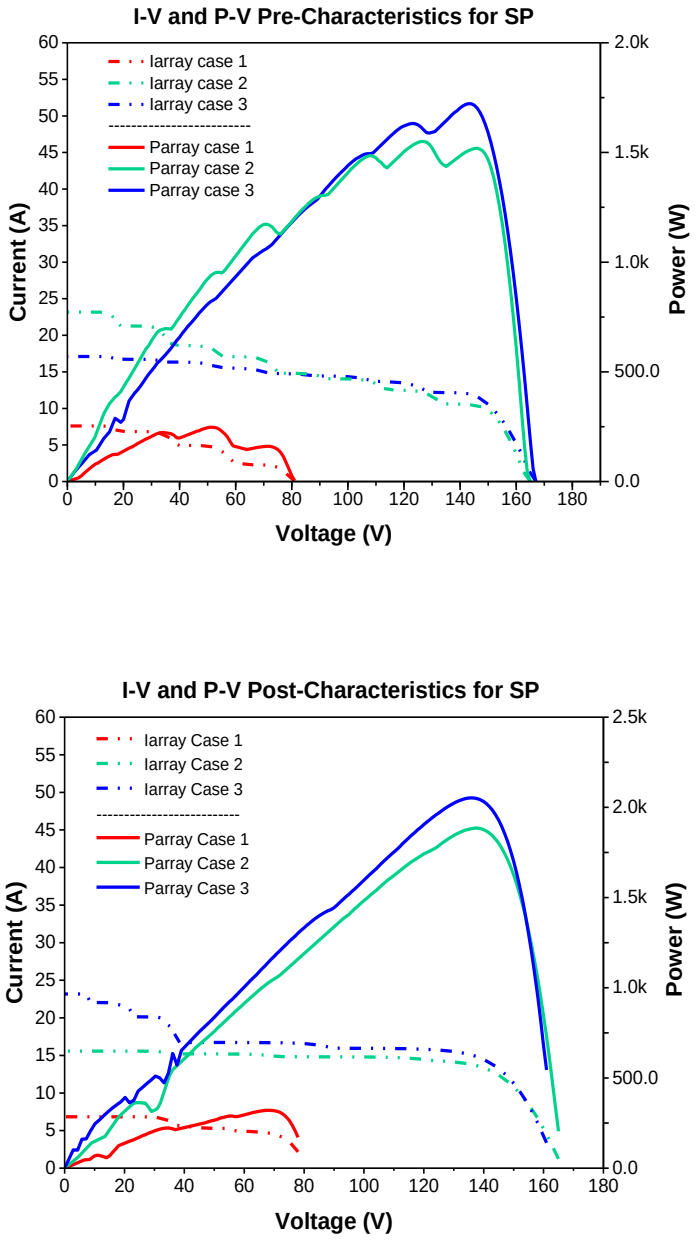

Figure 3.9: The outputs of a PV Arrays pre and post reconfigurations.

3.4.1.6 Conclusion

Non-uniform aging processes in PV arrays are the focus of the present chapter, with results showing that these arrays' power production is affected by the positions of aged PV modules in the PV arrays. A new algorithm for rearranging PV arrays is therefore put forward to attenuate the impact of PV arrays with non-uniform aging and increase the amount of power they can produce while precluding the necessity to

substitute aged PV modules. Furthermore, to minimise the incompatibility effect caused by the non-uniform aging between PV modules, the algorithm sorted the PV modules repetitively and hierarchically. Thus, the maximum power output was increased by 29.7% for the 3 × 4 PV array, by 9.47% for the 5 × 8 arrays and 32.5% for the 7 × 8 arrays. It can be concluded that the suggested strategy for reconfiguring PV modules can successfully increase the maximum power output of PV systems with a lower number of relays than the current online approaches for the rearrangement of PV arrays. Wherefore, the reconfiguration plan depends on the cost and benefit. So, providing the aging map of a PV plant is requisite, which propose a reconfiguration method to calculate the efficiency improvement and the corresponding profit. Then the workforce cost for reconfiguration its needs to be calculated. Consequently, if the profit in more power generation can cover the workforce's cost in the reconfiguration, then it is suggested that the PV plant owner undergoes reconfiguration to improve the benefits. Therefore, the proposed strategy's advantage is to employ a workforce to swap PV modules' positions only.

3.5 Reconfiguration of PV Array Based on Genetic Algorithm

After sorting the PV modules repeatedly and hierarchically in the previous section, the approach was followed by proposes GA-supported reconfiguration for medium and large PV arrays exhibiting non-uniform aging.

3.5.1.1 PV Array Reconfiguration Scheme

Figure 3.10 (a) shows an ($n \times m$) PV array where n represents the number of strings connected in parallel and m represents the number of PV modules connected in series per line. In the *P-V* curve, the voltage at a PV array's GMPP indicates the number of active modules for a given string voltage. Therefore, it is possible to derive

the PV array's full power from the product of the sum of all string currents multiplied by the string voltage of all the active modules.

To illustrate this idea, a PV array consisting of 25 aging modules connecting in a 5×5 SP configuration. The PV array consists of five parallel-connected strings (rows) and five series-connected modules (columns) in Figure 3.10. The values per unit values give the PV array's non-uniform aging status directly related to its short circuit currents.

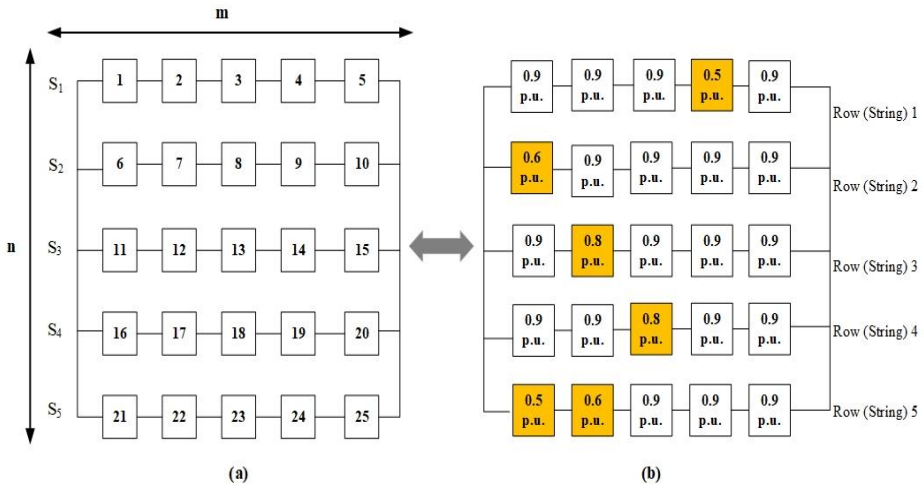

Figure 3.10: A series- parallel (SP) configuration PV array involving n × m and (b) A 5 × 5 SP configuration with non-uniform aging.

The standard test condition (STC) in the appropriate module defines the short-circuit current to be 1 per unit (p.u.), which corresponds to 1000 W/m2. The digits indicate the various aging factors (AF) directly correlated with their different short-circuit current associated with the PV modules in the array. For example, the optimisation problem is discussed the present work based on a GEA, which is applied to a 5×5 PV array arrangement in Figure 3.10. Therefore, several parameters need to be identified before presenting the suggested algorithm's two steps to explain the rearrangement work mentioned below. Before and after arrangements, there are two guidelines indicated for this function.

Several parameters need to be defined before presenting the suggested algorithm's nine steps to elucidate the rearrangement work mentioned below.

- n = 1, 2, 3…, n, $n-1$, where the number of strings in the PV array calledn.
- $\sum Af$ = Summation of aging factors in a series of connected modules.
- $m_{\min(n)} = Af_n$ a series-connection for a string (n) (n).
- $m_{max(n)} = Af_n$ a series-connection for a string $(n+1)$ (n+1).
- $PV_{n(min)}$ = position of PV module with a minimum Af_n a series of connected modules.
- $PV_{n(max)n+1}$ = position of PV module with a maximum Af_n a series of connected modules.

First step: initialize the summation of $PV_n = Af_n$ for each string before arrangement, as follows in Figure 3.11 and Equation (4.1):

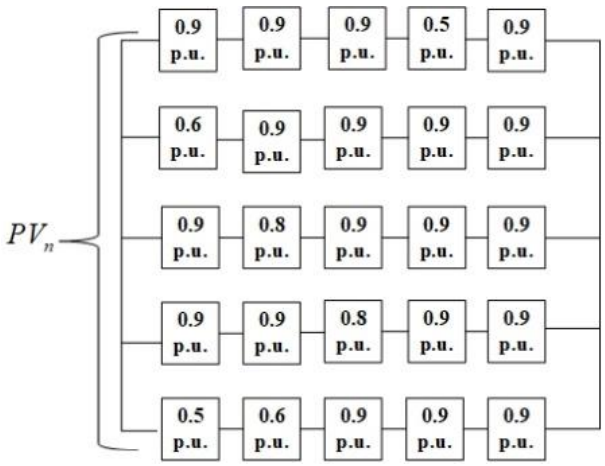

Figure 3.11: Each string before arrangement per-unit.

$$PV_n = \begin{matrix} \sum Af_1 = 0.9+0.9+0.9+0.5+0.9 = 4.1 \\ \sum Af_2 = 0.6+0.9+0.9+0.9+0.9 = 4.2 \\ \sum Af_3 = 0.9+0.8+0.9+0.9+0.9 = 4.4 \\ \sum Af_4 = 0.9+0.9+0.8+0.9+0.9 = 4.4 \\ \sum Af_5 = 0.5+0.6+0.9+0.9+0.9 = 3.8 \end{matrix} \quad p.u. \qquad (3.21)$$

Second step*:* the rule specifies that, in a string, the minimal number represents the Af_n output. This means that the output is the lowest among all values from high to low.

Arrange all the $P_n = Af_n \times PV_n$ before arrangement in descending order to find the total of PV_5, $PV4$ … and PV_1, presented in Equations (10–12) for the case study.

$$PV_5 = \begin{pmatrix} S_1 = 0.5\times 5 = 2.5 \\ S_2 = 0.6\times 5 = 3 \\ S_3 = 0.8\times 5 = 4 \\ S_4 = 0.8\times 5 = 4 \\ S_2 = 0.5\times 5 = 2.5 \end{pmatrix} p.u. \text{ and } PV_4 = \begin{pmatrix} S_1 = 0.9\times 4 = 3.6 \\ S_2 = 0.9\times 4 = 3.6 \\ S_3 = 0.9\times 4 = 3.6 \\ S_4 = 0.9\times 4 = 3.6 \\ S_2 = 0.6\times 4 = 2.4 \end{pmatrix} p.u. \quad (3.22)$$

$$PV_3 = \begin{pmatrix} S_1 = 0.9\times 3 = 2.7 \\ S_2 = 0.9\times 3 = 2.7 \\ S_3 = 0.9\times 3 = 2.7 \\ S_4 = 0.9\times 3 = 2.7 \\ S_2 = 0.9\times 3 = 2.7 \end{pmatrix} p.u. \quad \text{and} \quad PV_2 = \begin{pmatrix} S_1 = 0.9\times 3 = 2.7 \\ S_2 = 0.9\times 3 = 2.7 \\ S_3 = 0.9\times 3 = 2.7 \\ S_4 = 0.9\times 3 = 2.7 \\ S_2 = 0.9\times 3 = 2.7 \end{pmatrix} p.u. \quad (3.23)$$

$$PV_1 = \begin{pmatrix} S_1 = 0.9 \\ S_2 = 0.9 \\ S_3 = 0.9 \\ S_4 = 0.9 \\ S_2 = 0.9 \end{pmatrix} p.u. \quad (3.24)$$

3.5.1.2 Optimal Reconfiguration Based on GEA

A gene evaluation algorithm is applied to determine the configuration which has the maximum generated power among all possible connection patterns. The genetic algorithm has two significant advantages: firstly, it allows the genetic algorithm to have a certain degree of local random search-ability. When the iteration is close to a better solution for a certain number of times, the convergence to a better solution can be accelerated through mutation operations. Secondly, it can maintain that the diversity of feasible solutions can prevent the appearance of precocity. To use GEA, each configuration must be represented by a row of numbers that play a role as a chromosome in GEA. Also, there must be a fitness function to calculate the power generated by each configuration. The inputs of fitness function are chromosomes prepared before. Then according to outputs of the fitness function, GEA decides which

chromosomes should be selected as parents to produce chromosomes of the next generation. Therefore, in order to do optimisation for this problem, the following steps must be done.

$$\mathrm{n} \times \mathrm{m}_{\text{ matrix}} = \begin{bmatrix} 0.9 & 0.9 & 0.9 & 0.5 & 0.9 \\ 0.6 & 0.9 & 0.9 & 0.9 & 0.9 \\ 0.9 & 0.8 & 0.9 & 0.9 & 0.9 \\ 0.9 & 0.9 & 0.8 & 0.9 & 0.9 \\ 0.5 & 0.6 & 0.9 & 0.9 & 0.9 \end{bmatrix} \tag{3.25}$$

First step: the fitness function was designed as a normalised quantity. Equation (14) describes the proposed fitness function PV_i Equation (4.6), where $S_n = Af_1 + Af_2 + Af_3 + Af_4 + Af_5$ represent the short-circuit current of the modules, V_{OC} represents the open-circuit voltage, PV_{power} represents the power delivered by the PV array and n_{PV} represent the number of modules in the system. Therefore, the objective of the GEA is to maximise the value of PV_i as much as possible.

$$PV_i = \frac{PV_{pwoer}}{\sum_{j=1}^{n_{PV}} S_{n(j)} \bullet V_{OC}} \tag{3.26}$$

Second step: parametric design based on three points:

- Population size count = 300
- Chromosome length = *nm*
- Evolution times = 3000

Third step: the encoding strategy uses a decimal. Directly encode with the number of the PV module. For example, the chromosome can be expressed as the sequence $\{1, 2, 3\ldots \mathrm{nm}\}$.

Initialise the random population. In order to speed up the running of the program, some better individuals should be selected in the initial population selection. We first use the improved circle algorithm to obtain a better initial population. The idea of the algorithm is to randomly generate a chromosome, such as $\{1, 2, 3\ldots \mathrm{nm}\}$, and exchange the sequential position of the two modules arbitrarily. Continue the following two to convert a one-dimensional list into a two-dimensional matrix. If the value of the PV_i that needs to be optimised increases, the chromosome is updated and changed.

Fourth step: evaluate the fitness of each chromosome in the population. The chromosome is transformed into a two-dimensional array (nm). Then according to the fitness function designed, calculate PV_i.

Fifth step: judge to accomplish iterations or optimisation goal. If successful, then go to step nine, else go to step six.

Sixth step: parent's selection for next-generation. Firstly, to select the surviving chromosomes, the fitness is sorted from large to small, then the random selection is performed to select individuals who have small fitness but survive.

Seventh step: crossover of parent's chromosome. The crossover strategy is the difficulty of this problem. If the point cross is used directly, the offspring chromosomes will have the issues of PV- model duplication and omission. Therefore the order crossover method is used. The sequential hybridisation algorithm first randomly selects two hybridisation points among parents and then exchanges

hybridisation segments. The other positions are determined according to the relative positions of the parents' models.

For example, the chromosome can be expressed as the sequence $\{1, 2, \dots, 10\}$. Suppose:

- Parent one = $\{10, 8, 6, 3, 7, 4, 1, 5, 9, 2\}$
- Parent two = $\{1, 5, 10, 6, 9, 8, 2, 4, 3, 7\}$. Then the random hybridisation points are 4 and 7. As shown in Table 3.8.

Table 3.8: Two chromosomes and the random hybridisation point are set to 4-7.

Parent one'	**10**	**8**	**6**	**3**	**7**	**4**	**1**	**5**	**9**	**2**
Parent two'	**1**	**5**	**10**	**6**	**9**	**8**	**2**	**4**	**3**	**7**

First, swap the hybrids as shown in Table 3.9:

Parent one' = $\{\#, \#, \#, \#, \mid 9, 8, 2, 4 \mid, \#, \#\}$

Parent two'= $\{\#, \#, \#, \#, \mid 7, 4, 1, 5 \mid, \#, \#\}$

Table 3.9: Swap substrings in parents.

Parent one'	**#**	**#**	**#**	**#**	**9**	**8**	**2**	**4**	**#**	**#**
Parent two'	**#**	**#**	**#**	**#**	**7**	**4**	**1**	**5**	**#**	**#**

And then starting from the second hybridisation point of parent one, getting the collection $\{9, 2, 10, 8, 6, 3, 7, 4, 1, 5\}$; then removing the elements in the hybridisation segment $\{9, 8, 2, 4\}$, finally obtaining $\{10, 6, 3, 7, 1, 5\}$, match the hybridization point 7 filled in parent one', at last, parent one'= $\{3, 7, 1, 5, 9, 8, 2, 4, 10, 6\}$ from the second crossing point in turn. Similarly, parent two'=$\{4, 9, 10, 2, 7, 3, 1, 6, 8, 5\}$. As shown in Table 3.10.

Table 3.10: Crossover of parent's chromosomes.

Parent one'	**3**	**7**	**1**	**5**	**9**	**8**	**2**	**4**	**10**	**6**
Parent two'	**6**	**9**	**8**	**2**	**7**	**4**	**1**	**5**	**3**	**10**

Eighth step: mutation of the chromosome. A mutation is also a means to achieve group diversity, as well as a guarantee for global optimisation. The specific design is as follows. According to the given mutation rate, for the selected mutant individuals, three integers are randomly taken to satisfy $1 < u < v < w < nm$ and the genes between v and u (including u and v) the paragraph are inserted after w. Then we go to step four.

Final step: output the best chromosome. The optimal configuration for the PV array is displayed in the last step of Figure 3.12. Equation (4.7) demonstrates how each configuration that reached each step is compared with the original configuration. The optimal configuration for a non-uniformly aging 5 × 5 PV array took just nine iterations to achieve. Therefore, the reconfigured 5 × 5 PV array is the optimal

configuration. Figure 8 shows the before and after reconfiguration PV arrays for direct comparison.

$$PV_n = \begin{matrix} \sum Af_1 = 0.9+0.5+0.9+0.9+0.9 = 4.1 \\ \sum Af_2 = 0.9+0.9+0.9+0.8+0.9 = 4.4 \\ \sum Af_3 = 0.9+0.5+0.9+0.8+0.9 = 4 \\ \sum Af_4 = 0.9+0.6+0.9+0.9+0.9 = 4.2 \\ \sum Af_5 = 0.9+0.6+0.9+0.9+0.9 = 4.2 \end{matrix} \quad p.u. \qquad (3.27)$$

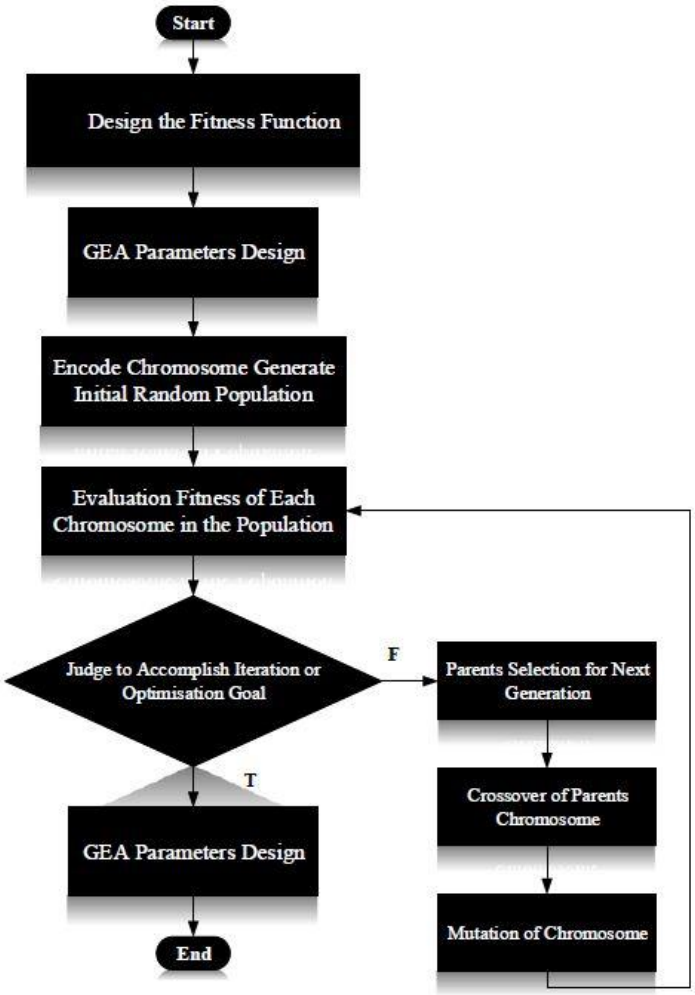

Figure 3.12: Flow chart of GEA procedure of PV array reconfiguration.

3.5.1.3 Cases Studies and Simulation Results

To demonstrate validation of the proposed algorithm, several PV arrays of different sizes will be evaluated 5 × 5 and 7 × 20 PV arrays.

3.5.1.4 Case 1 (5×5 PV Array)

Verification of the results using MATLAB can be obtained from Figure 3.11. The maximum short-circuits currents in a healthy module is set as 1 p.u. (STC), where standard test conditions represent 1000 W/m^2 irradiance at 25 °C module temperature. The reconfiguration of the PV array via the developed algorithm is presented in Table 5. Based on this data, Figure 3.13 and Figure 3.14 displays corresponding *I–V* and *P–V* curves. Figure 3.13 shows that before the reconfiguration the peak output power and voltage were 1055.4 W and 89 V, respectively, with global maximum power point (GMPP) current 11.8 A. Figure 3.14 shows that after the reconfiguration these were 1077.5 W and 68 V, respectively, with GMPP current 15.73 A. Clearly, the algorithm has enabled an overall improvement of 2.08% to the output power. As shown in Table 3.12, the total time to compute the reconfiguration was 0.015625 s.

Table 3.11: Arrangement of the first PV array before and after reconfiguration.

Before arrangement						*After arrangement*				
0.9 p.u.	0.9 p.u.	0.9 p.u.	0.5 p.u.	0.9 p.u.		0.9 p.u.	0.5 p.u.	0.9 p.u.	0.9 p.u	0.9 p.u.
0.6 p.u.	0.9 p.u.	0.9 p.u.	0.9 p.u.	0.9 p.u.		0.9 p.u.	0.9 p.u.	0.9 p.u.	0.8 p.u.	0.9 p.u.
0.9 p.u.	0.8 p.u.	0.9 p.u.	0.9 p.u.	0.9 p.u.		0.9 p.u.	0.5 p.u.	0.9 p.u.	0.8 p.u.	0.9 p.u.
0.9 p.u.	0.9 p.u.	0.8 p.u.	0.9 p.u.	0.9 p.u.		0.9 p.u.	0.6 p.u.	0.9 p.u.	0.9 p.u.	0.9 p.u.
0.5 p.u.	0.6 p.u.	0.9 p.u.	0.9 p.u.	0.9 p.u.		0.9 p.u.	0.6 p.u.	0.9 p.u.	0.9 p.u.	0.9 p.u.

Table 3.12: The 5 × 5 PV array parameters before and after the arrangement.

PV Array 5 × 5 parameters				
Parameters	*Before*	*After*	*Power Improvement*	*Computing time (s)*
Current I_{mpp} I_{mpp}	11.8 A	15.79 A		
Voltage V_{mpp} V_{mpp}	89 V	68 V	2.08 %	0.015625
Power W_L	1055.4 W	1077.5 W		

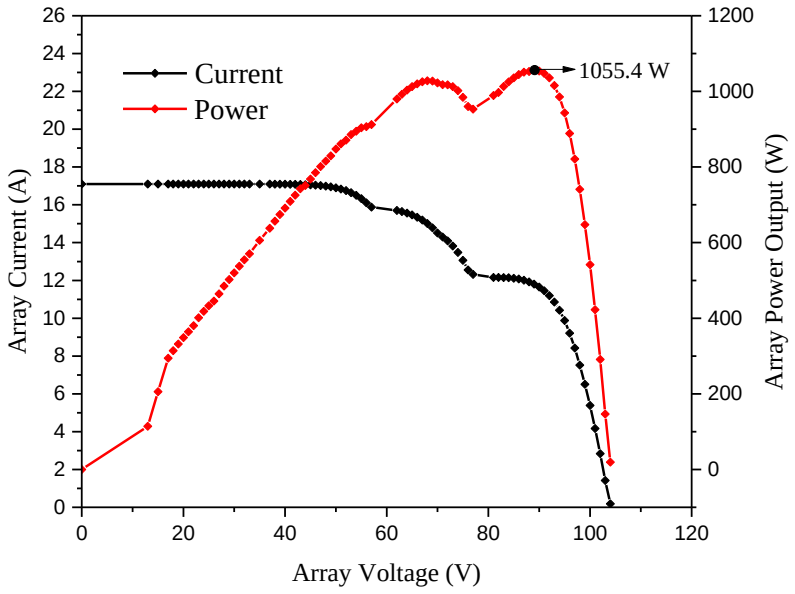

Figure 3.13: The 5 × 5 PV array outputs power results before arrangements.

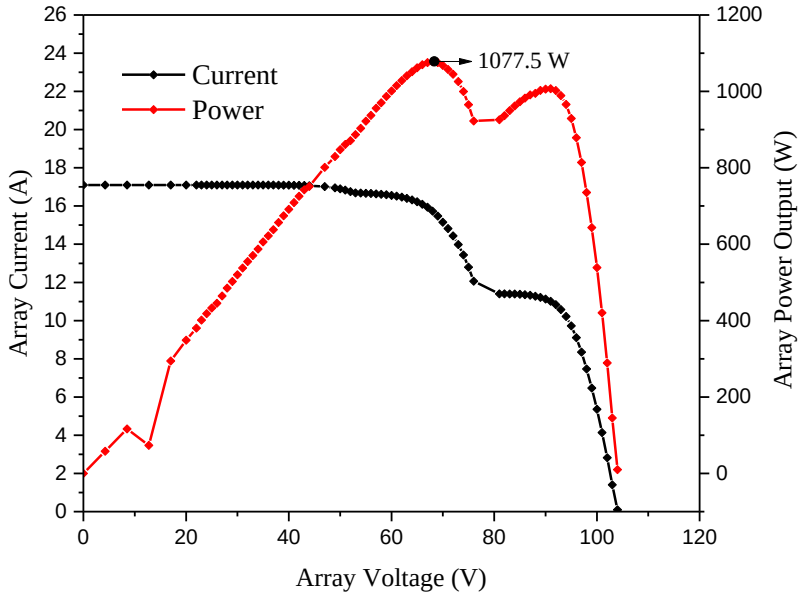

Figure 3.14: The 5 × 5 PV array outputs power results after arrangements.

3.5.1.5 Case 2 (7×20 PV Array)

Here, non-uniform aging factors were randomly generated for a large 7 × 20 PV array, comprising twenty parallel-connected strings and seven series-connected modules. The aging factors, ranging from 0.9 p.u. to 0.5 p.u. as shown in Table 3.13, were randomly generated, as in the second case. A power improvement of 9.74% was

observed following the application of the proposed algorithm, as presented in Table 8, *I–V* and *P*–V curves were plotted as depicted in Figure 3.15 and Figure 3.16 with a mean computational time of 0.129375 s.

Table 3.13: PV array before arrangement for the second case.

Before arrangement																			
0.9 p.u.	0.9 p.u.	0.9 p.u.	0.6 p.u.	0.9 p.u.	0.5 p.u.	0.9 p.u.	0.9 p.u.	0.6 p.u.	0.9 p.u.	0.9 p.u.	0.9 p.u.	0.9 p.u.	0.9 p.u.	0.9 p.u.	0.8 p.u.	0.9 p.u.	0.9 p.u.	0.9 p.u.	0.6 p.u.
0.8 p.u.	0.9 p.u.	0.9 p.u.	0.9 p.u.	0.5 p.u.	0.9 p.u.	0.9 p.u.	0.9 p.u.	0.9 p.u.	0.9 p.u.	0.6 p.u.	0.9 p.u.	0.9 p.u.	0.5 p.u.	0.9 p.u.	0.9 p.u.	0.9 p.u.	0.9 p.u.	0.9 p.u.	0.9 p.u.
0.9 p.u.	0.9 p.u.	0.5 p.u.	0.9 p.u.	0.8 p.u.	0.9 p.u.	0.9 p.u.	0.8 p.u.	0.8 p.u.	0.9 p.u.	0.6 p.u.	0.9 p.u.	0.9 p.u.	0.9 p.u.	0.9 p.u.	0.9 p.u.	0.9 p.u.	0.9 p.u.	0.9 p.u.	0.9 p.u.
0.9 p.u.	0.5 p.u.	0.9 p.u.	0.5 p.u.	0.5 p.u.	0.9 p.u.	0.9 p.u.	0.9 p.u.	0.9 p.u.	0.9 p.u.	0.9 p.u.	0.9 p.u.	0.9 p.u.	0.6 p.u.	0.6 p.u.	0.9 p.u.	0.9 p.u.	0.9 p.u.	0.9 p.u.	0.8 p.u.
0.8 p.u.	0.8 p.u.	0.9 p.u.	0.9 p.u.	0.9 p.u.	0.9 p.u.	0.9 p.u.	0.9 p.u.	0.9 p.u.	0.9 p.u.	0.9 p.u.	0.9 p.u.	0.9 p.u.	0.8 p.u.	0.9 p.u.	0.9 p.u.	0.9 p.u.	0.9 p.u.	0.5 p.u.	0.9 p.u.
0.9 p.u.	0.9 p.u.	0.9 p.u.	0.9 p.u.	0.9 p.u.	0.9 p.u.	0.9 p.u.	0.9 p.u.	0.9 p.u.	0.9 p.u.	0.9 p.u.	0.6 p.u.	0.9 p.u.	0.9 p.u.	0.9 p.u.	0.9 p.u.	0.9 p.u.	0.6 p.u.	0.9 p.u.	0.9 p.u.
0.9 p.u.	0.9 p.u.	0.9 p.u.	0.8 p.u.	0.9 p.u.	0.9 p.u.	0.9 p.u.	0.8 p.u.	0.9 p.u.	0.9 p.u.	0.9 p.u.	0.9 p.u.	0.9 p.u.	0.9 p.u.	0.6 p.u.	0.9 p.u.	0.9 p.u.	0.9 p.u.	0.9 p.u.	0.9 p.u.
After arrangement																			
0.9 p.u.	0.9 p.u.	0.8 p.u.	0.9 p.u.	0.9 p.u.	0.9 p.u.	0.9 p.u.	0.9 p.u.	0.8 p.u.	0.5 p.u.	0.8 p.u.	0.9 p.u.	0.9 p.u.	0.9 p.u.	0.8 p.u.	0.8 p.u.	0.9 p.u.	0.9 p.u.	0.9 p.u.	0.9 p.u.
0.9 p.u.	0.9 p.u.	0.9 p.u.	0.9 p.u.	0.9 p.u.	0.9 p.u.	0.9 p.u.	0.9 p.u.	0.9 p.u.	0.6 p.u.	0.9 p.u.	0.9 p.u.	0.9 p.u.	0.9 p.u.	0.9 p.u.	0.9 p.u.	0.9 p.u.	0.9 p.u.	0.9 p.u.	0.9 p.u.
0.9 p.u.	0.9 p.u.	0.9 p.u.	0.9 p.u.	0.9 p.u.	0.9 p.u.	0.9 p.u.	0.9 p.u.	0.9 p.u.	0.9 p.u.	0.9 p.u.	0.9 p.u.	0.9 p.u.	0.9 p.u.	0.6 p.u.	0.9 p.u.	0.9 p.u.	0.9 p.u.	0.9 p.u.	0.9 p.u.
0.8 p.u.	0.9 p.u.	0.9 p.u.	0.5 p.u.	0.9 p.u.	0.8 p.u.	0.9 p.u.	0.9 p.u.	0.9 p.u.	0.9 p.u.	0.8 p.u.	0.9 p.u.	0.9 p.u.	0.9 p.u.	0.9 p.u.	0.9 p.u.	0.9 p.u.	0.9 p.u.	0.9 p.u.	0.8 p.u.
0.6 p.u.	0.9 p.u.	0.5 p.u.	0.5 p.u.	0.5 p.u.	0.5 p.u.	0.9 p.u.	0.9 p.u.	0.9 p.u.	0.6 p.u.	0.6 p.u.	0.8 p.u.	0.6 p.u.	0.6 p.u.	0.9 p.u.	0.6 p.u.	0.5 p.u.	0.5 p.u.	0.6 p.u.	0.9 p.u.
0.8 p.u.	0.9 p.u.	0.9 p.u.	0.9 p.u.	0.9 p.u.	0.9 p.u.	0.9 p.u.	0.9 p.u.	0.9 p.u.	0.9 p.u.	0.9 p.u.	0.9 p.u.	0.9 p.u.	0.9 p.u.	0.9 p.u.	0.9 p.u.	0.9 p.u.	0.9 p.u.	0.9 p.u.	0.9 p.u.
0.9 p.u.	0.9 p.u.	0.9 p.u.	0.6 p.u.	0.9 p.u.	0.9 p.u.	0.9 p.u.	0.9 p.u.	0.9 p.u.	0.9 p.u.	0.9 p.u.	0.9 p.u.	0.9 p.u.	0.9 p.u.	0.9 p.u.	0.9 p.u.	0.9 p.u.	0.9 p.u.	0.9 p.u.	0.9 p.u.

Table 3.14: PV array 7 × 20 parameters before and after the arrangement.

PV Array 7 × 20 parameters				
Parameters	*Before*	*After*	*Power Improvement*	*Computing time (s)*
Current I_{mpp} I_{mpp}	19.38 A	20.4 A		
Voltage V_{mpp} V_{mpp}	314 V	329 V	9.74%	0.129375
Power W_L	6.095 W	6.721 kW		

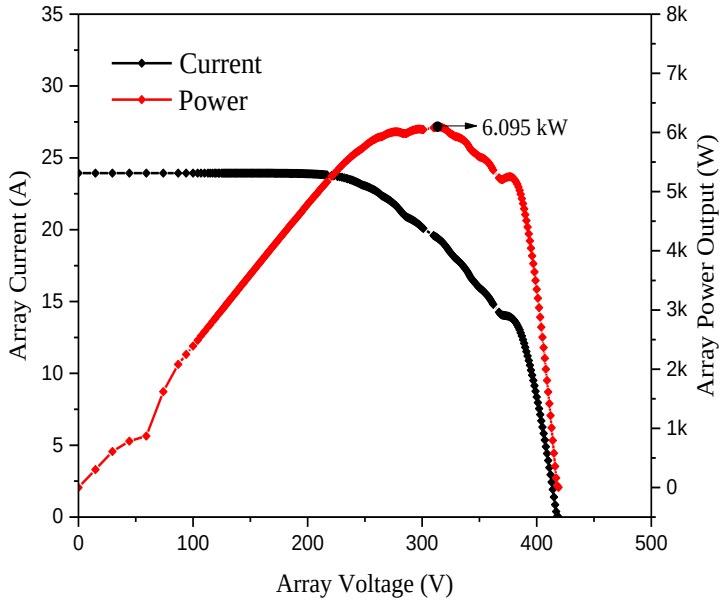

Figure 3.15: The output power of PV array 7 × 20 before rearrangement.

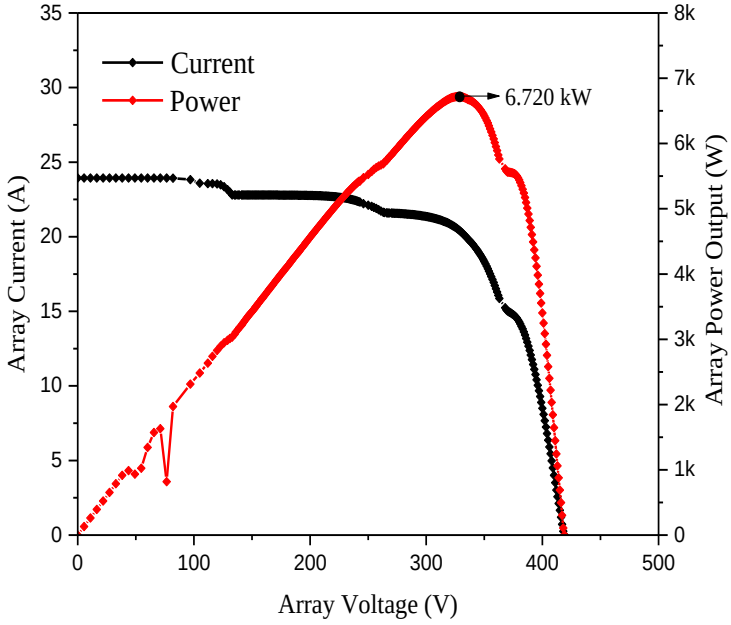

Figure 3.16: The output power of PV array 7 × 20 after rearrangement.

3.5.1.6 Discussion

These findings demonstrate that the proposed algorithm applies randomly to various PV array sizes. The findings also indicate that the algorithm improved maximum power output for both cases. Additionally, the algorithm reduced the bypass diodes' impact by rearranging the positions of separate PV modules in each string, based on their appropriate aging factors. This minimised the impact of mismatch losses over PV modules in any specified string, but voltage limitation was not considered. However, this has been discussed elsewhere in the literature [210]. The proposed algorithm utilises a hierarchical and iterative sorting of PV modules. The resulting $P-V$ curves for the two worked examples, as presented in Figure 3.15 and Figure 3.16, demonstrate that the influence of PV module mismatch reduced before rearrangement. From case 1 as an example, comparing the maximum power point with maximum power 1077.5 W improved significantly, concluding that PV array rearrangement is an important method to improve system efficiency and decrease system operation cost.

Furthermore, there is no requirement for the proposed algorithm to access every possible on- offline configuration for any specified PV array, which would be a massive undertaking. This is what enables the algorithm to produce results relatively quickly. For example, in case 1, only nine steps were required for the algorithm to identify the optimum PV module arrangement. So there was no requirement to analyse huge numbers of arrangements. Relevant computational times for the two cases are reported in Table 3.12 and Table 3.14. Therefore, the proposed algorithm can quickly determine the optimal module configuration, which can also be implemented quickly. Another advantage is that the affected PV modules are the only ones that require rearrangement, while the rest can remain in their original positions. This has the additional benefit of keeping the number of relays required for switching purposes to

a minimum, thereby offering cost and time savings compared to other approaches [210, 216, 218, 219]. However, it is worth bearing in mind that the prohibitive expense associated with the number of switches and cables required for this method makes it impractical. Achieving online reconfiguration with electric switches would necessitate the use of countless switches and cables, which corresponds to a prohibitive cost for real-world applications. Therefore, the offline optimal reconfirmation is more comfortable with calculating, without a need for high-performance controllers. A summary of online and offline reconfiguration methods, as shown in Table 3.15.

Table 3.15: Comparison of offline and online reconfiguration methods.

Item	*Online Reconfiguration*	*Offline Reconfiguration*
Health monitoring	Real-time monitoring	Periodic monitoring
Implementations of reconfiguration	On-site switching reconfiguration	Manual connection
Computation of reconfiguration	On-site computation with powerful controllers	Offline computation
Applicable array	Small-scale PV arrays	Any arrays

3.5.1.7 Conclusion

In conclusion, the phenomenon of non-uniform aging is prevalent in large-scale PV plants due to the long period of service required and the harsh environments PV arrays are exposed to. Therefore, this study derived modelling and computing GEA that simulates and analyses the possible rearrangement of aging PV arrays and the resulting output power. A non-linear integer programming solution was devised to improve power output by rearranging the PV panels. Voltage restrictions were considered, and a 5 × 5 and a 7 × 20 PV array was used to test and prove the devised algorithm. Thus, the maximum power output was increased by 2.08% for the first case and 9.74% for the second case. When comparatively examined with the current online PV array reconfiguration techniques, the proposed method does not need as many relays. It also enhances the maximum power output of the PV system. Simultaneously,

because the algorithm necessitates only that the positions of the PV modules are switched around, it can be implemented straightforwardly.

This rearrangement offered efficient maintenance management. The plan for offline reconfiguration is dependent on issues such as the benefit and the cost. Generating a PV plant’s aging map is critical, making it necessary to devise offline a reconfiguration technique for calculating the improvement in efficiency, profitability and the workforce cost for reconfiguration. If the profit gained from generating greater amounts of power can pay for the costs associated with the workforce's reconfiguration, then it is reasonable to conclude that the owner of a PV plant should undertake a reconfiguration to leverage the advantageous aspects of this practice. Given these considerations, the proposed strategy's benefit involves employing a workforce to swap PV modules positions only.

Chapter 4. AN EXPERIMENTAL INVESTIGATION ON OUTPUT POWER ENHANCEMENT WITH OFFLINE RECONFIGURATION FOR NON-UNIFORM AGING PHOTOVOLTAIC ARRAY TO MAXIMISE ECONOMIC BENEFIT

The content of this chapter has been submitted in the following paper:

1. M. Alkahtani, J. Zhou, Y. Hu, F. Alkasmoul, Z. H. Kiani and C. S. Kuka, "An Experimental Investigation on Output Power Enhancement with Offline Reconfiguration for Non-uniform Aging Photovoltaic Array to Maximise Economic Benefit," in IEEE Access, doi: 10.1109/ACCESS.2021.3088386.

The current study concentrates on non-uniform ageing processes in PV arrays. An AI-based algorithm is presented in the previous chapter. The included experiment presents the finding that PV array power production is impacted by the position of aged PV modules in the PV arrays, which was not presented in the previous chapter. Thus, the suggested current chapter is scientific proof that the theoretical reconfiguration of PV array through the MATLAB/Python software in the previous chapter has been scientifically tested in the laboratory.

4.1 Methodology

4.1.1.1 PV module Characteristics

This experiment used a 2 × 4 PV array to assess the efficiency of different array interconnection topologies for reducing mismatch loss due to aging factors. In turn, eight polycrystalline small PV modules (0.36 W/m2 and 25°C) were used as shown

Figure 4.1, and the electrical specifications of single PV modules are clearly in Table 4.1 and Figure 4.2 [227]. The experimental tests were conducted inside an indoor laboratory at home because of the ongoing pandemic (COVID-19). Five different aging patterns were employed to effectively analyses the performance when linked in a series-parallel SP topology. The details of array configuration, aging patterns, and detail experimental procedure are described in the following subsections.

Figure 4.1: The type of small solar power panel 0.36W 2V Polycrystalline SunPower DIY module.

Table 4.1: Electrical specification of monocrystalline ANYSOLAR Ltd (SM301K09L-ND) module and array.

Parameter	*Unit*	*Symbol*	*PV module (8 Cell)*
Open Circuit Voltage	V	V_{OC}	2.5
Short Circuit Current	A	I_{SC}	0.180
Maximum Power Point Voltage	V	V_{mpp}	2
Maximum Power Point Current	A	I_{mpp}	0.160
Maximum Power Point	W	P_{mpp}	0.36
Operating Temperature	T	$°C$	25

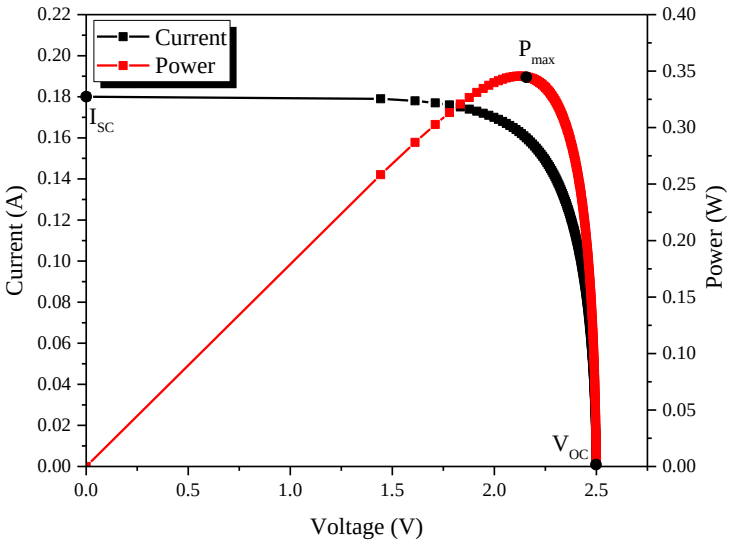

Figure 4.2: I-V and P-V curves of single PV (At standard test conditions) of the healthy module.

4.1.1.2 PV Array Aging Patterns Example

An example, random 16 PV modules connected in the PV string series for medium size PV array are commonly used for the MPPT investigation. Besides, PV module aging is achieved through films, and In Figure 4.3, shows the suggested aging patterns, which can be used as examples of the SP configuration. In aging pattern-I, (a) four modules are aging (in the first string) horizontally. In aging pattern-II, (b) two strings are aging as (a) horizontally. Finally, in aging pattern-III, (c) eight modules are aging vertically, and the modules are connected in parallel. This type of aging technique was employed on eight modules in order to produce aging pattern-IV, (d). These aging patterns' significance is evaluated using array current, array voltage, and power for the array configuration SP. As a result, Figure 4.4 shows the first PV string of pattern-I (a) as an example with three peaks in the top right corner and two PV modules (D and C) with ageing patterns for P–V curves. Simultaneously, the PV string

in the top left identified four different ageing of second patterns-II, (b), with modules (D and C) exhibiting ageing factors. In contrast, the others (B and A) remained stable.

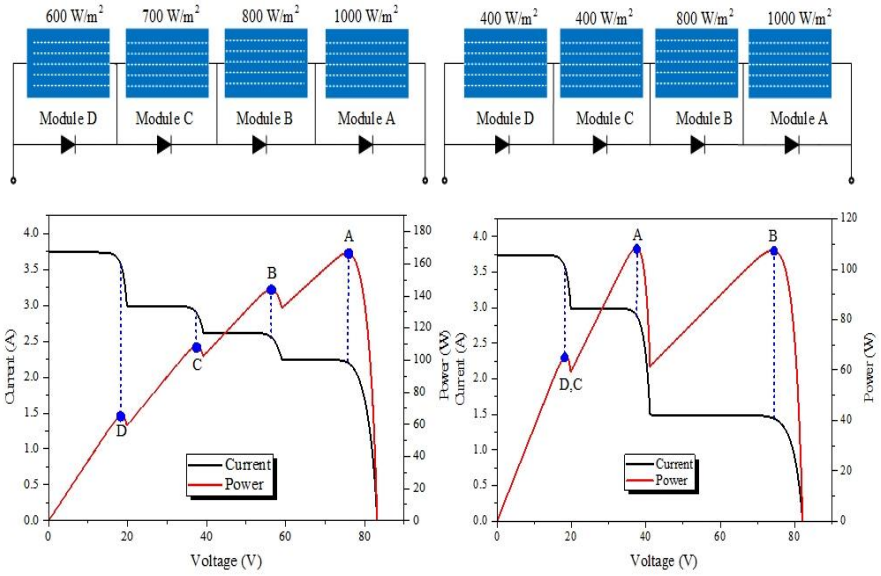

Figure 4.3. Example of connecting PV panels/module in series and parallel, where the healthy module begins 1000W/m^2.

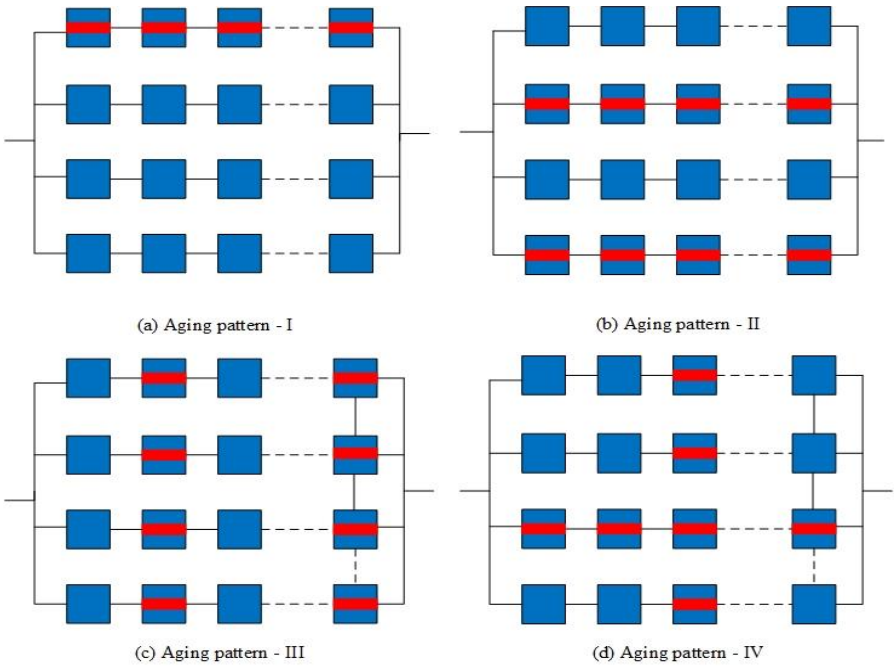

Figure 4.4. Four different PV modules aging patterns for SP configuration (a,b,c and d).

4.1.1.3 Experimental Study

This section discusses the research setup and measurement processes. The experiment involved 2 × 4 arrays in confirming the suggested approach, depending on availability. In Figure 4.5, three halogen bulbs are employed as artificial sunlight (0.5kW each), positioned parallel to the display modules. Practical used flexible wires and clips to link the individual PV modules' output edges to make the connections more manageable. In turn, commercial multimeters were used to evaluate the PV array's output I−V and P−V parameters, along with an irradiance sensor and temperature sensor. The room temperature was 25°C during the experiment, with a variable speed cooling fan used.

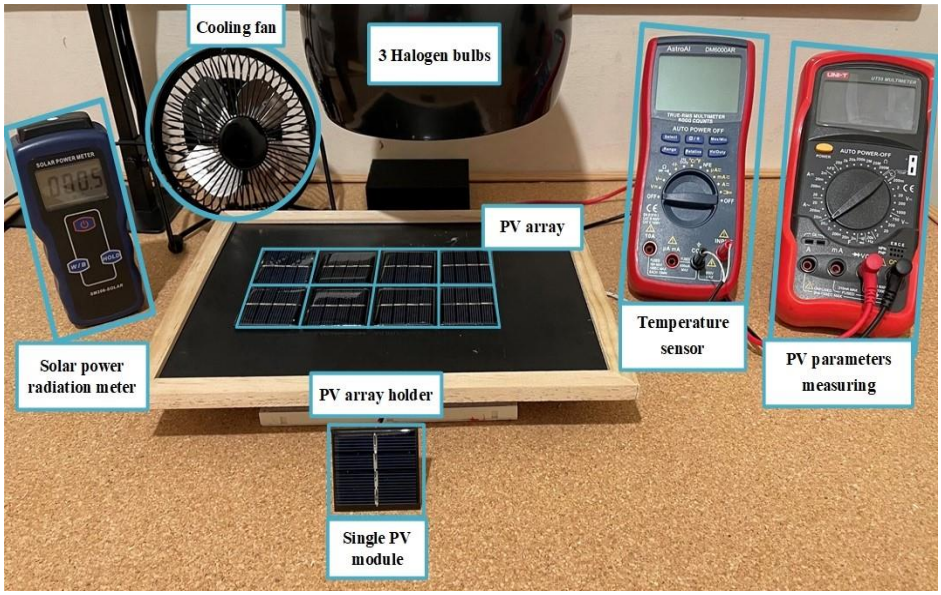

Figure 4.5. Experimental prototype to investigate before and after arranging the I-V and P-V characteristics of the PV array by offline reconfiguration.

Following the experiment, the results are shown in the

Table 4.2 below.

Table 4.2: The output of the I-V tracer parameters.

I-V Parameters	*Accuracy of Measurement*	*Range of Measurement*
Voltage measurement (V)	±1%	7.5-7.8
Current measurement (A)	±1%	0.170-0.174
Temperature (°C)	±2%	+25 to +50
Irradiance (W/m^2)	±3%	0-1200

Furthermore, the requirements for describing the setup of this experiment Figure 4.6 illustrated in order to obtain the performance characteristics of PV single and array modules must be identified below:

- As in the full sun, a solar cell is positioned at a fixed distance from a light source (using artificial sunlight).
- The voltage probe was connected to the solar cell's output, with the black lead to the negative and the red lead to the positive.
- The current probe was connected in series with a battery load to the solar cell's output.
- Figure 4.2 displayed the I-V and P-V using Python MPPT code and then saved output data.
- In a PV array, the measurement was repeated with a different solar cell.
- The calculation was repeated with different illumination levels, to get the best results, such as changing the artificial sunlight.

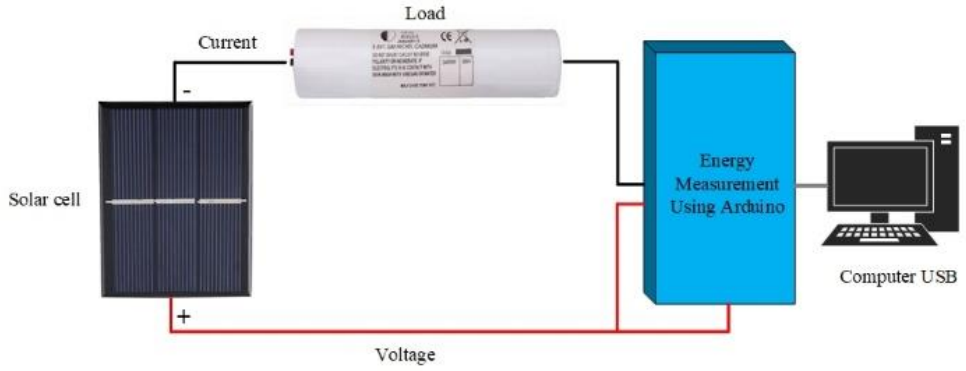

Figure 4.6. Experimental setup to investigate the I-V and P-V characteristics of the single module and array.

Following the experiment, the results of the healthy PV modules are shown in Table 4.3 below.

Table 4.3: The output of the I-V tracer parameters.

PV cell parameters	*Values*	*Units*
Voltage Cell	2.27	V
Current Cell	0.16	A
Power Cell	0.36	W
Voltage Array	18.16	V
Current Array	0.16	A
Power Array	2.91	W

4.2 Analysis of the Study

4.2.1.1 2 × 4 PV Array Before Rearrangement

Table 4.3 shows the exact PV module parameters in the experiment. A plastic cling film is used to cover the four modules positioned in both two strings (module11, module13, module22, module23 and module24) in order to achieve the aging condition. The maximum short-circuits currents in a healthy module are set as per unit (1 p.u.), from standard test conditions STC (1000 W/m^2) at 25 °C module temperature. Figure 4.8 shows the test results seen before the arrangement, with the module output characteristics for both strings shown in Table 4.4 and illtreats in Figure 4.7.

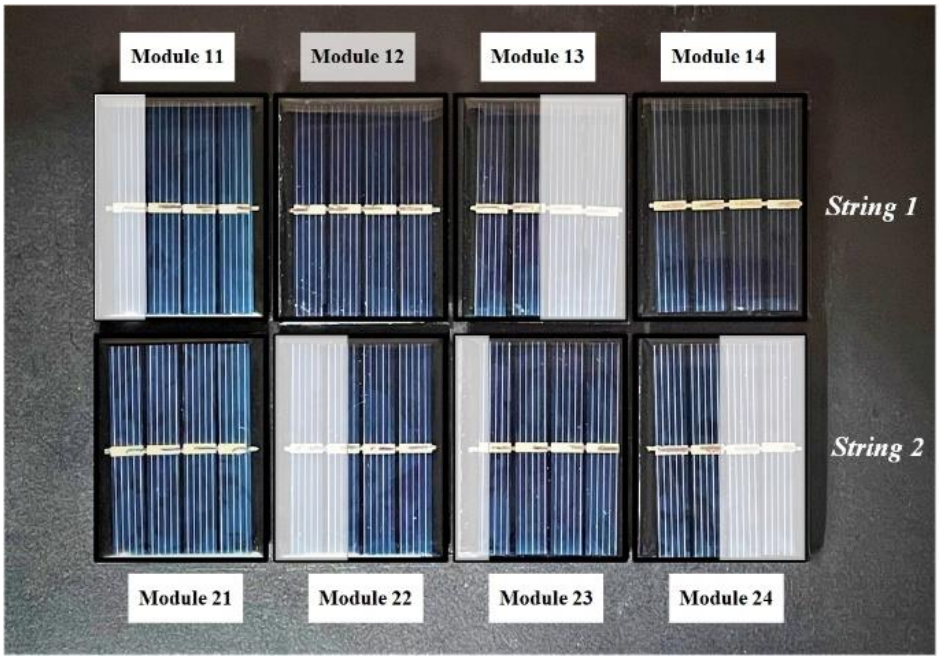

Figure 4.7. The non-uniform aging PV modules without reconfiguration (covered with a black plastic membrane)

Table 4.4: A 2 × 4 PV array before reconfiguration.

The PV age module condition (per unit)				
0.7 p.u.	1 p.u.	0.5 p.u.	1 p.u.	*Row (string 1)*
1 p.u.	0.6 p.u.	0.9 p.u.	0.5 p.u.	*Row (string 2)*

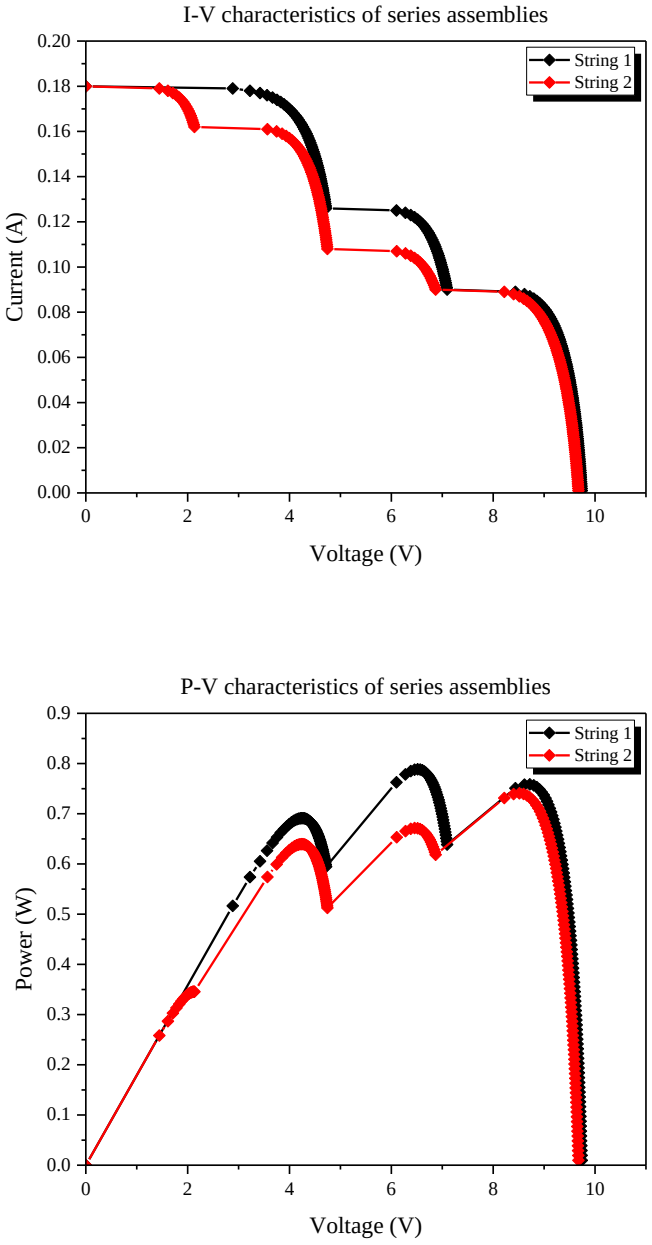

Figure 4.8. The 2 × 4 PV modules output characteristics of I-V and P-V before reconfiguration.

Before applying the suggested PV array method, and I-V and P-V were not reconfigured, the PV array maximum output power was 1.498 W. The voltage was 7.8 V, and the current was 0.174 A, respectively, depicted in Table 4.5 and Figure 4.9 describes the final parameters before rearrangement.

Table 4.5: PV array 2 × 4 output parameters before reconfiguration.

Parameters	*Parameters*	*Parameters*
Voltage	7.8	V
Current	0.174	A
Power	1.498	W

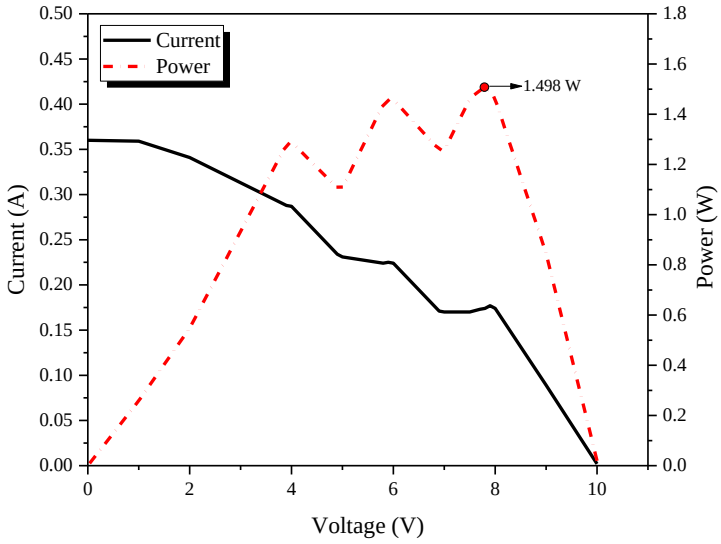

Figure 4.9. The outputs of the 2 × 4 PV array (before rearrangement)

4.2.1.2 2 × 4 PV Array After Rearrangement

Once the suggested strategy is used on the PV array, nine iterations were used to define the optimal reconfiguration for a 2 × 4 PV array with non-uniform aging, as depicted in Table 4.6. The last stage, with the smallest amount of swap times seen in Figure 4.10, as well as greatest output power.

```
0.5 row 1, col 1 is swapped by 1.0  row 4, col 2
0.9 row 1, col 2 is swapped by 0.5  row 4, col 1
0.6 row 2, col 1 is swapped by 1.0  row 3, col 2
0.7 row 2, col 2 is swapped by 1.0  row 3, col 1
1.0 row 3, col 1 is swapped by 0.7  row 2, col 2
1.0 row 3, col 2 is swapped by 0.6  row 2, col 1
0.5 row 4, col 1 is swapped by 0.9  row 1, col 2
1.0 row 4, col 2 is swapped by 0.5  row 1, col 1

Total swaps: 8
>>>
```

Figure 4.10. Final iterations to obtain the ideal configuration for proposed method.

Identifying the optimal reconfiguration allowed the final stage to be reached through greater output power and reduced swap to the greatest degree. Thus, the ideal PV modules were replaced with ones that could boost final output power, described with:

- (PV module 11 in string 1 “swapped” with PV module 21 in string 2).
- (PV module 12 in string 1 “swapped” with PV module 13 in string 2).

This shows that the reconfiguration established the lowest swap times where only four PV modules shifted position to boost output power, while the others (module14, module22, module23 and module24) did not move, as seen in Figure 4.11. In addition, the PV module output properties of I-V and P-V after reconfiguration are depicted in Figure 4.12 as a series connection.

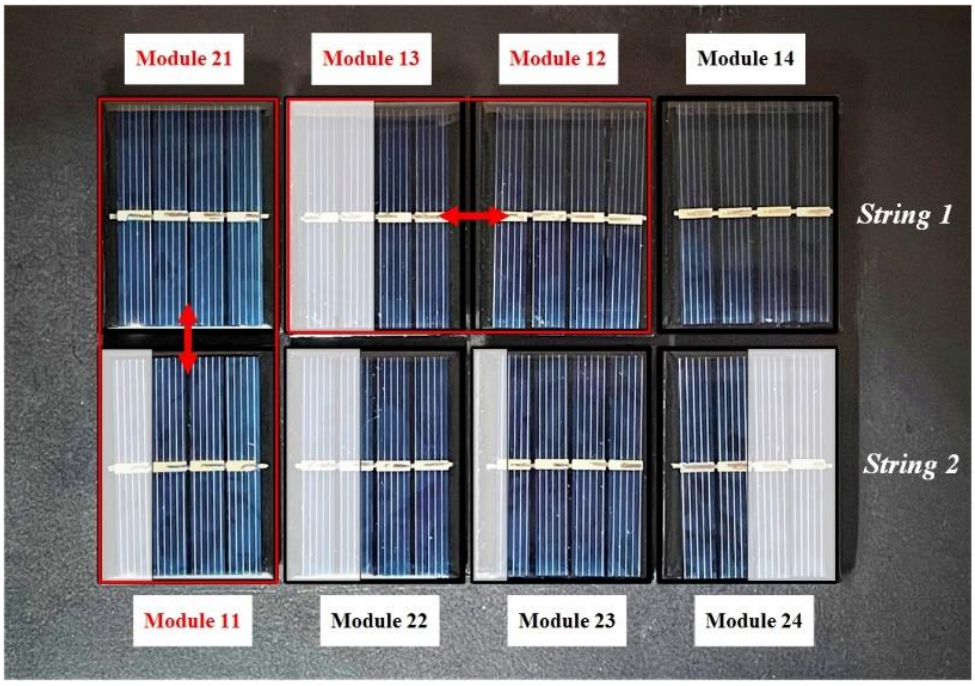

Figure 4.11. The non-uniform aging PV modules with reconfiguration (where 4 modules have swapped marked with red boxes).

Table 4.6: A 2 × 4 PV array after reconfiguration

The PV age module condition (per unit)				
1 p.u.	0.5 p.u.	1 p.u.	1 p.u.	*Row (string 1)*
0.7 p.u.	0.6 p.u.	0.9 p.u.	0.5 p.u.	*Row (string 2)*

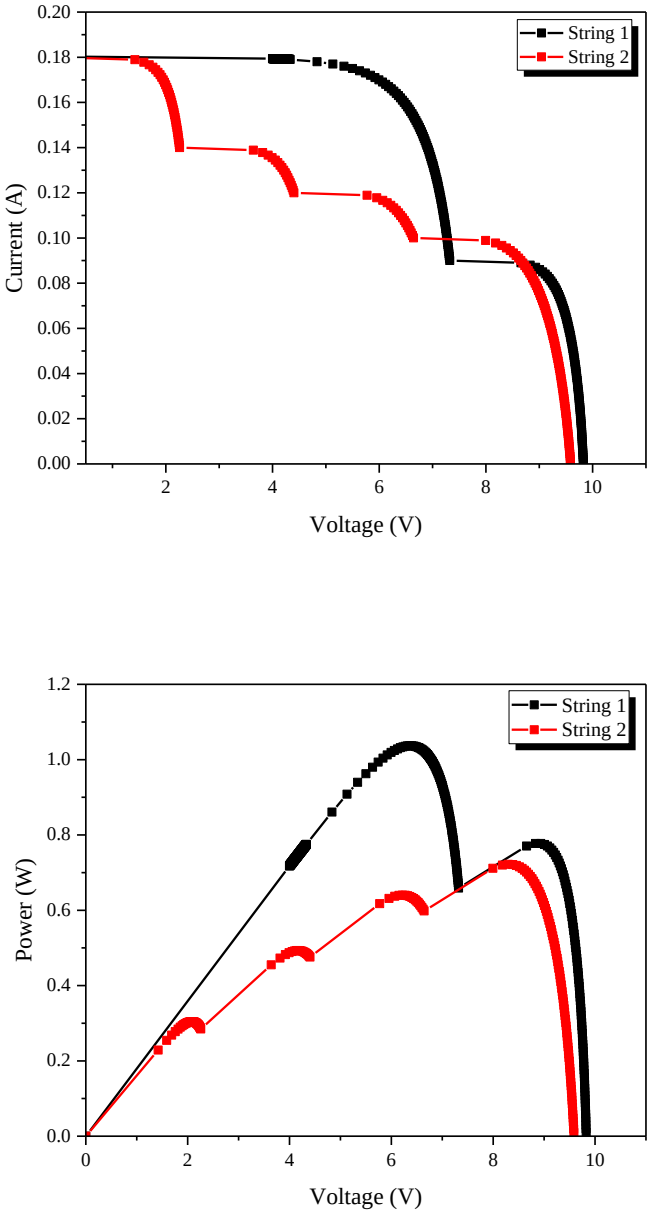

Figure 4.12. The series 2 × 4 PV modules output characteristics of I-V and P-V after reconfiguration.

Once the suggested PV array solution was applied, the algorithm's potential to uncover the optimal arrangement was ensured through simulating the two PV structures. The peak power output following rearrangement is shown in Figure 4.13,which was 1.669 W, with a PV array output voltage of 6 V and an MPPT current of 0.258 A. The computational time for the suggested algorithm for describing aged 2 × 4 PV array rearrangements are shown in Table 4.7.

Table 4.7: PV array 2 × 4 output parameters after reconfiguration.

Parameters	*Parameters*	*Parameters*
Voltage	6	V
Current	0.258	A
Power	1.669	W

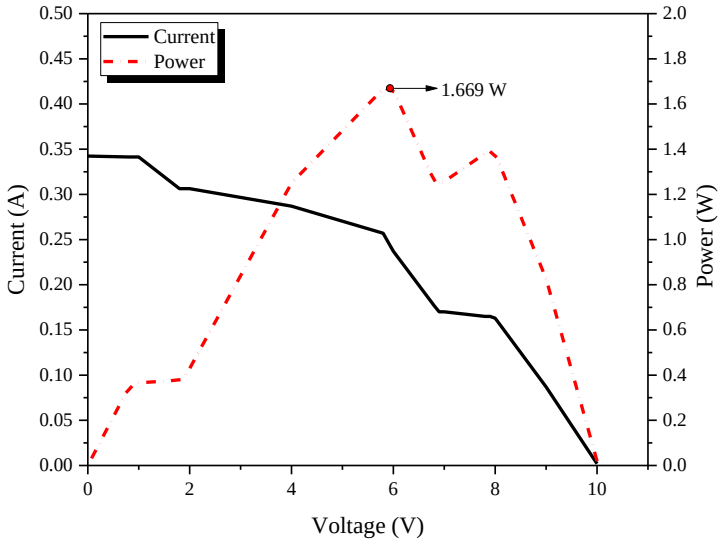

Figure 4.13. The outputs of the 2 × 4 PV array (after rearrangement).

4.3 Dissection

For PV arrays of varying dimensions, the proposed algorithm can be applied to support maximum power output. Besides, for the 2 × 4 PV arrays, the algorithm considered important aging factors for rearranging specific PV module positions in each string, therefore enhancing the impact of bypass diodes. In turn, all string PV modules suffered from mismatch loss to a smaller degree, but voltage limits were not considered. Additional studies which examine this area can be found [210], [225], [41]. The recommended algorithm has the ability to sort the PV modules iteratively and hierarchically. The produced P–V curves seen in Figure 4.14 depict the PV array reconfiguration strategy's potential to increase system efficiency and lower operating costs.

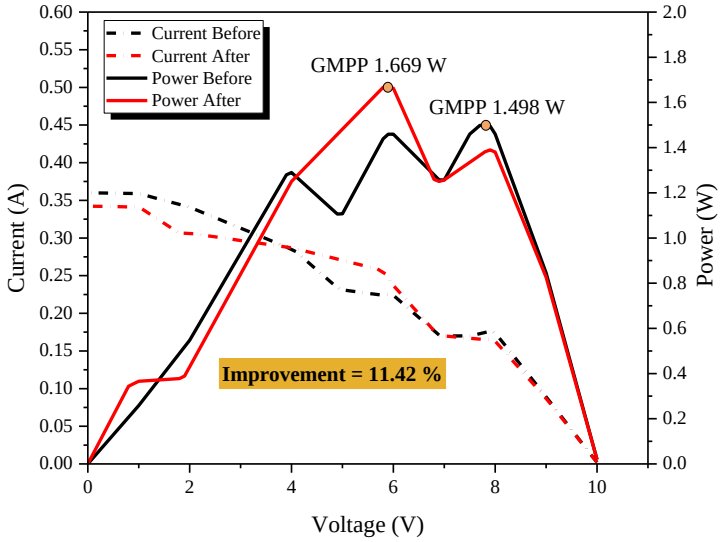

Figure 4.14. The outputs of PV arrays before and after rearrangements, including a percentage of improvement.

Besides, the proposed algorithm can bring about rapid results, as there is no requirement to access all potential configurations of a specific PV Array (Online or Offline), which streamlines the action. This was seen where the algorithm established the ideal PV module configuration in only nine steps, with an average computational time of 0.134325 s. Therefore, by finding an ideal module configuration quickly, the real-time implementation process is sped up. Another benefit of the proposed algorithm is that it only rearranges impacted PV modules, with others not being affected. Also, this chapter shows that rearrangement increases maintenance management efficiency. Notably, expenditures and benefits are the critical decision criteria for offline reconfiguration methods. The selected methods increase reconfiguration efficiency, profitability, and cost-effectiveness during operation, as developing an aging map for PV plants is crucial. Reconfiguration can be supported as a step towards maximising PV plant strengths once profitability and more outstanding power production outweigh the expense of labor force rearrangement. Once these elements are considered, the proposed methodology would provide many

benefits. PV module positions would be replaced in line with the workforce instead of replacing all aging modules with new ones.

4.4 Conclusion

The current chapter concentrates on non-uniform aging processes in PV arrays. The included experiment presents the finding that PV array power production is impacted by the position of aged PV modules in the PV arrays. Thus, the suggested algorithm for the reconfiguration of PV arrays will help limit the effect of PV arrays with non-uniform aging while boosting the amount of power produced while overcoming the need to replace aged PV modules. The algorithm arranges the PV modules repetitively and hierarchically to mitigate the incompatibility effect of non-uniform aging amongst PV modules. In turn, the output power increased by 11.42 % for the 2 × 4 PV array, as shown in Figure 4.14. Therefore, it is suggested that the proposed approach for the reconfiguration of PV modules can raise the maximum power output of PV systems with less relays than the current online approaches offer for PV array reconfiguration. It is concluded that the ideal reconfiguration plan is based on the cost and benefit involved. Thus, finding the aging map of a PV plant is necessary for an efficient reconfiguration approach to be found, which will also raise profits. The swapping cost of PV modules relating to the workforce should also be found. By comparing the above values, the PV plant owner can decide whether to undertake the suggested reconfiguration if the increase in profit through more significant power generation would surpass the expense incurred by the workforce's efforts in this regard. Thus, the suggested strategy's main benefit is to suggest suitable swaps of PV modules' positions only through a workforce.

Chapter 5. INVESTIGATING FOURTEEN COUNTRIES TO MAXIMUM THE ECONOMY BENEFIT BY USING OFFLINE RECONFIGURATION FOR MEDIUM SCALE PV ARRAY ARRANGEMENTS

The content of this chapter has been published in the following paper:

1. M. Alkahtani et al., "Investigating Fourteen Countries to Maximum the Economy Benefit by Using Offline Reconfiguration for Medium Scale PV Array Arrangements," Energies, vol. 14, no. 1, 2021, doi: 10.3390/en14010059.

An AI-based algorithm is presented in previous chapters 3 and 4. The included economy benefits present the finding that PV array power production is impacted by the position of aged PV modules in the PV arrays, which was not presented in the previous chapters. Thus, the suggested current chapter is proof that the reconfiguration of PV array through the MATLAB/Python software in the previous chapters has been scientifically tested. Therefore, the strategy offers the minimum swapping/replacing times to maximize the output power and improve electric revenue by reducing maintenance costs. However, solar power plants can achieve better financial increments within a decade.

5.1 The Offline Reconfiguration Strategy without Replacing Extremely Aged Modules

According to the authors of [131, 210] the short-circuit current (I_{SC}) varies more than the open-circuit voltage (V_{OC}) when a PV cell reaches an aging experiment, due to the p-n junction qualities of the cell. This work assesses the PV module's aging

status based on the I_{SC} while keeping the V_{OC} unchanged for various aging conditions. Besides, it is believed that uniform aging is experienced by each of the cell units in the same PV module so that the entire PV module can be characterised by a single maximum I_{SC} of each of the cell units. In the case of in-series PV modules forming a PV array, their output currents will be the same, while the module's total voltages will be applied to obtain the output voltage [210].

In the long service, the PV array's non-uniform aging is a well-known phenomenon resulting from dust, water corrosion, and shadow [41, 233]. An example of enhancement in aging and the global maximum power point (GMPP) is illustrated in Figure 5.2. It is important to change the PV modules' position based on the aging information regarding aging improvement. Once rearranged, the characteristic of the PV array output can still involve multi-maximum power points. GMPP refers to the algorithm that determines the global maximum power point. Further, the PV module parameters are as shown in Table 5.1. The modules are covered using a plastic membrane in Figure 5.1 to determine the aging condition. Further, the pre-rearrangement 10×10 PV array GMPP is 3.969 kW as a medium condition, while the post-rearrangement of the array GMPP is 4.2 kW, as shown in Figure 5.2 and Figure 5.4. There is a 5.7% improvement in the entire array efficiency when the array's working end is the GMPP (Figure 5.2). Hence, the proposed aging array rearrangement complements the GMPP.

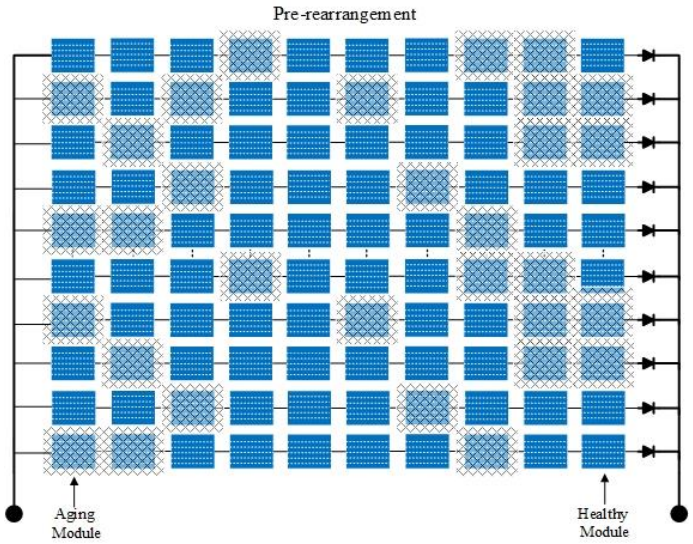

Figure 5.1: The aging modules were covered with a plastic cap for clarification.

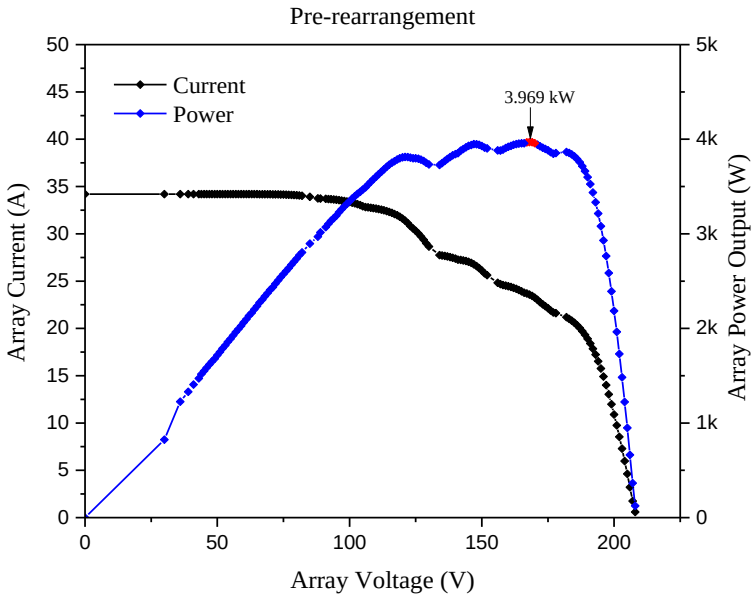

Figure 5.2: The output result for the 10 × 10 PV array without rearrangement.

Table 5.1: PV array 10×10 parameters before arrangements.

Pre-arrangement									
0.9 p.u.	0.9 p.u.	0.9 p.u.	0.4 p.u.	0.9 p.u.	0.9 p.u.	0.6 p.u.	0.9 p.u.	0.8 p.u.	0.9 p.u.
0.6 p.u.	0.9 p.u.	0.5 p.u.	0.9 p.u.	0.9 p.u.	0.8 p.u.	0.9 p.u.	0.9 p.u.	0.6 p.u.	0.8 p.u.
0.9 p.u.	0.8 p.u.	0.9 p.u.	0.9 p.u.	0.9 p.u.	0.9 p.u.	0.9 p.u.	0.9 p.u.	0.8 p.u.	0.8 p.u.
0.9 p.u.	0.9 p.u.	0.8 p.u.	0.9 p.u.	0.9 p.u.	0.9 p.u.	0.7 p.u.	0.9 p.u.	0.9 p.u.	0.9 p.u.
0.5 p.u.	0.6 p.u.	0.9 p.u.	0.9 p.u.	0.9 p.u.	0.9 p.u.	0.9 p.u.	0.7 p.u.	0.9 p.u.	0.9 p.u.
0.9 p.u.	0.9 p.u.	0.9 p.u.	0.4 p.u.	0.9 p.u.	0.9 p.u.	0.9 p.u.	0.8 p.u.	0.5 p.u.	0.9 p.u.
0.6 p.u.	0.9 p.u.	0.9 p.u.	0.9 p.u.	0.9 p.u.	0.8 p.u.	0.9 p.u.	0.9 p.u.	0.6 p.u.	0.8 p.u.
0.9 p.u.	0.8 p.u.	0.9 p.u.	0.9 p.u.	0.9 p.u.	0.9 p.u.	0.9 p.u.	0.9 p.u.	0.8 p.u.	0.8 p.u.

0.9 p.u.	0.9 p.u.	0.8 p.u.	0.9 p.u.	0.9 p.u.	0.9 p.u.	0.7 p.u.	0.9 p.u.	0.9 p.u.	0.9 p.u.
0.4 p.u.	0.6 p.u.	0.9 p.u.	0.9 p.u.	0.9 p.u.	0.9 p.u.	0.9 p.u.	0.7 p.u.	0.9 p.u.	0.9 p.u.

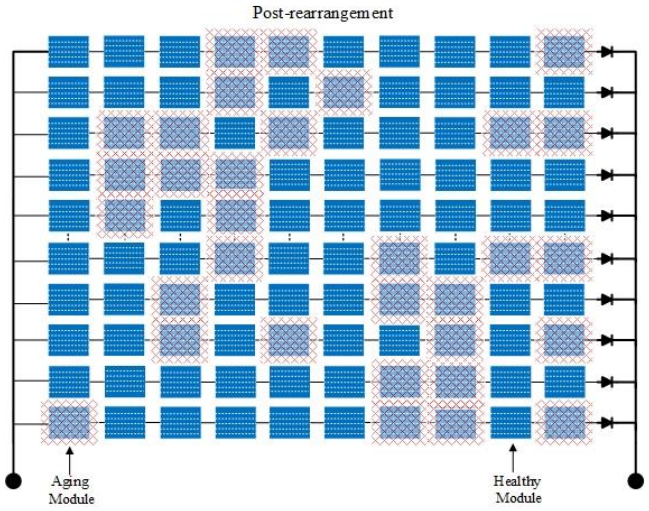

Figure 5.3: The aging modules were covered with a plastic cap for clarification.

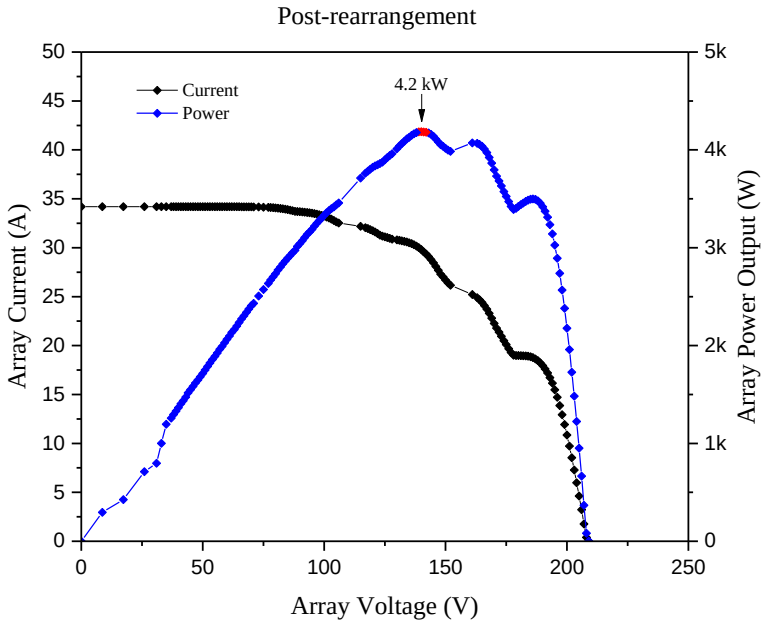

Figure 5.4: The output result for the 10 × 10 PV array with rearrangement.

To enhance effective service time, two important steps should be followed. First is the PV array fault diagnosis and second is the PV array reconfiguration. PV array fault diagnosis involves four well-known methods: thermal camera [234], time-

domain reflectometry (TDR) [131, 235], applying voltage/current sensors, and earth capacitance measurement (ECM) [235]. The thermal imaging camera can adapt to the faulty PV array's non-uniform temperature distribution to locate the defective PV module in the background of the online application [236]. The disconnection of the PV modules can be located using an ECM, and the degradation of the PV arrays can be calculated using a TDR. However, ECM and TDR can only be utilized in an offline fault diagnosis [234]. Power loss analysis is recommended concerning scale PV array fault diagnosis [126, 127]. To reconfigure the PV array, [212, 237] provided an example for small-scale reconfiguration. The authors in [221] suggested a classical optimization algorithm (COA) for reconfiguring (RTCT) reconfigurable total cross-tied arrays. A gene evaluation algorithm (GEA) was applied as the COA requires strong computational effort to minimise costs.

Furthermore, in small-scale PV arrays, the look-up table method has been developed, which cannot be used effectively for large PV arrays [237]. [231] Generated a thorough search algorithm [230] devised (sorting algorithm) according to the best and worst paradigm to make the configuration faster. The fuzzy logical algorithm was also suggested in [228] for identifying the best reconfiguration. Additionally, [231] summarized the most effective online reconfiguration concerning the PV array. However, no reports on large-scale PV array reconfiguration are available. PV array reconfiguration is currently mainly used by relay networks that need many relays and have a high device cost. In terms of large-scale PV arrays, the only viable option for reconfiguring PV is to swap PV modules offline by human labor. An example of such a solution is presented in Figure 5.5 and Figure 5.6).

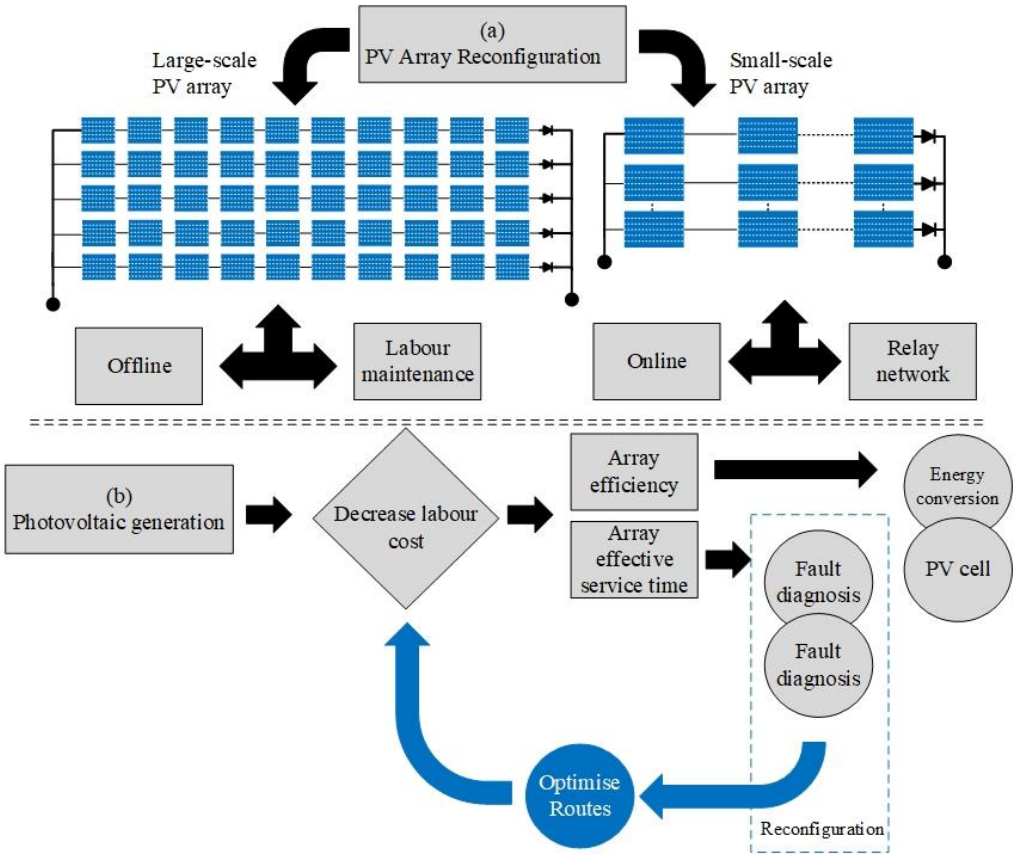

Figure 5.5: PV array reconfiguration considering the labor cost.

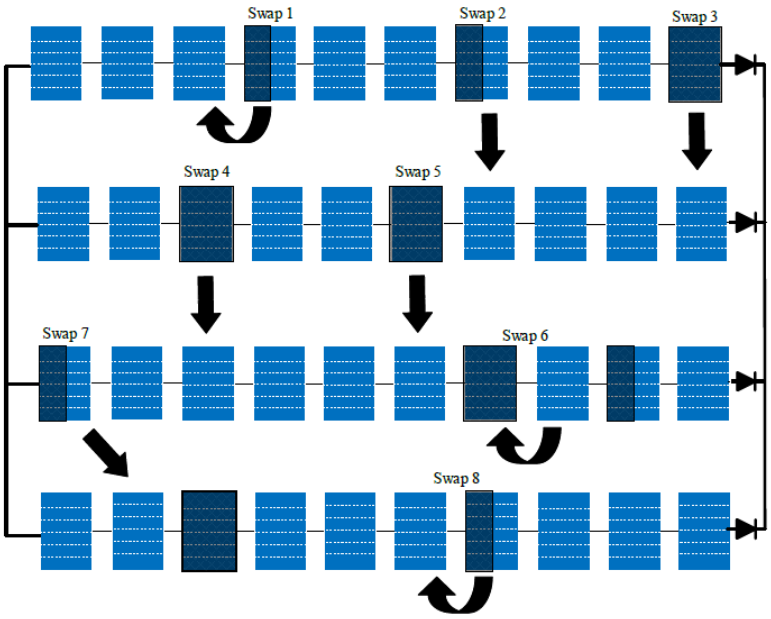

Figure 5.6: An example of the offline reconfiguration to swap PV modules through human labor in location.

Before flawed PV modules are substituted at higher financial costs, reorganization of such modules can be undertaken via a remedial measure following the PV array aging map's identification. A variety of reconfiguration strategies are available in the case of PV arrays of large scale, differing in terms of the duration of line reconnection and wiring distances, which determine how efficient and expensive each strategy is. Reconfiguration cost modelling is important for establishing the best reconfiguration strategy. To minimise complexity, the number of reconfigured panels can be used to estimate that cost.

5.1.1.1 Cost Analysis of Rearrangements for PV Array

According to the survey, the PV array is assumed to need to be rebuilt on average once a year, and the PV array will produce 8 h of power per day. To swap panels from one position to another, a professional grid worker requires an average of 45 mints and 30 mints to install a new module [238].

Some criteria need to be identified to explain the economic benefit work outlined be-low for the aging PV collection:

- PV_{pre} is the PV array output power before arrangements
- PV_{post} is the output power after arrangements
- A_e is the additional electricity
- H_w is the average hourly wage of the manpower (60 min)
- E_p is the electricity price
- N_s is the number of swaps/replace
- T_s is the time per swap/replace
- C_{per} is the cost per swap/replace
- C_{sawp} is the cost of swaps

- $C_{replace}$ is the cost of replacing
- W_t Cost is the cost per watt peak (cents/Wp)
- S_s is the size per module (Wp)
- *USD* is the United States Dollar ($)

PV array output difference:

$$A_e = PV_{post} - PV_{pre} \tag{5.1}$$

Next, equations are subject to swap PV modules:

1. Compute the cost per swap

$$\mathrm{C}_{per} = \frac{45}{H_w} \times T_s \tag{5.2}$$

2. Compute the cost of swap

$$\mathrm{C}_{swap} = \mathrm{C}_{per} \times N_s \tag{5.3}$$

Here, equations are subject to replace PV modules:

1. Compute the cost per replace

$$\mathrm{C}_{per} = \frac{30}{H_w} \times T_s \tag{5.4}$$

2. Compute the cost of replace

$$\mathrm{C}_{replace} = (N_s \times New\ pnael) + (N_s \times C_{per}) \tag{5.5}$$

The total economic benefit in the next equations from swap/replace:

1. A year electric revenue

$$A_e \times 8 \times 365 \times year \times E_p - C_{swap/replace} \tag{5.6}$$

2. Total electric revenue

$$= \text{A year electric revenue} \times 10 \text{ years} \quad (5.7)$$

The cost-effectiveness of the topology reconstruction technique for PV arrays was validated by considering 2020 as the PV system benchmark, the average cost of electricity price, average handling cost associated with PV panel replacement, and average labor cost in various countries [239-242]. Table 5.2 outlines these aspects.

Table 5.2: Electricity price and labor cost in 2020.

Country	*Electricity Prices $/kWh*	*Hourly Wage $/hr*	*Cost Per Swap $/time*	*Cost Per Replace $/time*
Saudi Arabia	0.059	7.98	5.98	3.99
Pakistan	0.108	1.42	1.07	0.71
India	0.097	1.19	0.89	0.60
France	0.177	24.87	18.65	12.44
United Kingdom	0.242	17.2	12.9	8.60
Germany	0.301	27.91	20.93	13.96
Greece	0.179	8.28	6.21	4.14
Cyprus	0.263	7.11	5.21	3.56
Jamaica	0.219	1.24	0.93	0.62
China	0.091	9.57	7.17	4.79
Japan	0.249	26.33	19.74	13.17
Australia	0.227	33.35	25.02	16.68
Brazil	0.127	6.05	4.54	3.03
US states	0.126	15.47	11.8	7.78

The following part explores two cases regarding the economic advantages of pre-post arrangements of the proposed method.

5.2 Cases Studies and Simulation Results

5.2.1.1 Case 1 (Arrange Aging Modules of 10 × 10 PV Array)

Under typical test conditions of 1000 W/m2 irradiance and 25 °C module temperature, a normal module has a maximum short-circuit current of 1 p.u. (STC). Table 5.3 shows a standard large-scale PV array with non-uniform aging, which serves as a testing branch, with every number denoting the highest aging-related output power. As is conventional for PV arrays available on the market, every string contains PV

modules within a series connection, while the strings have a parallel connection (SP). Furthermore, the aging factors are in the spectrum of 0.9–0.4 p.u. (Table 5.3), so the plotting of the I–V and P–V curves were undertaken as shown in Figure 5.7, with the suggested algorithm enabling output power enhancement of 3.87% for the 18-kW 10 × 10 PV array and 1.76% for the 43-kW 10 × 10 PV array, respectively. The increase in power was reflected by the fact that the mean average computation time was 0.129375 s.

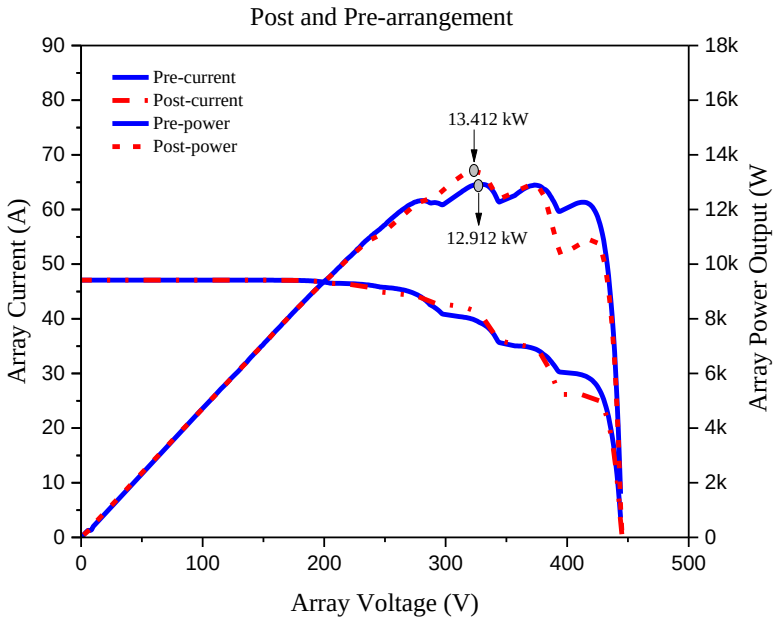

Figure 5.7: The outputs associated with the two types of 10 × 10 PV arrays of 18-kW before and after reconfiguration.

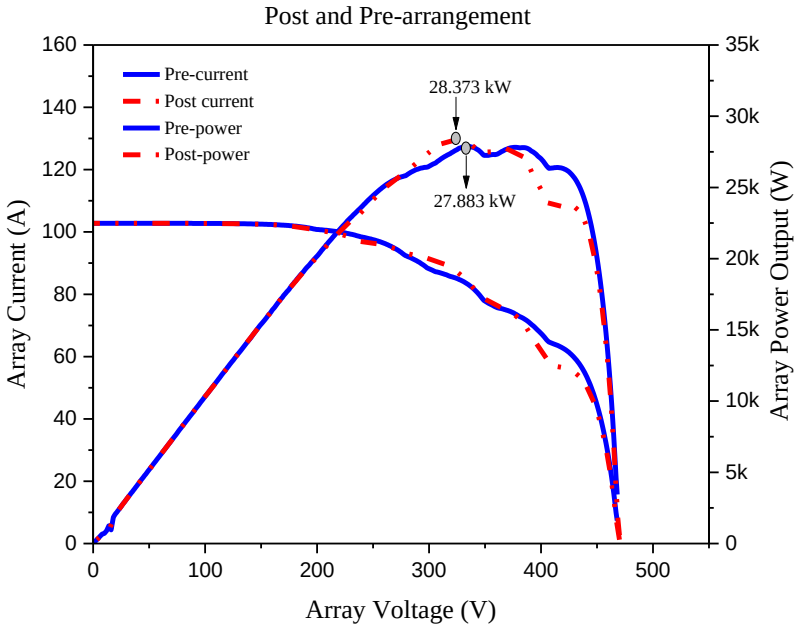

Figure 5.8: The outputs associated with the two types of 10 × 10 PV arrays of 43-kW before and after reconfiguration.

Table 5.3: The parameters associated with the two types of 10 × 10 PV arrays (i.e., 18-kW and 43-kW) after application of reconfiguration in 14 different countries.

Pre-arrangement									
0.9 p.u.	0.9 p.u.	0.9 p.u.	0.4 p.u.	0.9 p.u.	0.9 p.u.	0.6 p.u.	0.9 p.u.	0.8 p.u.	0.9 p.u.
0.6 p.u.	0.9 p.u.	0.5 p.u.	0.9 p.u.	0.9 p.u.	0.8 p.u.	0.9 p.u.	0.9 p.u.	0.6 p.u.	0.8 p.u.
0.9 p.u.	0.8 p.u.	0.9 p.u.	0.9 p.u.	0.9 p.u.	0.9 p.u.	0.9 p.u.	0.9 p.u.	0.8 p.u.	0.8 p.u.
0.9 p.u.	0.9 p.u.	0.8 p.u.	0.9 p.u.	0.9 p.u.	0.9 p.u.	0.7 p.u.	0.9 p.u.	0.9 p.u.	0.9 p.u.
0.5 p.u.	0.6 p.u.	0.9 p.u.	0.9 p.u.	0.9 p.u.	0.9 p.u.	0.9 p.u.	0.7 p.u.	0.9 p.u.	0.9 p.u.
0.9 p.u.	0.9 p.u.	0.9 p.u.	0.4 p.u.	0.9 p.u.	0.9 p.u.	0.9 p.u.	0.8 p.u.	0.5 p.u.	0.9 p.u.
0.6 p.u.	0.9 p.u.	0.9 p.u.	0.9 p.u.	0.9 p.u.	0.8 p.u.	0.9 p.u.	0.9 p.u.	0.6 p.u.	0.8 p.u.
0.9 p.u.	0.8 p.u.	0.9 p.u.	0.9 p.u.	0.9 p.u.	0.9 p.u.	0.9 p.u.	0.9 p.u.	0.8 p.u.	0.8 p.u.
0.9 p.u.	0.9 p.u.	0.8 p.u.	0.9 p.u.	0.9 p.u.	0.9 p.u.	0.7 p.u.	0.9 p.u.	0.9 p.u.	0.9 p.u.
0.4 p.u.	0.6 p.u.	0.9 p.u.	0.9 p.u.	0.9 p.u.	0.9 p.u.	0.9 p.u.	0.7 p.u.	0.9 p.u.	0.9 p.u.
Post-arrangement									
0.9 p.u.	0.9 p.u.	0.9 p.u.	0.4 p.u.	0.8 p.u.	0.9 p.u.	0.9 p.u.	0.9 p.u.	0.9 p.u.	0.8 p.u.
0.9 p.u.	0.9 p.u.	0.9 p.u.	0.4 p.u.	0.9 p.u.	0.7 p.u.	0.9 p.u.	0.9 p.u.	0.9 p.u.	0.9 p.u.
0.9 p.u.	0.9 p.u.	0.7 p.u.	0.9 p.u.	0.8 p.u.	0.9 p.u.	0.9 p.u.	0.9 p.u.	0.8 p.u.	0.6 p.u.
0.9 p.u.	0.5 p.u.	0.5 p.u.	0.8 p.u.	0.9 p.u.	0.9 p.u.	0.9 p.u.	0.9 p.u.	0.9 p.u.	0.9 p.u.
0.9 p.u.	0.8 p.u.	0.9 p.u.	0.6 p.u.	0.9 p.u.	0.9 p.u.	0.9 p.u.	0.9 p.u.	0.9 p.u.	0.9 p.u.
0.9 p.u.	0.9 p.u.	0.9 p.u.	0.6 p.u.	0.9 p.u.	0.9 p.u.	0.8 p.u.	0.9 p.u.	0.8 p.u.	0.8 p.u.
0.9 p.u.	0.9 p.u.	0.4 p.u.	0.9 p.u.	0.9 p.u.	0.9 p.u.	0.6 p.u.	0.8 p.u.	0.9 p.u.	0.9 p.u.
0.9 p.u.	0.9 p.u.	0.7 p.u.	0.9 p.u.	0.8 p.u.	0.9 p.u.	0.9 p.u.	0.8 p.u.	0.9 p.u.	0.5 p.u.
0.9 p.u.	0.9 p.u.	0.9 p.u.	0.9 p.u.	0.9 p.u.	0.9 p.u.	0.7 p.u.	0.6 p.u.	0.9 p.u.	0.9 p.u.
0.8 p.u.	0.9 p.u.	0.9 p.u.	0.9 p.u.	0.9 p.u.	0.9 p.u.	0.8 p.u.	0.6 p.u.	0.9 p.u.	0.6 p.u.

5.2.1.2 Scenario One (Initial–Final Rates Return of Electricity Revenue)

Figure 5.7 and Figure 5.8 illustrates the output power enhancement in the case of a 10 × 10 PV array. At the same time, Table 5.3 details the simulation outcomes based on the cost of electric power and labor in fourteen countries necessitating forty-four manual swap times. Table 6 indicates the initial and final rate returns of electric revenue for the two types of 10 × 10 PV arrays (i.e., 18-kW and 43-kW), without considering the most remarkable economic advantage. Thus, in the 18-kW 10 × 10 PV array, the post-reconfiguration electric revenue increased by 3.87%. In the case of the 43-kW array, the increase achieved by the suggested approach was 1.76%, according to Table 5.4.

Table 5.4: The original and final rate returns of electric revenue associated with the two types of 10 × 10 PV arrays, without taking into account the greatest annual economic advantage.

Country	Initial Rate Return of Electric Revenue 18-kW ($)	Final Rate Return of Electric Revenue 18-kW ($)	Initial Rate Return of Electric revenue 43-kW ($)	Final Rate Return of Electric revenue 43-kW ($)
Saudi Arabia	17,795.83	18,484.95	33,625.78	34,216.7
Pakistan	4071.93	4229.61	8793.18	8947.71
India	3657.19	3798.81	7897.58	8036.37
France	46,714.07	48,523.01	100,877.35	102,650.11
United Kingdom	36,496.54	37,909.82	78,812.97	80,197.99
Germany	56,743.08	58,940.38	122,534.63	124,687.99
Greece	20,246.53	21,030.55	43,721.66	44,490.01
Cyprus	19,831.8	20,599.76	42,826.06	43,578.66
Jamaica	8256.97	8576.71	17,830.62	18,143.97
China	17,154.88	17,819.18	44,454.42	45,235.64
Japan	46,940.28	48,757.98	121,639.03	12,3776.65
Australia	59,910.13	62,230.07	147,855.74	150,454.07
Brazil	14,364.86	14,921.12	31,020.4	31,565.53
US states	28,503.5	29,607.26	71,810.99	73,072.96

5.2.1.3 Scenario Two (Net Profits of Additional Electric Revenue)

Regarding the cost of high labor and low electricity price in some countries, Table 5.5 and Equation (5.4) reflect that, by reducing the number of swap times, the suggested approach can make the offline reconfiguration more cost-effective, whilst also significantly enhancing overall profit (Table 5.6). However, it is unclear how the process benefits profitability in countries where labor price is high. Still, the electricity price is low, in which case the labor cost can be diminished. Still, the electric revenue profit cannot be increased.

Table 5.5: Assessment of economic advantages taking into account minimum handling times.

Country	*Cost of Swapping 44 Modules $/time*	*Best Cost-Effective Maintenance Period Time*	*Additional Electric Revenue 18-kW ($)*	*Cost of Swapping 44 Modules $/time*	*Best Cost-Effective Maintenance Period Time*	*Additional Electric Revenue 43-kW ($)*
Saudi Arabia	263.34	8	607.9	263.34	7	327.58
Pakistan	46.86	1	110.82	46.86	1	107.67
India	39.27	1	102.35	39.27	1	99.52
France	820.71	7	988.23	820.71	7	952.05
United Kingdom	567.60	4	845.68	567.60	4	817.41

Germany	921.03	5	1276.27	921.03	5	1232.32
Greece	273.24	3	510.78	273.24	3	495.10
Cyprus	234.63	2	533.33	234.63	2	517.97
Jamaica	40.92	1	278.82	40.92	1	272.43
China	315.81	5	348.49	315.81	6	465.41
Japan	868.89	5	948.81	868.89	6	1268.73
Australia	1100.55	7	1219.39	1100.55	8	1497.78
Brazil	199.65	3	356.61	199.65	3	345.48
US states	510.51	6	593.25	510.51	7	751.46

Table 5.6: The original and final rate returns of electric revenue associated with the two types of 10 × 10 PV arrays, taking into account the greatest annual economic advantage.

Country	*The Initial Value of Electric Revenue without Considering Labor Cost 18-kW ($)*	*Net Profit of Final Value Electric Revenue by Considering Labor Cost 18-kW ($)*	*The Initial Value of Electric Revenue without Considering Labor cost 43-kW ($)*	*Net Profit of Final Value Electric Revenue by Considering Labor Cost 43-kW ($)*
Saudi Arabia	17,795.83	18,221.61	33,625.78	33,953.36
Pakistan	4071.93	4182.75	8793.18	8900.85
India	3657.19	3759.54	7897.58	7997.1
France	46,714.07	47,702.3	100,877.35	101,829.4
United Kingdom	36,496.54	37,342.22	78,812.97	79,630.39
Germany	56,743.08	58,019.35	122,534.63	123,766.96
Greece	20,246.53	20,757.31	43,721.66	44,216.77
Cyprus	19,831.8	20,365.13	42,826.06	43,344.03
Jamaica	8256.97	8535.79	17,830.62	18,103.05
China	17,154.88	17,503.37	44,454.42	44,919.83
Japan	46,940.28	47,889.09	121,639.03	122,907.76
Australia	59,910.13	61,129.52	147,855.74	149,353.52
Brazil	14,364.86	14,721.47	31,020.4	31,365.88
US states	28,503.5	29,096.75	71,810.99	72,562.45

The outcomes of the simulation are presented in Table 5.6. It can be seen that manual swap had to be performed forty-four times, according to the costs associated with electricity and labor force in the fourteen countries examined. The suggested algorithm considered one decade following PV module installation was used to determine the most remarkable economic advantage. Meanwhile, Table 5.5 indicates the extra electric revenue profit made possible by the (18-kW and 43-kW) PV array and the associated cost of labor, the calculation of which was undertaken based on Equations (5.2)–(5.8). Furthermore, the proportion of net electric revenue profit

achieved after the reconfiguration was carried out based on the suggested approach is provided in Figure 5.9 and Figure 5.10.

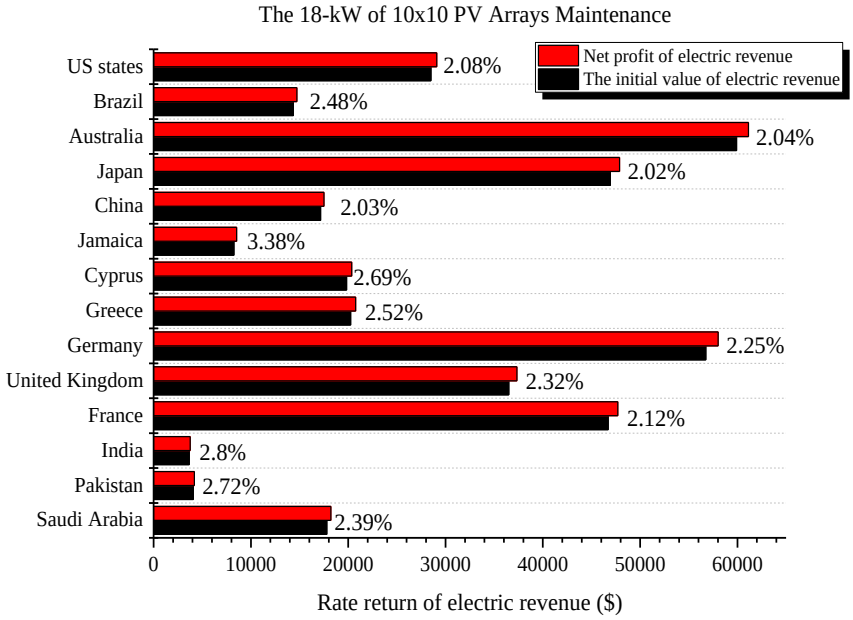

Figure 5.9: The increase in rate returns of electric revenue associated with the 18-kW of 10 x 10 PV arrays, taking into account the greatest annual economic advantage.

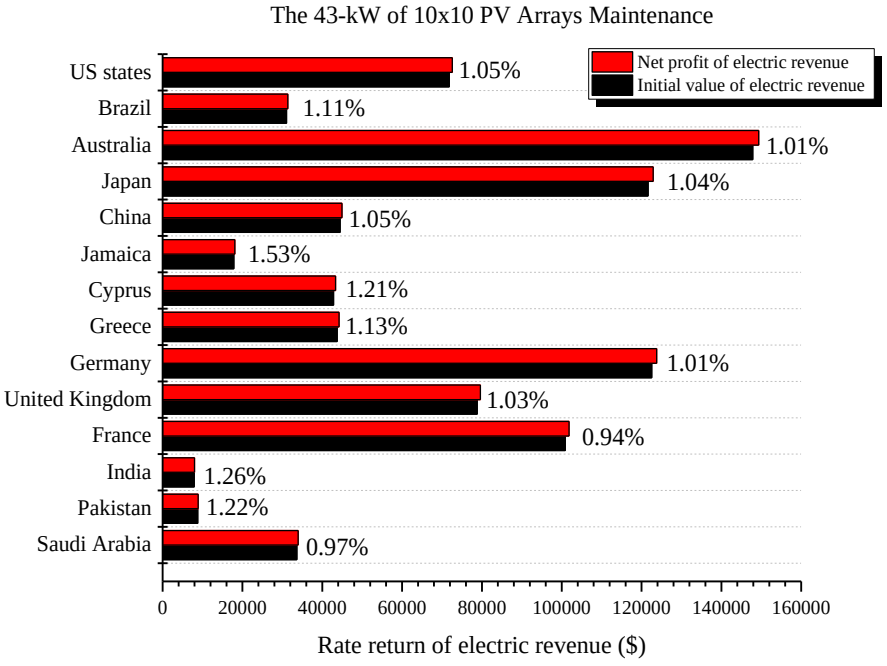

Figure 5.10: The increase in rate returns of electric revenue associated with the 43-kW of 10 x 10 PV arrays, taking into account the greatest annual economic advantage.

In order to achieve the maximum net profit return, the suggested algorithm yielded a particular maintenance time in each case. This explains the discrepancies that

have been noted concerning maintenance times. For example, the algorithm indicated that, in countries like Pakistan, India, and Jamaica, maintenance could be carried out in the first year to achieve a net profit from the electric revenue due to the high cost of electricity but low labor cost. On the other hand, the algorithm indicated that maintenance could be conducted in the second year in countries like Cyprus to better net profit from electric revenue. In contrast, maintenance can be conducted in the third year in Greece and Brazil and in the fourth year in the UK to benefit net profit. Furthermore, maintenance can be carried out in the fifth year in Germany, China, Japan, and in the sixth year in the US. Moreover, the increase in electric revenue profit in France and Australia could be enhanced by undertaking maintenance in the seven-year after PV installation, according to the suggested algorithm. Last, the algorithm indicated that in a country like Saudi Arabia maintenance can be carried out in the year eight to achieve a net profit from the electric revenue due to the low cost of electricity and high labor cost. Figure 5.11 and Figure 5.12 illustrates the increase in electric revenue.

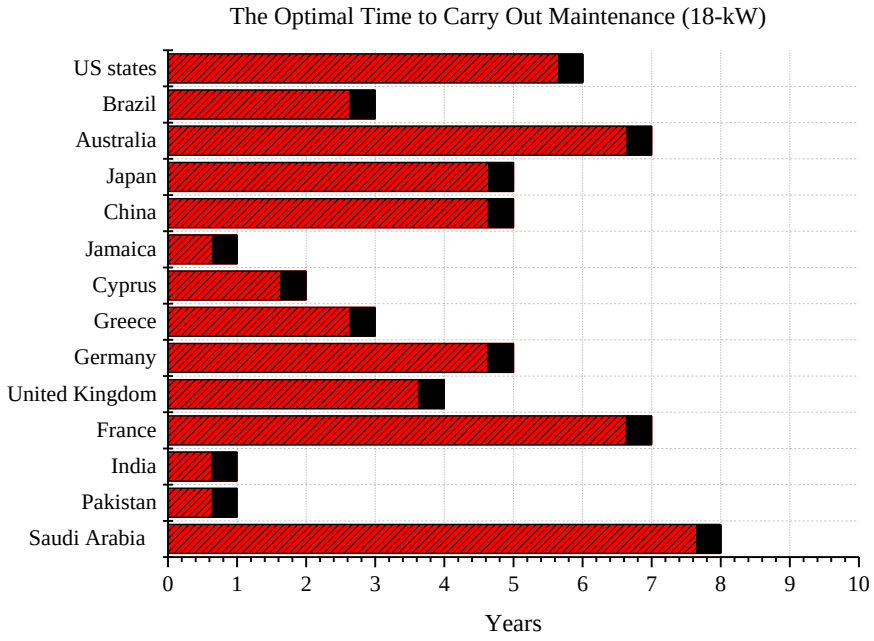

Figure 5.11: The year identified by the suggested algorithm as the optimal time to carry out maintenance in order to achieve the greatest economic advantage in 10*10 PV array (18-kW).

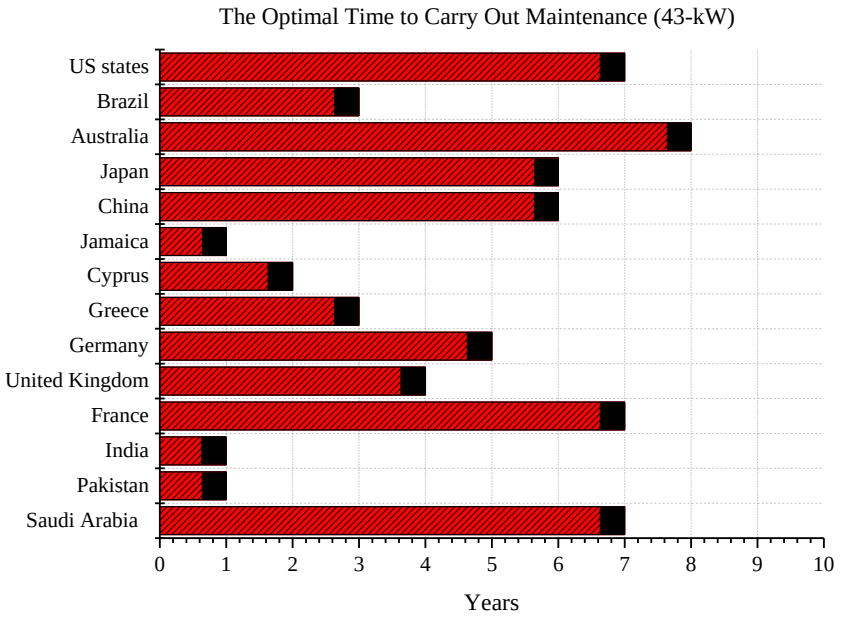

Figure 5.12: The year identified by the suggested algorithm as the optimal time to carry out maintenance in order to achieve the greatest economic advantage in 10*10 PV array (43-kW).

5.2.1.4 Case 2 (Combine Swap/Replace Aging Modules of 10 × 10 PV Array)

Concerning the second case that was explored, the outcomes produced by the assessment of the maintenance costs associated with the two types of PV arrays served as the basis for concluding concerning the extent to which the profit from the electric revenue could be increased to enhance the economic advantages in the fourteen countries that were considered. Besides, as indicated in Table 5.8 related to the conditions before reconfiguration, aging factors in the range of (0.9-0.4 p.u.) and lacking homogeneity were produced arbitrarily for a 10 x 10 PV array of large scale, which consisted of ten strings within a parallel connection and ten modules within a series connection. Once the aging factors were identified in the PV array, it is necessary to undertake the aged PV panel substitution with a new PV panel (1 p.u.). In other words, substitution is required in the case of all aged PV panels with less than (0.6 p.u.). The conditions refer to this after reconfiguration in Table 5.8. Furthermore, Table 5.8 also shows that, when the suggested method was applied, the PV array of 18 kW displayed an enhancement in the power of 11.35% after the reconfiguration. The same table reveals that the PV array of 43 kW achieved an enhancement in the power of 10.8% after the reconfiguration. Meanwhile, Figure 5.13 and Figure 5.14 illustrates the *I-V* curve's plotting and the *P-V* curve, which was accomplished in a mean computational time of 0.159364 s. Table 5.7 lists the parameters that need to be taken into account concerning electric power and labor costs in the fourteen countries examined.

Table 5.7: The PV array 10×10 parameters inputs.

Parameters input	*10 × 10 PV array 18 kW*	*10 × 10 PV array 43 kW*	*Unit*
Number of Replace	6	6	PV module
Number of Swap	38	38	PV module
Time per replace	30	30	Minute

Time per swap	45	45	Minute
Cost per panel	40	70	USD
Cost per watt peak	0.22	0.36	Cents/Wp
Size per module	180	430	Wp
Initial Output	12.912	27.883	kW
Final Output	15.957	33.990	kW
Difference	3.045	6.108	kW
Number of Replace	6	6	PV module
Number of Swap	38	38	PV module

Table 5.8: The parameters associated with the two types of 10x10 PV arrays (i.e. 18 kW and 43 kW) after application of reconfiguration in 14 different countries.

Pre-arrangement									
0.9 p.u.	0.9 p.u.	0.9 p.u.	0.4 p.u.	0.9 p.u.	0.9 p.u.	0.6 p.u.	0.9 p.u.	0.8 p.u.	0.9 p.u.
0.6 p.u.	0.9 p.u.	0.5 p.u.	0.9 p.u.	0.9 p.u.	0.8 p.u.	0.9 p.u.	0.9 p.u.	0.6 p.u.	0.8 p.u.
0.9 p.u.	0.8 p.u.	0.9 p.u.	0.9 p.u.	0.9 p.u.	0.9 p.u.	0.9 p.u.	0.9 p.u.	0.8 p.u.	0.8 p.u.
0.9 p.u.	0.9 p.u.	0.8 p.u.	0.9 p.u.	0.9 p.u.	0.9 p.u.	0.7 p.u.	0.9 p.u.	0.9 p.u.	0.9 p.u.
0.5 p.u.	0.6 p.u.	0.9 p.u.	0.9 p.u.	0.9 p.u.	0.9 p.u.	0.9 p.u.	0.7 p.u.	0.9 p.u.	0.9 p.u.
0.9 p.u.	0.9 p.u.	0.9 p.u.	0.4 p.u.	0.9 p.u.	0.9 p.u.	0.9 p.u.	0.8 p.u.	0.5 p.u.	0.9 p.u.
0.6 p.u.	0.9 p.u.	0.9 p.u.	0.9 p.u.	0.9 p.u.	0.8 p.u.	0.9 p.u.	0.9 p.u.	0.6 p.u.	0.8 p.u.
0.9 p.u.	0.8 p.u.	0.9 p.u.	0.9 p.u.	0.9 p.u.	0.9 p.u.	0.9 p.u.	0.9 p.u.	0.8 p.u.	0.8 p.u.
0.9 p.u.	0.9 p.u.	0.8 p.u.	0.9 p.u.	0.9 p.u.	0.9 p.u.	0.7 p.u.	0.9 p.u.	0.9 p.u.	0.9 p.u.
0.4 p.u.	0.6 p.u.	0.9 p.u.	0.9 p.u.	0.9 p.u.	0.9 p.u.	0.9 p.u.	0.7 p.u.	0.9 p.u.	0.9 p.u.
Post-arrangement									
0.9 p.u.	0.9 p.u.	0.9 p.u.	1 p.u.	0.8 p.u.	0.9 p.u.	0.9 p.u.	0.9 p.u.	0.9 p.u.	0.8 p.u.
0.9 p.u.	0.9 p.u.	0.9 p.u.	1 p.u.	0.9 p.u.	0.7 p.u.	0.9 p.u.	0.9 p.u.	0.9 p.u.	0.9 p.u.
0.9 p.u.	0.9 p.u.	0.7 p.u.	0.9 p.u.	0.8 p.u.	0.9 p.u.	0.9 p.u.	0.9 p.u.	0.8 p.u.	0.6 p.u.
0.9 p.u.	1 p.u.	1 p.u.	0.8 p.u.	0.9 p.u.	0.9 p.u.	0.9 p.u.	0.9 p.u.	0.9 p.u.	0.9 p.u.
0.9 p.u.	0.8 p.u.	0.9 p.u.	0.6 p.u.	0.9 p.u.	0.9 p.u.	0.9 p.u.	0.9 p.u.	0.9 p.u.	0.9 p.u.
0.9 p.u.	0.9 p.u.	0.9 p.u.	0.6 p.u.	0.9 p.u.	0.9 p.u.	0.8 p.u.	0.9 p.u.	0.8 p.u.	0.8 p.u.
0.9 p.u.	0.9 p.u.	1 p.u.	0.9 p.u.	0.9 p.u.	0.9 p.u.	0.6 p.u.	0.8 p.u.	0.9 p.u.	0.9 p.u.
0.9 p.u.	0.9 p.u.	0.7 p.u.	0.9 p.u.	0.8 p.u.	0.9 p.u.	0.9 p.u.	0.8 p.u.	0.9 p.u.	1 p.u.
0.9 p.u.	0.9 p.u.	0.9 p.u.	0.9 p.u.	0.9 p.u.	0.9 p.u.	0.7 p.u.	0.6 p.u.	0.9 p.u.	0.9 p.u.
0.8 p.u.	0.9 p.u.	0.9 p.u.	0.9 p.u.	0.9 p.u.	0.9 p.u.	0.8 p.u.	0.6 p.u.	0.9 p.u.	0.6 p.u.

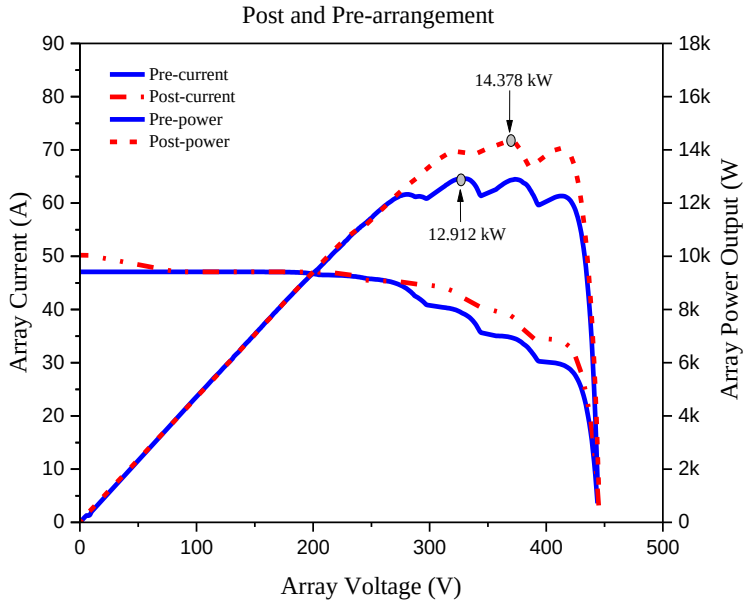

Figure 5.13: The outputs associated with the two types of 10 x 10 PV arrays, namely, 18-kW before and after the implementation of reconfiguration.

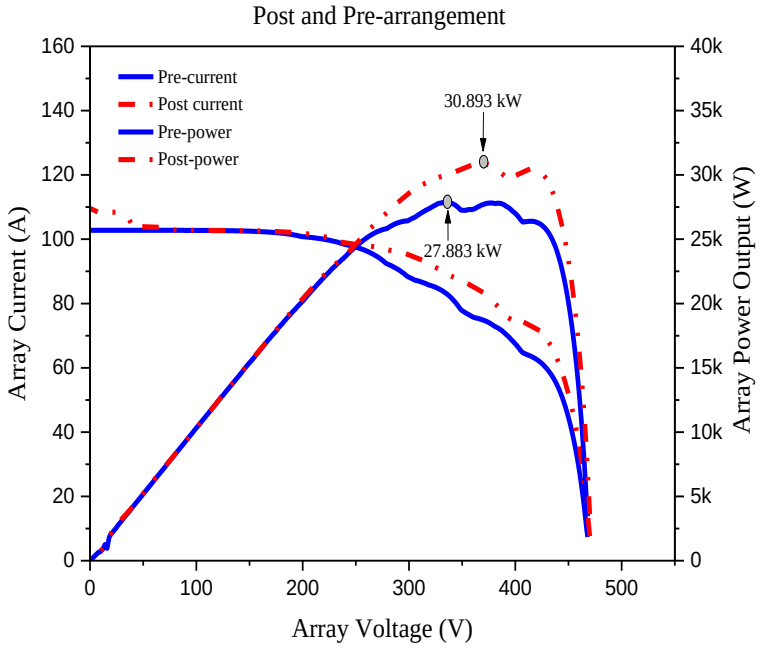

Figure 5.14: The outputs associated with the two types of 10 x 10 PV arrays, namely, 43-kW before and after the implementation of reconfiguration.

5.2.1.5 Scenario one (Initial-Final Rates Return of Electricity Revenue)

In the earlier part, the enhancement of the output power associated with the 10 x 10 PV arrays were addressed, and the process is illustrated in Figure 5.17 and Figure

5.18. The outcomes of the simulation are presented in Table 5.9. It can be seen that manual swap had to be performed 38 times and 6 manual replacing, according to the costs associated with electric power and labor force in the fourteen countries examined. Meanwhile, Table 5.9 provides the initial and final rate returns related to the electric revenue of both the 18-kW 10 x 10 PV array and the 43-kW 10 x 10 PV array, but without considering the most significant economic advantage. Thus, it can be observed that, by comparison to the final rate return of electric revenue, the initial rate return of electric revenue before reconfiguration is lower. This reflects the positive effect of the suggested approach, which determined an 11.35% increase in the electric revenue of the 18-kW 10 x 10 PV array in all of the examined countries following the implementation of reconfiguration. Similarly, the approach also had a favorable impact on the 43-kW 10 x 10 PV array, increasing the related electric revenue by 10.8% in all fourteen countries, according to Table 5.9.

Table 5.9: The original and final rate returns associated with the 18-kW and 43-kW 10x10 PV arrays, without taking into account the greatest economic advantage per year.

Country	*Initial rate return of electric revenue 18-kW ($)*	*Final rate return of electric revenue 18-kW ($)*	*Initial rate return of electric revenue 43-kW ($)*	*Final rate return of electric revenue 43-kW ($)*
Saudi Arabia	8897.92	9908.17	14411.05	15966.74
Pakistan	8143.86	9068.49	17586.37	19484.83
India	7314.39	8144.85	15795.16	17500.27
France	20020.31	22293.38	28822.1	31933.48
United Kingdom	18248.27	20320.14	19703.24	21830.23
Germany	22697.23	25274.22	24506.93	27152.48
Greece	13497.69	15030.19	14573.89	16147.15
Cyprus	9915.91	11041.73	21413.03	23724.59
Jamaica	8256.97	9194.44	17830.62	19755.46
China	10292.93	11461.57	14818.14	16417.78
Japan	28164.17	31361.87	40546.34	44923.36
Australia	25675.77	28590.94	36963.94	40954.23
Brazil	9576.57	10663.88	20680.26	22912.72
US states	14251.75	15869.86	20517.43	22732.31

5.2.1.6 Scenario two (Net Profits of Additional Electric Revenue)

As can be deduced from Table 5.10 and equation (5.4-5.8) about the costs of labor and electricity price in the investigated countries, the approach put forth in this work can reduce the number of times that substitutions are performed, thus making offline reconfiguration less expensive. At the same time, this would determine a significant rise in overall profit (Table 5.10). On the other hand, there is a lack of clarity about how the approach benefits profitability in countries where labor and electricity price are expensive; in such countries, the cost of labor can be diminished, but the electric revenue profit cannot be increased.

Table 5.10: The assessment of economic advantage, taking into account the lowest number of times that handling is required.

Country	*Cost of swap/replace modules $/time*	*Best cost-effective maintenance period time*	*Additional electric revenue 18 kW ($)*	*Cost of swap/replace modules $/time*	*Best cost-effective maintenance period time*	*Additional electric revenue 43 kW ($)*
Saudi Arabia	491.37	4	518.88	671.37	3	884.32
Pakistan	284.73	2	639.91	464.73	2	1433.74
India	277.49	2	552.97	457.49	2	1247.62
France	1023.41	3	1249.66	1203.41	2	1907.97
United Kingdom	781.8	2	1290.07	961.8	1	1165.19
Germany	1119.17	2	1457.83	1299.17	1	1346.38
Greece	500.82	2	1031.68	680.82	1	892.45
Cyprus	463.97	1	661.86	643.97	1	1667.59
Jamaica	279.06	1	658.42	459.06	1	1465.77
China	541.46	3	627.18	721.46	2	878.18
Japan	1069.4	3	2128.3	1249.4	2	3127.63
Australia	1290.53	3	1624.65	1470.53	2	2519.77
Brazil	430.58	2	656.73	610.58	2	1621.88
US states	727.31	3	890.81	907.31	2	1307.57

Table 5.11: The original and final rate returns associated with the substituting modules of the 10x10 PV arrays, taking into account the greatest economic advantage per year.

Country	*The initial value of electric revenue without considering labor cost 18 kW ($)*	*Net profit of final value electric revenue by considering labor cost 18 kW ($)*	*The initial value of electric revenue without considering labor cost 43 kW ($)*	*Net profit of final value electric revenue by considering labor cost 43 kW ($)*

Saudi Arabia	8897.92	9416.8	14411.05	15295.37
Pakistan	8143.86	8783.76	17586.37	19020.1
India	7314.39	7867.36	15795.16	17042.78
France	20020.31	21269.97	28822.1	30730.07
United Kingdom	18248.27	19538.34	19703.24	20868.43
Germany	22697.23	24155.06	24506.93	25853.31
Greece	13497.69	14529.37	14573.89	15466.33
Cyprus	9915.91	10577.76	21413.03	23080.62
Jamaica	8256.97	8915.38	17830.62	19296.4
China	10292.93	10920.11	14818.14	15696.32
Japan	28164.17	30292.47	40546.34	43673.97
Australia	25675.77	27300.42	36963.94	39483.71
Brazil	9576.57	10233.3	20680.26	22302.15
US states	14251.75	15142.56	20517.43	21825.01

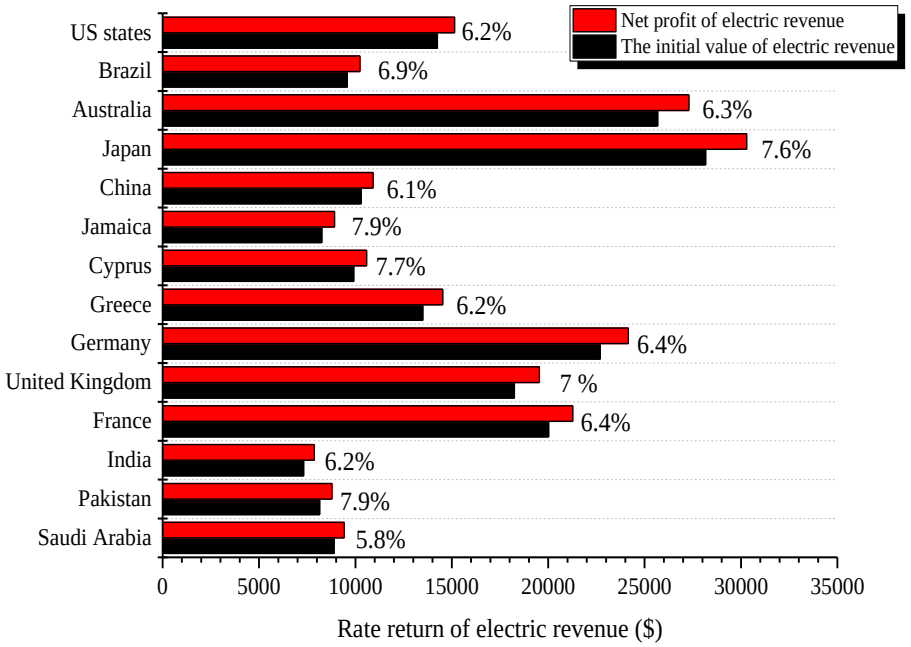

Figure 5.15: The increase in rate returns of electric revenue associated with the 18-kW 10x10 PV arrays, taking into account the greatest economic advantage per year.

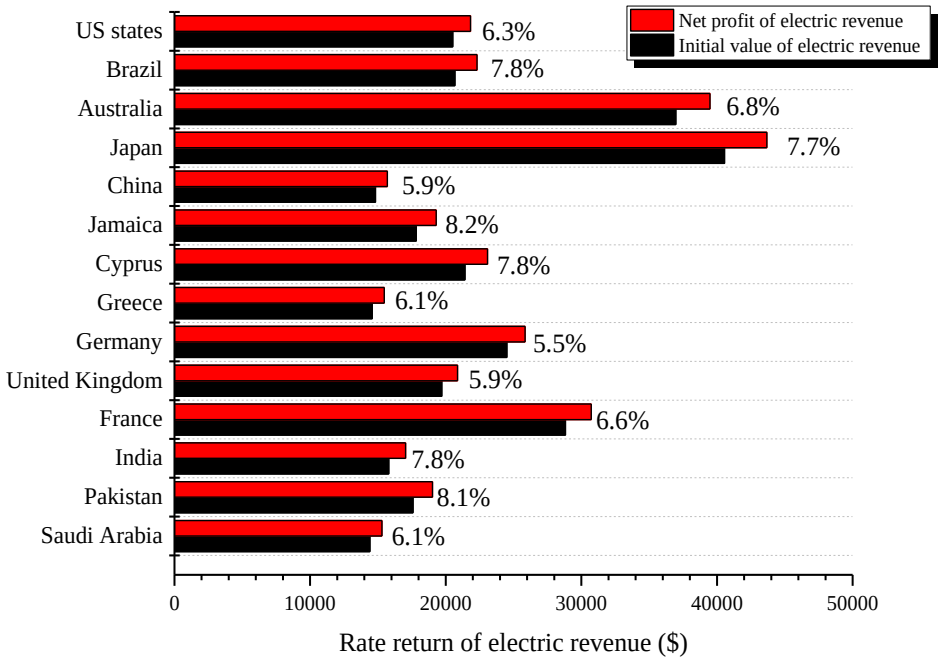

Figure 5.16: The increase in rate returns of electric revenue associated with the 43-kW 10x10 PV arrays, taking into account the greatest economic advantage per year.

The outcomes of the simulation presented in

Table 5.11 point to the fact that manual swap had to be performed thirty-eight times, while substitution had to be performed six replace times, according to the costs associated with electric power and labor force in the fourteen countries that were examined. Meanwhile, equation (5.3-5.8) facilitated calculating the extra electric revenue profit associated with the (18-kW and 43-kW) PV array and the equivalent cost of labor. The figures that were thus obtained are given in Table 5.5. What is more, the proportion of the net profit of electric revenue that was achieved following the application of the reconfiguration based on the suggested approach is indicated in Figure 5.15 and Figure 5.16.

The analysis performed based on the same interval of maintenance applied in the earlier part revealed that suboptimal electric revenue was achieved. This can be attributed to the fact that solar panels' substitution with new ones in countries like Pakistan, India, and Jamaica is costly. On the other hand, the electric revenue rate was medium in the case of the other countries that were analysed. Thus, it was concluded that, in the case of the latter, maintenance could begin from the second to the fourth year, as indicated in Figure 5.17 and Figure 5.18. Despite such observations, it is attested that an approach involving a mixture of PV panel swap and substitution could ensure that the performance of midlife maintenance is advantageous in most countries.

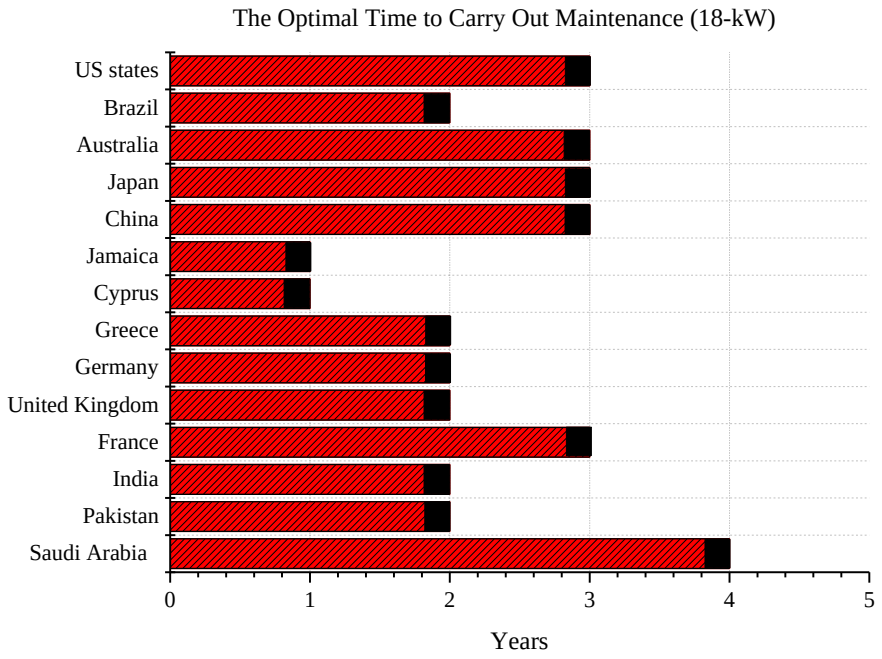

Figure 5.17: The year identified by the suggested algorithm as the optimal time to carry out maintenance to achieve the greatest economic advantage in 10*10 PV Array (18-kW).

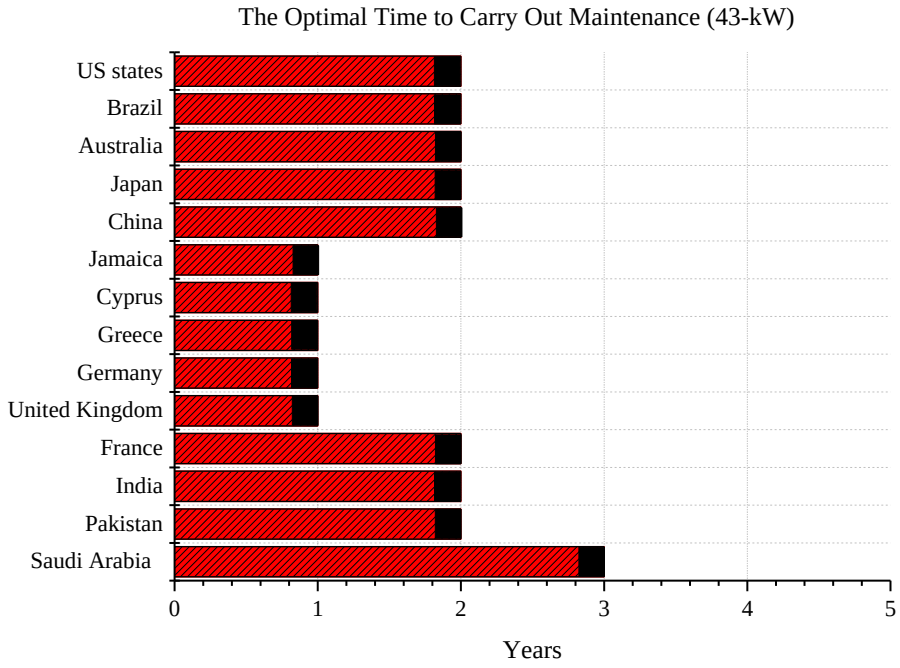

Figure 5.18: The year identified by the suggested algorithm as the optimal time to carry out maintenance to achieve the greatest economic advantage in 10*10 PV Array (43-kW).

5.3 Discussion

To establish the extent to which electric revenue can be increased to enhance economic advantages in the 14 countries analysed, the outcomes of maintenance cost analysis for the two types of PV arrays are discussed in the following part. According to those outcomes, the suggested algorithm is arbitrarily applicable to PV arrays of different dimensions and enhanced the maximum power output for both types of PV arrays considered. Furthermore, in the first case, the algorithm considered relevant aging factors to reorganise individual PV modules' positions in every string, thus attenuating the effect of the bypass diodes. Consequently, PV modules in all strings were less affected by mismatch losses, although voltage limits were overlooked. Other studies addressing this issue are available [210, 238, 243-245]. The suggested algorithm hierarchically and iteratively sorts of PV modules. The generated P-V curves in Figure 5.7, Figure 5.8, Figure 5.13 and Figure 5.14 reflect the usefulness of PV array reconfiguration strategy for making systems more efficient and reducing their operating costs.

Furthermore, the suggested algorithm can yield results speedily because it does not need access to all potential online and offline configurations for a given PV array, thus simplifying the process. For instance, the algorithm determined the best PV module configuration in the first case based on just nine steps, with an average computational time of 0.129375 s. Thus, by identifying the ideal module configuration rapidly, the algorithm accelerates the real-time implementation process. The suggested algorithm is also advantageous because it involves reorganisation solely of the affected PV modules, leaving the others unchanged. Moreover, in the first case, the reorganisation enhanced the efficiency of maintenance management. Costs and advantages are the main determinants of offline reconfiguration methods. Such

methods are needed to make reconfiguration more efficient, more profitable, and more cost-effective in labor since the creation of an aging map for PV plants is essential. Reconfiguration as a way of capitalising on a PV plant's strengths is justified when the profitability engendered by higher power production offsets the costs of labor force reorganisation. Considering these aspects, the suggested approach is useful as it involves the substitution of just PV module positions based on manpower rather than complete substitution of aging modules with new ones.

An overview of the approach put forth in the present study to address the intended research question is provided in the following part. More specifically, two particular strategies have been identified as a viable way to make solar power plants more efficient, on the one hand, and to achieve higher financial returns, on the other hand, based on the application of a suitable reconfiguration. The proposed strategies were underpinned by the (GEA), which is an algorithm capable of both simulation and analysis of the potential manner in which aging PV arrays can be reorganised and the output power and economic advantages associated with the various solutions of reorganisation. Hence, the first case study revealed that the reorganisation of the PV modules that showed signs of aging acceptably improved the PV array's output power and, at the same time, increased the electric revenue. Meanwhile, the second case study also demonstrated a rise in the output power of the PV array as well as a marked increase in financial returns; this was attributed to the fact that the suggested algorithm helped to establish the best reconfiguration not only in terms of identifying the PV modules that had to be position swapped but also in terms of identifying the PV modules that had to be substituted completely. The following example can serve to illustrate the capability of the suggested algorithm. Based on the instruction given by the algorithm, aged PV modules with a production of less than (0.5p.u.) should be

substituted, whereas PV modules with production higher than (0.6p.u.) should be retained; in this way, it is possible to preserve the PV modules that display signs of aging instead of recycling them. This kind of strategy can be a viable option for PV plants of a medium-to-large size that require maintenance. The extent to which the suggested algorithm's application can increase the financial returns of electric revenue is indicated in Table 5.12, with the figures being expressed as a percentage.

Table 5.12: Comparative analysis of electric revenue rate returns in 14 countries over a period of one decade.

	Case one (Swapping age modules)				*Case two (Swap/Replace age modules)*			
Country	*Net profit of electric revenue 18 kW ($)*	*Profits return*	*Net profit of electric revenue 43 kW ($)*	*Profits return*	*Net profit of electric revenue 18 kW ($)*	*Profits return*	*Net profit of electric revenue 43 kW ($)*	*Profits return*
Saudi Arabia	18484.95	2.39%	33953.36	0.97%	9416.8	5.8%	15295.37	6.1%
Pakistan	4229.61	2.72%	8900.85	1.22%	8783.76	7.9%	19020.1	8.1%
India	3798.81	2.8%	7997.1	1.26%	7867.36	7.6%	17042.78	7.8%
France	48523.01	2.12%	101829.4	0.94%	21269.97	6.4%	30730.07	6.6%
United Kingdom	37909.82	2.32%	79630.39	1.04%	19538.34	7.01%	20868.43	5.9%
Germany	58940.38	2.25%	123766.96	1.01%	24155.06	6.4%	25853.31	5.5%
Greece	21030.55	2.52%	44216.77	1.13%	14529.37	7.6%	15466.33	6.1%
Cyprus	20599.76	2.69%	43344.03	1.21%	10577.76	7.7%	23080.62	7.8%
Jamaica	8576.71	3.38%	18103.05	1.53%	8915.38	7.9%	19296.4	8.2%
China	17819.18	2.03%	44919.83	1.05%	10920.11	6.1%	15696.32	5.9%
Japan	48757.98	2.02%	122907.76	1.04%	30292.47	7.6%	43673.97	7.7%
Australia	62230.07	2.04%	149353.52	1.01%	27300.42	6.3%	39483.71	6.8%
Brazil	14921.12	2.48%	31365.88	1.11%	10233.3	6.9%	22302.15	7.8%
US states	29607.26	2.08%	72562.45	1.05%	15142.56	6.2%	21825.01	6.3%

5.4 Conclusion

A persistent issue for PV arrays of large scale is that PV modules do not age homogeneously. If it is not addressed, this issue diminishes the PV array output power and causes PV module deterioration. Standard online global-MPPT methods are limited to monitoring the affected maximum instead of the maximum possible power of PV arrays with non-uniform aging, with no attempt to reorganise such PV arrays. Therefore, a new algorithm for 10 x 10 PV array reconfiguration was put forth in this

study, considering the costs associated with labor force and electric power in fourteen countries, namely, Saudi Arabia, Pakistan, India, France, the UK, Germany, Greece, Cyprus, Jamaica, China, Japan, Australia, Brazil, and the US. Owing to cost discrepancies between the examined countries, the outcomes obtained were more favourable in both cases study related to the reconfiguration of aged PV modules and the substitution of aged PV modules with new ones Table 5.6 and

Table 5.11. They were switching the PV panels' positions led to a slight increase in the output power of the PV array.

Nevertheless, the advantage gained in terms of electric revenue enhanced production and decreased maintenance costs over the period of a decade in the investigated countries. Hence, the approach applied in the first case and second case could be employed to maintain aged PV arrays in other countries (e.g. South Africa, Turkey, etc.). It can be concluded that, based on the suggested algorithm, solar power plants can achieve better financial increment within a decade.

Chapter 6. CONCLUSION AND FUTURE WORK

6.1 Conclusion

This thesis aims to design an algorithm that is arbitrarily applicable to PV arrays for any size and increase the potential power output of a PV array over a decade and decrease maintenance costs. However, a new algorithm for the offline configuration of PV arrays is then put forward to attenuate the effect of non-uniform aging PV arrays and maximise the power output it can deliver while excluding the need to replacement aged PV modules. The algorithm sorted the PV modules repeatedly and hierarchically to minimise the incompatibility effect induced by the non-uniform aging between PV modules. The following tasks have been completed, reflect contributions to the current body of information, and are of interest to the field of photovoltaic systems.

1. ***A critical review of the current methods has been carried out and concluded by a critical comparison between offline and online configurations.***

The algorithm's capability to speedily generate results stems from the fact that it does not need to access all potential arrangements for a given PV array. For example, the ideal PV module configuration was determined by the algorithm in chapter 3, based solely on five steps. The potential (2,627,625) arrangements did not have to examine in their entirety. Where Table 3.3, Table 3.5 and Table 3.7 respectively show the computational times for each scenario. Thus, it is apparent that the ideal module arrangement can be identified quickly by the suggested algorithm and subsequently applied rapidly in real-time. However, this algorithm is helpful since only the damaged PV modules are repositioned; the others remain unchanged; therefore, the number of relays needed for switching purposes is reduced. Makes the algorithm more

economical and time-consuming than any other technique. Due to the electric switches which would require several switches and cables online reconfiguration, the high costs make this kind of solution in a real application challenging to afford.

2. ***A Gene Evaluation Algorithm (GEA) offline reconfiguration has been designed out to improve non-uniform PV array in chapters 3, 4 and 5.***

The offline arrangement is useful for maintenance. The offline reconfiguration strategy depends on the benefits and costs. A photovoltaic aging map is essential for developing a reconfiguration technique offline to measure performance improvement, profitability and reconfiguration workforce costs. Suppose the service obtained from further power generation will cover the costs of reconfiguration of the employee. In that case, it is fair to assume that a PV plant owner can make a redefine to take advantage of this configuration method. Because of these factors, only workers can swap PV modules positions to gain the proposed strategy.

3. ***The proposed GEA offline reconfiguration method applied to the 2 × 4 PV arrays in the experiment to improve the non-uniform PV array output power.***

The included experiment demonstrates in chapter 5 how age affects PV module output power in PV arrays. The proposed algorithm for PV array reconfiguration would limit PV arrays with non-uniform aging while increasing output power and limiting the need to replace aged PV modules. The algorithm arranges the PV modules in a repetitive and hierarchical attempt to avoid non-uniform aging incompatibility across PV modules. As a result, the 2 × 4 PV array's output power increased by 11.42 %.

4. ***A maximum attempt was made to use offline reconfiguration of PV array to support the economic benefit.***

The study presented a new algorithm for PV reconfiguration on a medium-large scale in fourteen countries, considering labor force and energy costs. Due to cost differences between the studied countries, the results achieved were more positive in both cases study related to the offline reconfiguration of aged PV modules and replacing aged PV modules with new ones as shown in Table 5.9. Table 5.11 swapped the PV panels' locations, contributing to a slight increase in the PV array's output efficiency. Nevertheless, over a decade in the examined countries, the benefit achieved in electric revenue increased efficiency and lowered maintenance costs. Therefore, the algorithm used in the first and second case can be used in any other countries. Furthermore, the suggested method can be inferred that solar plants can achieve more critical financial development within a decade based on the proposed algorithm.

5. The main contributions can summarise as follows:

- This thesis analyses the PV module's aging status based on the short-circuit current for different aging conditions while keeping the open-circuit voltage constant. In the case of PV modules connected in series to form a PV array, their output currents will be the same, while the total module voltages will be added to obtain the output voltage.

- A Gene Evaluation Algorithm (GEA) is used in this thesis to evaluate the configuration with the most generated power among all possible relation patterns. The genetic algorithm has two major advantages: first, it allows for some local random searchability. When an iteration is similar to a better solution for a certain number of iterations, mutation operations speed up the convergence to a better solution. Second, it should maintain that the diversity of viable solutions can prevent precocity from occurring.

- Maximise the economic benefit and testing benchmark and consider the electricity price and workforce cost using offline reconfiguration to reducing the maintenance cost of large-scale PV array plants.

6.2 Future Work

The future work of this study is challenging the soiling and fire risks management of the solar plant. Solar power is obtaining increased attention, including reducing the risk of fire and increased maintenance. In past fire incidents, it has been known that the soiling effects and aging of panels may be caused by the environmental conditions around the PV array, the PV array material framework. Preventive fire hazard remedies can be distinguished by the PV modules reconfiguration and the fire detection algorithm. However, the advantages of PV module reconfiguration; first is decreasing soiling. Secondly increases PV output power performance where the main benefit of the algorithm for detecting fire faults is to see defective locations correctly. There are technical requirements to comply with in order to minimise the risk of PV fire accidents.

For further development of this work, the following recommendations are presented, such as study the performance of soiling and fire hazard in solar modules. To develop a new algorithm for the offline reconfiguration of PV modules is then put forward to attenuate the effect caused by soiling.

REFERENCE

[1] K. Sundareswaran, V. Vigneshkumar, P. Sankar, S. P. Simon, P. S. R. Nayak, and S. Palani, "Development of an Improved P&O Algorithm Assisted Through a Colony of Foraging Ants for MPPT in PV System," *IEEE Transactions on Industrial Informatics*, vol. 12, no. 1, pp. 187-200, 2016, doi: 10.1109/TII.2015.2502428.

[2] Y. Zhang and L. Cai, "Dynamic Charging Scheduling for EV Parking Lots With Photovoltaic Power System," *IEEE Access*, vol. 6, pp. 56995-57005, 2018, doi: 10.1109/ACCESS.2018.2873286.

[3] A. Jäger-Waldau, "Snapshot of Photovoltaics—February 2020," *Energies*, vol. 13, no. 4, 2020, doi: 10.3390/en13040930.

[4] I. E. A. (IEA). "Renewables 2020, IEA, Paris " https://www.iea.org/reports/renewables-2020 (accessed 01 February, 2021).

[5] Statista. "Demand of solar photovoltaic power globally from 2015 to 2019, with forecast until 2024." https://www.statista.com/statistics/500250/solar-photovoltaic-demand-outlook-worldwide/ (accessed 23-03, 2021).

[6] A. Jäger-Waldau. "PV Status Report 2019." https://ec.europa.eu/jrc/sites/jrcsh/files/kjna29938enn_1.pdf (accessed 2021).

[7] CNN. solar park rises from Dubai desert [Online] Available: https://edition.cnn.com/style/article/mbr-solar-park-dubai-desert-intl/index.html

[8] M. B. Hayat, D. Ali, K. C. Monyake, L. Alagha, and N. Ahmed, "Solar energy—A look into power generation, challenges, and a solar-powered future," *International Journal of Energy Research*, https://doi.org/10.1002/er.4252 vol. 43, no. 3, pp. 1049-1067, 2019/03/10 2019, doi: https://doi.org/10.1002/er.4252.

[9] A. Agarwal, "Solar Powered Mobile Power Bank Systems," *American Journal of Electrical and Electronic Engineering*, vol. 4, pp. 148-151, 12/12 2016, doi: 10.12691/ajeee-4-5-4.

[10] H. Ludditus. Nostalgia & Fun With Calculators [Online] Available: https://ludditus.com/2019/02/10/nostalgia-fun-with-calculators/

[11] P. Padmavathi and S. Natarajan, "A Novel Switched Capacitor based High Gain Boost Converter with efficient MPPT controller for LED Lighting Applications," in *2019 Innovations in Power and Advanced Computing Technologies (i-PACT)*, 22-23 March 2019 2019, vol. 1, pp. 1-7, doi: 10.1109/i-PACT44901.2019.8959976.

[12] P. Primiceri and P. Visconti, "Solar-powered LED-based lighting facilities: An overview on recent technologies and embedded IoT devices to obtain wireless control, energy savings and quick maintenance," *Journal of Engineering and Applied Sciences*, vol. 12, pp. 140-150, 01/10 2017.

[13] S. Vision. Solar Road Studs [Online] Available: http://www.solarroadstud.com/

[14] S. B. Wali *et al.*, "Battery storage systems integrated renewable energy sources: A biblio metric analysis towards future directions," *Journal of Energy Storage*, vol. 35, p. 102296, 2021/03/01/ 2021, doi: https://doi.org/10.1016/j.est.2021.102296.

[15] A. R. Prasad and E. Natarajan, "Optimization of integrated photovoltaic–wind power generation systems with battery storage," *Energy*, vol. 31, no. 12, pp.

1943-1954, 2006/09/01/ 2006, doi: https://doi.org/10.1016/j.energy.2005.10.032.
[16] N. C. Davy *et al.*, "Pairing of near-ultraviolet solar cells with electrochromic windows for smart management of the solar spectrum," *Nature Energy*, vol. 2, no. 8, p. 17104, 2017/06/30 2017, doi: 10.1038/nenergy.2017.104.
[17] D. RAZNICK. ADAPTIVE SOLAR SKIN [Online] Available: https://danielraznick.com/about/adaptive-solar-skin/
[18] M. K. H. Rabaia *et al.*, "Environmental impacts of solar energy systems: A review," *Science of The Total Environment*, vol. 754, p. 141989, 2021/02/01/ 2021, doi: https://doi.org/10.1016/j.scitotenv.2020.141989.
[19] P. Balakrishnan, M. S. Shabbir, A. F. Siddiqi, and X. Wang, "Current status and future prospects of renewable energy: A case study," *Energy Sources, Part A: Recovery, Utilization, and Environmental Effects*, vol. 42, no. 21, pp. 2698-2703, 2020/11/01 2020, doi: 10.1080/15567036.2019.1618983.
[20] S. Quereshi, P. R. Jadhao, A. Pandey, E. Ahmad, and K. K. Pant, "1 - Overview of sustainable fuel and energy technologies," in *Sustainable Fuel Technologies Handbook*, S. Dutta and C. Mustansar Hussain Eds.: Academic Press, 2021, pp. 3-25.
[21] P. Manganiello, M. Balato, and M. Vitelli, "A Survey on Mismatching and Aging of PV Modules: The Closed Loop," *IEEE Transactions on Industrial Electronics*, vol. 62, no. 11, pp. 7276-7286, 2015, doi: 10.1109/TIE.2015.2418731.
[22] J. D. Andy Walker, and Donna Heimiller. Performance of Photovoltaic Systems Recorded by Open Solar Performance and Reliability Clearinghouse (oSPARC) [Online] Available: https://www.nrel.gov/docs/fy20osti/75162.pdf
[23] M. A. Green, "Photovoltaics: coming of age," in *IEEE Conference on Photovoltaic Specialists*, 21-25 May 1990 1990, pp. 1-8 vol.1, doi: 10.1109/PVSC.1990.111582.
[24] W. G. Adams and R. E. Day, "IX. The action of light on selenium," *Philosophical Transactions of the Royal Society of London*, vol. 167, pp. 313-349, 1877/01/01 1877, doi: 10.1098/rstl.1877.0009.
[25] D. M. Chapin, C. S. Fuller, and G. L. Pearson, "A New Silicon p-n Junction Photocell for Converting Solar Radiation into Electrical Power," *Journal of Applied Physics*, vol. 25, p. 676, May 01, 1954 1954, doi: 10.1063/1.1721711.
[26] S. B. Kjær, *Design and Control of an Inverter for Photovoltaic Applications*. Aalborg Universitet: Institut for Energiteknik, Aalborg Universitet, 2005, p. 236.
[27] L. E. Chaar, L. A. Lamont, and N. Elzein, "PV Technology - Industry update," in *IEEE PES General Meeting*, 25-29 July 2010 2010, pp. 1-6, doi: 10.1109/PES.2010.5589568.
[28] S. MAGAZINE. Types of Solar Panels: On the Market and in the Lab [Online] Available: https://solarmagazine.com/solar-panels/#Thinfilm_solar_panels
[29] G. Gaspar, A. Autruffe, and M. Pó, "Silicon Growth Technologies for PV Applications," 2017.
[30] L. El Chaar, L. A. lamont, and N. El Zein, "Review of photovoltaic technologies," *Renewable and Sustainable Energy Reviews*, vol. 15, no. 5, pp. 2165-2175, 2011/06/01/ 2011, doi: https://doi.org/10.1016/j.rser.2011.01.004.
[31] T. N. R. E. L. (NREL). Photovoltaic Device Performance Calibration Services [Online] Available: https://pvdpc.nrel.gov/

[32] T. K. Manna and S. M. Mahajan, "Nanotechnology in the Development of Photovoltaic Cells," in *2007 International Conference on Clean Electrical Power*, 21-23 May 2007 2007, pp. 379-386, doi: 10.1109/ICCEP.2007.384240.
[33] N. C. f. S. Growth. Solar Panel Efficiency [Online] Available: https://evergreensolar.com/how/efficiency/
[34] J. Li, R. Li, Y. Jia, and Z. Zhang, "Prediction of I–V Characteristic Curve for Photovoltaic Modules Based on Convolutional Neural Network," *Sensors*, vol. 20, no. 7, 2020, doi: 10.3390/s20072119.
[35] J. Ramos-Hernanz, I. Uriarte, J. M. Lopez-Guede, U. Fernandez-Gamiz, A. Mesanza, and E. Zulueta, "Temperature based maximum power point tracking for photovoltaic modules," *Scientific Reports*, vol. 10, no. 1, p. 12476, 2020/07/27 2020, doi: 10.1038/s41598-020-69365-5.
[36] J. P. Storey, "Advanced reconfigurable photovoltaic arrays," ed: University of Southampton, 2015.
[37] B. N. Nguyen, V. T. Nguyen, M. Q. Duong, K. H. Le, H. H. Nguyen, and A. T. Doan, "Propose a MPPT Algorithm Based on Thevenin Equivalent Circuit for Improving Photovoltaic System Operation," (in English), *Frontiers in Energy Research*, Original Research vol. 8, no. 14, 2020-February-18 2020, doi: 10.3389/fenrg.2020.00014.
[38] H. Tian, F. Mancilla-David, K. Ellis, E. Muljadi, and P. Jenkins, "A cell-to-module-to-array detailed model for photovoltaic panels," *Solar Energy*, vol. 86, no. 9, pp. 2695-2706, 2012/09/01/ 2012, doi: https://doi.org/10.1016/j.solener.2012.06.004.
[39] X. H. Nguyen and M. P. Nguyen, "Mathematical modeling of photovoltaic cell/module/arrays with tags in Matlab/Simulink," *Environmental Systems Research*, vol. 4, no. 1, p. 24, 2015/12/09 2015, doi: 10.1186/s40068-015-0047-9.
[40] R. Kadri, J. Gaubert, and G. Champenois, "An Improved Maximum Power Point Tracking for Photovoltaic Grid-Connected Inverter Based on Voltage-Oriented Control," *IEEE Transactions on Industrial Electronics*, vol. 58, no. 1, pp. 66-75, 2011, doi: 10.1109/TIE.2010.2044733.
[41] M. Alkahtani, Y. Hu, Z. Wu, C. S. Kuka, M. S. Alhammad, and C. Zhang, "Gene Evaluation Algorithm for Reconfiguration of Medium and Large Size Photovoltaic Arrays Exhibiting Non-Uniform Aging," *Energies*, vol. 13, no. 8, p. 1921, 2020. [Online]. Available: https://www.mdpi.com/1996-1073/13/8/1921.
[42] K. K. Ilse, B. W. Figgis, V. Naumann, C. Hagendorf, and J. Bagdahn, "Fundamentals of soiling processes on photovoltaic modules," *Renewable and Sustainable Energy Reviews*, vol. 98, pp. 239-254, 2018/12/01/ 2018, doi: https://doi.org/10.1016/j.rser.2018.09.015.
[43] M. R. Maghami, H. Hizam, C. Gomes, M. A. Radzi, M. I. Rezadad, and S. Hajighorbani, "Power loss due to soiling on solar panel: A review," *Renewable and Sustainable Energy Reviews*, vol. 59, pp. 1307-1316, 2016, doi: 10.1016/j.rser.2016.01.044.
[44] J. J. John, S. Warade, G. Tamizhmani, and A. Kottantharayil, "Study of Soiling Loss on Photovoltaic Modules With Artificially Deposited Dust of Different Gravimetric Densities and Compositions Collected From Different Locations in India," *IEEE Journal of Photovoltaics*, vol. 6, no. 1, pp. 236-243, 2016, doi: 10.1109/JPHOTOV.2015.2495208.

[45] A. Rao, R. Pillai, M. Mani, and P. Ramamurthy, "Influence of Dust Deposition on Photovoltaic Panel Performance," *Energy Procedia*, vol. 54, pp. 690-700, 2014/01/01/ 2014, doi: https://doi.org/10.1016/j.egypro.2014.07.310.

[46] W. Javed, Y. Wubulikasimu, B. Figgis, and B. Guo, "Characterization of dust accumulated on photovoltaic panels in Doha, Qatar," *Solar Energy*, vol. 142, pp. 123-135, 2017/01/15/ 2017, doi: https://doi.org/10.1016/j.solener.2016.11.053.

[47] W. Javed, B. Guo, Y. Wubulikasimu, and B. W. Figgis, "Photovoltaic performance degradation due to soiling and characterization of the accumulated dust," in *2016 IEEE International Conference on Power and Renewable Energy (ICPRE)*, 21-23 Oct. 2016 2016, pp. 580-584, doi: 10.1109/ICPRE.2016.7871142.

[48] H. Zitouni *et al.*, "Experimental investigation of the soiling effect on the performance of monocrystalline photovoltaic systems," *Energy Procedia*, vol. 157, pp. 1011-1021, 2019/01/01/ 2019, doi: https://doi.org/10.1016/j.egypro.2018.11.268.

[49] P. D. Burton and B. H. King, "Application and Characterization of an Artificial Grime for Photovoltaic Soiling Studies," *IEEE Journal of Photovoltaics*, vol. 4, no. 1, pp. 299-303, 2014, doi: 10.1109/JPHOTOV.2013.2270343.

[50] P. D. Burton and B. H. King, "Artificial soiling of photovoltaic module surfaces using traceable soil components," in *2013 IEEE 39th Photovoltaic Specialists Conference (PVSC)*, 16-21 June 2013 2013, pp. 1542-1545, doi: 10.1109/PVSC.2013.6744438.

[51] M. Saidan, A. G. Albaali, E. Alasis, and J. K. Kaldellis, "Experimental study on the effect of dust deposition on solar photovoltaic panels in desert environment," *Renewable Energy*, vol. 92, pp. 499-505, 2016/07/01/ 2016, doi: https://doi.org/10.1016/j.renene.2016.02.031.

[52] M. García, L. Marroyo, E. Lorenzo, and M. Pérez, "Soiling and other optical losses in solar-tracking PV plants in navarra," *Progress in Photovoltaics: Research and Applications*, vol. 19, no. 2, pp. 211-217, 2011, doi: https://doi.org/10.1002/pip.1004.

[53] F. Mejia, J. Kleissl, and J. L. Bosch, "The Effect of Dust on Solar Photovoltaic Systems," *Energy Procedia*, vol. 49, pp. 2370-2376, 2014/01/01/ 2014, doi: https://doi.org/10.1016/j.egypro.2014.03.251.

[54] J. R. Caron and B. Littmann, "Direct Monitoring of Energy Lost Due to Soiling on First Solar Modules in California," *IEEE Journal of Photovoltaics*, vol. 3, no. 1, pp. 336-340, 2013, doi: 10.1109/JPHOTOV.2012.2216859.

[55] A. Kimber, L. Mitchell, S. Nogradi, and H. Wenger, "The Effect of Soiling on Large Grid-Connected Photovoltaic Systems in California and the Southwest Region of the United States," in *2006 IEEE 4th World Conference on Photovoltaic Energy Conference*, 7-12 May 2006 2006, vol. 2, pp. 2391-2395, doi: 10.1109/WCPEC.2006.279690.

[56] M. Gostein, J. R. Caron, and B. Littmann, "Measuring soiling losses at utility-scale PV power plants," in *2014 IEEE 40th Photovoltaic Specialist Conference (PVSC)*, 8-13 June 2014 2014, pp. 0885-0890, doi: 10.1109/PVSC.2014.6925056.

[57] H. Pedersen, J. Strauss, and J. Selj, "Effect of Soiling on Photovoltaic Modules in Norway," *Energy Procedia*, vol. 92, pp. 585-589, 2016/08/01/ 2016, doi: https://doi.org/10.1016/j.egypro.2016.07.023.

[58] E. Andenæs, B. P. Jelle, K. Ramlo, T. Kolås, J. Selj, and S. E. Foss, "The influence of snow and ice coverage on the energy generation from photovoltaic solar cells," *Solar Energy*, vol. 159, pp. 318-328, 2018/01/01/ 2018, doi: https://doi.org/10.1016/j.solener.2017.10.078.

[59] J. R. B. Marion, J. Pruett. Instrumentation for evaluating PV system performance losses from snow [Online] Available: https://www.nrel.gov/docs/fy09osti/45380.pdf

[60] R. E. Pawluk, Y. Chen, and Y. She, "Photovoltaic electricity generation loss due to snow – A literature review on influence factors, estimation, and mitigation," *Renewable and Sustainable Energy Reviews*, vol. 107, pp. 171-182, 2019/06/01/ 2019, doi: https://doi.org/10.1016/j.rser.2018.12.031.

[61] N. Heidari, J. Gwamuri, T. Townsend, and J. M. Pearce, "Impact of Snow and Ground Interference on Photovoltaic Electric System Performance," *IEEE Journal of Photovoltaics*, vol. 5, no. 6, pp. 1680-1685, 2015, doi: 10.1109/JPHOTOV.2015.2466448.

[62] R. W. Andrews, A. Pollard, and J. M. Pearce, "The effects of snowfall on solar photovoltaic performance," *Solar Energy*, vol. 92, pp. 84-97, 2013/06/01/ 2013, doi: https://doi.org/10.1016/j.solener.2013.02.014.

[63] B. Marion, R. Schaefer, H. Caine, and G. Sanchez, "Measured and modeled photovoltaic system energy losses from snow for Colorado and Wisconsin locations," *Solar Energy*, vol. 97, pp. 112-121, 2013/11/01/ 2013, doi: https://doi.org/10.1016/j.solener.2013.07.029.

[64] L. Powers, J. Newmiller, and T. Townsend, "Measuring and modeling the effect of snow on photovoltaic system performance," in *2010 35th IEEE Photovoltaic Specialists Conference*, 20-25 June 2010 2010, pp. 000973-000978, doi: 10.1109/PVSC.2010.5614572.

[65] J. Bogenrieder, C. Camus, M. Hüttner, P. Offermann, J. Hauch, and C. J. Brabec, "Technology-dependent analysis of the snow melting and sliding behavior on photovoltaic modules," *Journal of Renewable and Sustainable Energy*, vol. 10, no. 2, p. 021005, 2018/03/01 2018, doi: 10.1063/1.5001556.

[66] A. Rahmatmand, S. J. Harrison, and P. H. Oosthuizen, "Numerical and experimental study of an improved method for prediction of snow melting and snow sliding from photovoltaic panels," *Applied Thermal Engineering*, vol. 158, p. 113773, 2019/07/25/ 2019, doi: https://doi.org/10.1016/j.applthermaleng.2019.113773.

[67] J. M. Pinar-Pérez and F. P. García Márquez, "Managing Costs and Review for Icing Problems," in *Renewable Energies: Business Outlook 2050*, F. P. García Márquez, A. Karyotakis, and M. Papaelias Eds. Cham: Springer International Publishing, 2018, pp. 97-109.

[68] R. Carriveau, A. Edrisy, P. Cadieux, and R. Mailloux, "Ice Adhesion Issues in Renewable Energy Infrastructure," *Journal of Adhesion Science and Technology*, vol. 26, no. 4-5, pp. 447-461, 2012/03/01 2012, doi: 10.1163/016942411X574592.

[69] R. Pawluk, Y. Chen, and Y. She, "Observations of Ice at the Interface Between Snow Accumulations and Photovoltaic Panel Surfaces," in *2018 6th International Renewable and Sustainable Energy Conference (IRSEC)*, 5-8 Dec. 2018 2018, pp. 1-5, doi: 10.1109/IRSEC.2018.8703019.

[70] Á. Huerta Herraiz, A. Pliego Marugán, and F. P. García Márquez, "Photovoltaic plant condition monitoring using thermal images analysis by convolutional neural network-based structure," *Renewable Energy*, vol. 153,

pp. 334-348, 2020/06/01/ 2020, doi: https://doi.org/10.1016/j.renene.2020.01.148.
[71] R. Moretón, E. Lorenzo, and L. Narvarte, "Experimental observations on hot-spots and derived acceptance/rejection criteria," *Solar Energy*, vol. 118, pp. 28-40, 2015/08/01/ 2015, doi: https://doi.org/10.1016/j.solener.2015.05.009.
[72] A. Arcos Jiménez, C. Q. Gómez Muñoz, and F. P. García Márquez, "Machine Learning for Wind Turbine Blades Maintenance Management," *Energies*, vol. 11, no. 1, 2018, doi: 10.3390/en11010013.
[73] A. K. V. d. Oliveira, M. Aghaei, U. E. Madukanya, L. Nascimento, and R. Rüther, "Aerial Infrared Thermography of a Utility-Scale PV Plant After a Meteorological Tsunami in Brazil," in *2018 IEEE 7th World Conference on Photovoltaic Energy Conversion (WCPEC) (A Joint Conference of 45th IEEE PVSC, 28th PVSEC & 34th EU PVSEC)*, 10-15 June 2018 2018, pp. 684-689, doi: 10.1109/PVSC.2018.8548019.
[74] P. Bharadwaj, K. Karnataki, and V. John, "Formation of Hotspots on Healthy PV Modules and Their Effect on Output Performance," in *2018 IEEE 7th World Conference on Photovoltaic Energy Conversion (WCPEC) (A Joint Conference of 45th IEEE PVSC, 28th PVSEC & 34th EU PVSEC)*, 10-15 June 2018 2018, pp. 0676-0680, doi: 10.1109/PVSC.2018.8548126.
[75] J. Solórzano and M. A. Egido, "Automatic fault diagnosis in PV systems with distributed MPPT," *Energy Conversion and Management*, vol. 76, pp. 925-934, 2013/12/01/ 2013, doi: https://doi.org/10.1016/j.enconman.2013.08.055.
[76] A. Ndiaye, A. Charki, A. Kobi, C. M. F. Kébé, P. A. Ndiaye, and V. Sambou, "Degradations of silicon photovoltaic modules: A literature review," *Solar Energy*, vol. 96, pp. 140-151, 2013/10/01/ 2013, doi: https://doi.org/10.1016/j.solener.2013.07.005.
[77] M. Islam, G. Hasan, I. Ahmed, M. Amin, S. Dewan, and M. M. Rahman, "Infrared Thermography Based Performance Analysis of Photovoltaic Modules," in *2019 International Conference on Energy and Power Engineering (ICEPE)*, 14-16 March 2019 2019, pp. 1-5, doi: 10.1109/CEPE.2019.8726565.
[78] M. Simon and E. L. Meyer, "Detection and analysis of hot-spot formation in solar cells," *Solar Energy Materials and Solar Cells*, vol. 94, no. 2, pp. 106-113, 2010/02/01/ 2010, doi: https://doi.org/10.1016/j.solmat.2009.09.016.
[79] K. Ramspeck, S. Schenk, D. Duphorn, A. Metz, and M. Meixner, "In-line Thermography for Reliable Hot Spot Detection and Process Control," *Energy Procedia*, vol. 55, pp. 133-140, 2014/01/01/ 2014, doi: https://doi.org/10.1016/j.egypro.2014.08.097.
[80] S. Deng *et al.*, "Research on hot spot risk for high-efficiency solar module," *Energy Procedia*, vol. 130, pp. 77-86, 2017/09/01/ 2017, doi: https://doi.org/10.1016/j.egypro.2017.09.399.
[81] H. J. Solheim, H. G. Fjær, E. A. Sørheim, and S. E. Foss, "Measurement and Simulation of Hot Spots in Solar Cells," *Energy Procedia*, vol. 38, pp. 183-189, 2013/01/01/ 2013, doi: https://doi.org/10.1016/j.egypro.2013.07.266.
[82] P. Rajput, G. N. Tiwari, and O. S. Sastry, "Thermal modelling and experimental validation of hot spot in crystalline silicon photovoltaic modules for real outdoor condition," *Solar Energy*, vol. 139, pp. 569-580, 2016/12/01/ 2016, doi: https://doi.org/10.1016/j.solener.2016.10.016.
[83] K. A. Kim and P. T. Krein, "Photovoltaic hot spot analysis for cells with various reverse-bias characteristics through electrical and thermal simulation,"

in *2013 IEEE 14th Workshop on Control and Modeling for Power Electronics (COMPEL)*, 23-26 June 2013 2013, pp. 1-8, doi: 10.1109/COMPEL.2013.6626399.

[84] K. A. Kim, G. Seo, B. Cho, and P. T. Krein, "Photovoltaic Hot-Spot Detection for Solar Panel Substrings Using AC Parameter Characterization," *IEEE Transactions on Power Electronics*, vol. 31, no. 2, pp. 1121-1130, 2016, doi: 10.1109/TPEL.2015.2417548.

[85] I. Geisemeyer, F. Fertig, W. Warta, S. Rein, and M. C. Schubert, "Prediction of silicon PV module temperature for hot spots and worst case partial shading situations using spatially resolved lock-in thermography," *Solar Energy Materials and Solar Cells*, vol. 120, pp. 259-269, 2014/01/01/ 2014, doi: https://doi.org/10.1016/j.solmat.2013.09.016.

[86] D. Rossi, M. Omaña, D. Giaffreda, and C. Metra, "Modeling and Detection of Hotspot in Shaded Photovoltaic Cells," *IEEE Transactions on Very Large Scale Integration (VLSI) Systems*, vol. 23, no. 6, pp. 1031-1039, 2015, doi: 10.1109/TVLSI.2014.2333064.

[87] M. O. Reese *et al.*, "Consensus stability testing protocols for organic photovoltaic materials and devices," *Solar Energy Materials and Solar Cells*, vol. 95, no. 5, pp. 1253-1267, 2011/05/01/ 2011, doi: https://doi.org/10.1016/j.solmat.2011.01.036.

[88] S. A. Gevorgyan *et al.*, "Interlaboratory outdoor stability studies of flexible roll-to-roll coated organic photovoltaic modules: Stability over 10,000h," *Solar Energy Materials and Solar Cells*, vol. 116, pp. 187-196, 2013/09/01/ 2013, doi: https://doi.org/10.1016/j.solmat.2013.04.024.

[89] J. Tracy, N. Bosco, and R. Dauskardt, "Encapsulant Adhesion to Surface Metallization on Photovoltaic Cells," *IEEE Journal of Photovoltaics*, vol. 7, no. 6, pp. 1635-1639, 2017, doi: 10.1109/JPHOTOV.2017.2746572.

[90] K. W. Jansen and A. E. Delahoy, "A laboratory technique for the evaluation of electrochemical transparent conductive oxide delamination from glass substrates," *Thin Solid Films*, vol. 423, no. 2, pp. 153-160, 2003/01/15/ 2003, doi: https://doi.org/10.1016/S0040-6090(02)01020-9.

[91] J. Tracy, N. Bosco, F. Novoa, and R. Dauskardt, "Encapsulation and backsheet adhesion metrology for photovoltaic modules," *Progress in Photovoltaics: Research and Applications*, https://doi.org/10.1002/pip.2817 vol. 25, no. 1, pp. 87-96, 2017/01/01 2017, doi: https://doi.org/10.1002/pip.2817.

[92] G. J. Jorgensen *et al.*, "Moisture transport, adhesion, and corrosion protection of PV module packaging materials," *Solar Energy Materials and Solar Cells*, vol. 90, no. 16, pp. 2739-2775, 2006/10/16/ 2006, doi: https://doi.org/10.1016/j.solmat.2006.04.003.

[93] N. C. Park, J. S. Jeong, B. J. Kang, and D. H. Kim, "The effect of encapsulant discoloration and delamination on the electrical characteristics of photovoltaic module," *Microelectronics Reliability*, vol. 53, no. 9, pp. 1818-1822, 2013/09/01/ 2013, doi: https://doi.org/10.1016/j.microrel.2013.07.062.

[94] A. Sinha, O. S. Sastry, and R. Gupta, "Nondestructive characterization of encapsulant discoloration effects in crystalline-silicon PV modules," *Solar Energy Materials and Solar Cells*, vol. 155, pp. 234-242, 2016/10/01/ 2016, doi: https://doi.org/10.1016/j.solmat.2016.06.019.

[95] E. E. van Dyk, J. B. Chamel, and A. R. Gxasheka, "Investigation of delamination in an edge-defined film-fed growth photovoltaic module," *Solar*

Energy Materials and Solar Cells, vol. 88, no. 4, pp. 403-411, 2005/09/15/ 2005, doi: https://doi.org/10.1016/j.solmat.2004.12.004.

[96] S. Meyer *et al.*, "Snail Trails: Root Cause Analysis and Test Procedures," *Energy Procedia*, vol. 38, pp. 498-505, 2013/01/01/ 2013, doi: https://doi.org/10.1016/j.egypro.2013.07.309.

[97] H. Yang, J. Chang, H. Wang, and D. Song, "Power Degradation Caused by Snail Trails in Urban Photovoltaic Energy Systems," *Energy Procedia*, vol. 88, pp. 422-428, 2016/06/01/ 2016, doi: https://doi.org/10.1016/j.egypro.2016.06.018.

[98] V. I. Madogni, B. Kounouhéwa, A. Akpo, M. Agbomahéna, S. A. Hounkpatin, and C. N. Awanou, "Comparison of degradation mechanisms in organic photovoltaic devices upon exposure to a temperate and a subequatorial climate," *Chemical Physics Letters*, vol. 640, pp. 201-214, 2015/11/01/ 2015, doi: https://doi.org/10.1016/j.cplett.2015.09.023.

[99] A. Bouraiou *et al.*, "Experimental evaluation of the performance and degradation of single crystalline silicon photovoltaic modules in the Saharan environment," *Energy*, vol. 132, pp. 22-30, 2017/08/01/ 2017, doi: https://doi.org/10.1016/j.energy.2017.05.056.

[100] S. Silvestre, S. Kichou, L. Guglielminotti, G. Nofuentes, and M. Alonso-Abella, "Degradation analysis of thin film photovoltaic modules under outdoor long term exposure in Spanish continental climate conditions," *Solar Energy*, vol. 139, pp. 599-607, 2016/12/01/ 2016, doi: https://doi.org/10.1016/j.solener.2016.10.030.

[101] A. Limmanee *et al.*, "Degradation analysis of photovoltaic modules under tropical climatic conditions and its impacts on LCOE," *Renewable Energy*, vol. 102, pp. 199-204, 2017/03/01/ 2017, doi: https://doi.org/10.1016/j.renene.2016.10.052.

[102] S. S. Chandel, M. Nagaraju Naik, V. Sharma, and R. Chandel, "Degradation analysis of 28 year field exposed mono-c-Si photovoltaic modules of a direct coupled solar water pumping system in western Himalayan region of India," *Renewable Energy*, vol. 78, pp. 193-202, 2015/06/01/ 2015, doi: https://doi.org/10.1016/j.renene.2015.01.015.

[103] L. Cristaldi, M. Faifer, M. Lazzaroni, M. M. A. F. Khalil, M. Catelani, and L. Ciani, "Diagnostic architecture: A procedure based on the analysis of the failure causes applied to photovoltaic plants," *Measurement*, vol. 67, pp. 99-107, 2015/05/01/ 2015, doi: https://doi.org/10.1016/j.measurement.2015.02.023.

[104] S. Gallardo-Saavedra *et al.*, "Nondestructive characterization of solar PV cells defects by means of electroluminescence, infrared thermography, I–V curves and visual tests: Experimental study and comparison," *Energy*, vol. 205, p. 117930, 2020/08/15/ 2020, doi: https://doi.org/10.1016/j.energy.2020.117930.

[105] M. Köntges, S. Kajari-Schröder, I. Kunze, and U. Jahn, *Crack Statistic of Crystalline Silicon Photovoltaic Modules*. 2011.

[106] S. Kajari-Schröder, I. Kunze, U. Eitner, and M. Köntges, "Spatial and orientational distribution of cracks in crystalline photovoltaic modules generated by mechanical load tests," *Solar Energy Materials and Solar Cells*, vol. 95, no. 11, pp. 3054-3059, 2011/11/01/ 2011, doi: https://doi.org/10.1016/j.solmat.2011.06.032.

[107] A. Kilikevičius, A. Čereška, and K. Kilikevičienė, "Analysis of external dynamic loads influence to photovoltaic module structural performance,"

Engineering Failure Analysis, vol. 66, pp. 445-454, 2016/08/01/ 2016, doi: https://doi.org/10.1016/j.engfailanal.2016.04.031.

[108] J. Käsewieter, F. Haase, M. H. Larrodé, and M. Köntges, "Cracks in Solar Cell Metallization Leading to Module Power Loss under Mechanical Loads," *Energy Procedia*, vol. 55, pp. 469-477, 2014/01/01/ 2014, doi: https://doi.org/10.1016/j.egypro.2014.08.011.

[109] M. Sander, S. Dietrich, M. Pander, M. Ebert, and J. Bagdahn, "Systematic investigation of cracks in encapsulated solar cells after mechanical loading," *Solar Energy Materials and Solar Cells*, vol. 111, pp. 82-89, 2013/04/01/ 2013, doi: https://doi.org/10.1016/j.solmat.2012.12.031.

[110] M. Dhimish, V. Holmes, P. Mather, C. Aissa, and M. Sibley, "Development of 3D graph-based model to examine photovoltaic micro cracks," *Journal of Science: Advanced Materials and Devices*, vol. 3, no. 3, pp. 380-388, 2018/09/01/ 2018, doi: https://doi.org/10.1016/j.jsamd.2018.07.004.

[111] M. Song, D. Cui, C. Yu, J. An, C. Chang, and M. Song, "Crack Detection Algorithm for Photovoltaic Image Based on Multi-Scale Pyramid and Improved Region Growing," in *2018 IEEE 3rd International Conference on Image, Vision and Computing (ICIVC)*, 27-29 June 2018 2018, pp. 128-132, doi: 10.1109/ICIVC.2018.8492810.

[112] M. Dhimish, V. Holmes, B. Mehrdadi, and M. Dales, "The impact of cracks on photovoltaic power performance," *Journal of Science: Advanced Materials and Devices*, vol. 2, no. 2, pp. 199-209, 2017/06/01/ 2017, doi: https://doi.org/10.1016/j.jsamd.2017.05.005.

[113] J. I. van Mölken *et al.*, "Impact of Micro-Cracks on the Degradation of Solar Cell Performance Based On Two-Diode Model Parameters," *Energy Procedia*, vol. 27, pp. 167-172, 2012/01/01/ 2012, doi: https://doi.org/10.1016/j.egypro.2012.07.046.

[114] O. Maier, *Operation & Maintenance Costs of Photovoltaic Power Plants: a Swiss Benchmark and Outlook*. 2015.

[115] H. Walker *et al.*, "Model of Operation-and-Maintenance Costs for Photovoltaic Systems," United States, 2020-06-22 2020. [Online]. Available: https://www.osti.gov/biblio/1659995

https://www.osti.gov/servlets/purl/1659995

[116] G. T. Klise *et al.*, "PV Reliability Operations and Maintenance (PVROM) Database Initiative: 2014 Project Report," United States, 2014-12-01 2014. [Online]. Available: https://www.osti.gov/biblio/1504104

https://www.osti.gov/servlets/purl/1504104

[117] J. D. Bastidas-Rodriguez, G. Petrone, C. A. Ramos-Paja, and G. Spagnuolo, "Photovoltaic modules diagnostic: An overview," in *IECON 2013 - 39th Annual Conference of the IEEE Industrial Electronics Society*, 10-13 Nov. 2013 2013, pp. 96-101, doi: 10.1109/IECON.2013.6699117.

[118] S. Manzano, R. Peña-Ortiz, D. Guevara, and A. Rios Villacorta, "AN OVERVIEW OF REMOTE MONITORING PV SYSTEMS: ACQUISITION, STORAGES, PROCESSING AND PUBLICATION OF REAL- TIME DATA BASED ON CLOUD COMPUTING," *Proceedings International Workshop on Solar Integration*, 11/09 2014.

[119] S. R. Madeti and S. N. Singh, "Monitoring system for photovoltaic plants: A review," *Renewable and Sustainable Energy Reviews*, vol. 67, pp. 1180-1207, 2017/01/01/ 2017, doi: https://doi.org/10.1016/j.rser.2016.09.088.

[120] S. Daliento *et al.*, "Monitoring, Diagnosis, and Power Forecasting for Photovoltaic Fields: A Review," *International Journal of Photoenergy*, vol. Volume 2017, p. 13, 01/11 2017, doi: 10.1155/2017/1356851.
[121] A. Woyte *et al.*, *Analytical Monitoring of Grid-connected Photovoltaic Systems: Good Practices for Monitoring and Performance Analysis*. 2014.
[122] K.-H. Chao, S.-H. Ho, and M.-H. Wang, "Modeling and fault diagnosis of a photovoltaic system," *Electric Power Systems Research*, vol. 78, no. 1, pp. 97-105, 2008/01/01/ 2008, doi: https://doi.org/10.1016/j.epsr.2006.12.012.
[123] D. Guasch, S. Silvestre, and R. Calatayud, "Automatic failure detection in photovoltaic systems," in *3rd World Conference onPhotovoltaic Energy Conversion, 2003. Proceedings of*, 11-18 May 2003 2003, vol. 3, pp. 2269-2271 Vol.3.
[124] D. Stellbogen, "Use of PV circuit simulation for fault detection in PV array fields," in *Conference Record of the Twenty Third IEEE Photovoltaic Specialists Conference - 1993 (Cat. No.93CH3283-9)*, 10-14 May 1993 1993, pp. 1302-1307, doi: 10.1109/PVSC.1993.346931.
[125] W. Chine, A. Mellit, A. M. Pavan, and S. A. Kalogirou, "Fault detection method for grid-connected photovoltaic plants," *Renewable Energy*, vol. 66, pp. 99-110, 2014/06/01/ 2014, doi: https://doi.org/10.1016/j.renene.2013.11.073.
[126] A. Chouder and S. Silvestre, "Automatic supervision and fault detection of PV systems based on power losses analysis," *Energy Conversion and Management*, vol. 51, no. 10, pp. 1929-1937, 2010/10/01/ 2010, doi: https://doi.org/10.1016/j.enconman.2010.02.025.
[127] S. Silvestre, A. Chouder, and E. Karatepe, "Automatic fault detection in grid connected PV systems," *Solar Energy*, vol. 94, pp. 119-127, 2013/08/01/ 2013, doi: https://doi.org/10.1016/j.solener.2013.05.001.
[128] A. Chouder, S. Silvestre, B. Taghezouit, and E. Karatepe, "Monitoring, modelling and simulation of PV systems using LabVIEW," *Solar Energy*, vol. 91, pp. 337-349, 2013/05/01/ 2013, doi: https://doi.org/10.1016/j.solener.2012.09.016.
[129] M. H. Ali, A. Rabhi, A. E. Hajjaji, and G. M. Tina, "Real Time Fault Detection in Photovoltaic Systems," *Energy Procedia*, vol. 111, pp. 914-923, 2017/03/01/ 2017, doi: https://doi.org/10.1016/j.egypro.2017.03.254.
[130] N. Gokmen, E. Karatepe, S. Silvestre, B. Celik, and P. Ortega, "An efficient fault diagnosis method for PV systems based on operating voltage-window," *Energy Conversion and Management*, vol. 73, pp. 350-360, 2013/09/01/ 2013, doi: https://doi.org/10.1016/j.enconman.2013.05.015.
[131] T. Takashima, J. Yamaguchi, K. Otani, T. Oozeki, K. Kato, and M. Ishida, "Experimental studies of fault location in PV module strings," *Solar Energy Materials and Solar Cells*, vol. 93, no. 6, pp. 1079-1082, 2009/06/01/ 2009, doi: https://doi.org/10.1016/j.solmat.2008.11.060.
[132] P. Guerriero, L. Piegari, R. Rizzo, and S. Daliento, "Mismatch Based Diagnosis of PV Fields Relying on Monitored String Currents," *International Journal of Photoenergy*, vol. 2017, p. 2834685, 2017/01/16 2017, doi: 10.1155/2017/2834685.
[133] Y. Hirata, S. Noro, T. Aoki, and S. Miyazawa, "Diagnosis photovoltaic failure by simple function method to acquire I–V curve of photovoltaic modules string," in *2012 38th IEEE Photovoltaic Specialists Conference*, 3-8 June 2012 2012, pp. 001340-001343, doi: 10.1109/PVSC.2012.6317848.

[134] B. P. Singh, S. K. Goyal, and S. A. Siddiqui, "Analysis and Classification of Maximum Power Point Tracking (MPPT) Techniques: A Review," in *Intelligent Computing Techniques for Smart Energy Systems*, Singapore, A. Kalam, K. R. Niazi, A. Soni, S. A. Siddiqui, and A. Mundra, Eds., 2020// 2020: Springer Singapore, pp. 999-1008.

[135] S. Spataru, D. Sera, T. Kerekes, and R. Teodorescu, "Photovoltaic array condition monitoring based on online regression of performance model," in *2013 IEEE 39th Photovoltaic Specialists Conference (PVSC)*, 16-21 June 2013 2013, pp. 0815-0820, doi: 10.1109/PVSC.2013.6744271.

[136] N. Gokmen, E. Karatepe, B. Celik, and S. Silvestre, "Simple diagnostic approach for determining of faulted PV modules in string based PV arrays," *Solar Energy*, vol. 86, no. 11, pp. 3364-3377, 2012/11/01/ 2012, doi: https://doi.org/10.1016/j.solener.2012.09.007.

[137] K.-H. Chao, P.-Y. Chen, M.-H. Wang, and C.-T. Chen, "An Intelligent Fault Detection Method of a Photovoltaic Module Array Using Wireless Sensor Networks," *International Journal of Distributed Sensor Networks*, vol. 10, no. 5, p. 540147, 2014, doi: 10.1155/2014/540147.

[138] L. L. Jiang and D. L. Maskell, "Automatic fault detection and diagnosis for photovoltaic systems using combined artificial neural network and analytical based methods," in *2015 International Joint Conference on Neural Networks (IJCNN)*, 12-17 July 2015 2015, pp. 1-8, doi: 10.1109/IJCNN.2015.7280498.

[139] M. N. Akram and S. Lotfifard, "Modeling and Health Monitoring of DC Side of Photovoltaic Array," *IEEE Transactions on Sustainable Energy*, vol. 6, no. 4, pp. 1245-1253, 2015, doi: 10.1109/TSTE.2015.2425791.

[140] D. Riley and J. Johnson, "Photovoltaic prognostics and heath management using learning algorithms," in *2012 38th IEEE Photovoltaic Specialists Conference*, 3-8 June 2012 2012, pp. 001535-001539, doi: 10.1109/PVSC.2012.6317887.

[141] A. Coleman and J. Zalewski, "Intelligent fault detection and diagnostics in solar plants," in *Proceedings of the 6th IEEE International Conference on Intelligent Data Acquisition and Advanced Computing Systems*, 15-17 Sept. 2011 2011, vol. 2, pp. 948-953, doi: 10.1109/IDAACS.2011.6072914.

[142] Z. Cheng, D. Zhong, B. Li, and Y. Liu, "Research on Fault Detection of PV Array Based on Data Fusion and Fuzzy Mathematics," in *2011 Asia-Pacific Power and Energy Engineering Conference*, 25-28 March 2011 2011, pp. 1-4, doi: 10.1109/APPEEC.2011.5749018.

[143] P. Ducange, M. Fazzolari, B. Lazzerini, and F. Marcelloni, "An intelligent system for detecting faults in photovoltaic fields," in *2011 11th International Conference on Intelligent Systems Design and Applications*, 22-24 Nov. 2011 2011, pp. 1341-1346, doi: 10.1109/ISDA.2011.6121846.

[144] Y. Yagi *et al.*, "Diagnostic technology and an expert system for photovoltaic systems using the learning method," *Solar Energy Materials and Solar Cells*, vol. 75, no. 3, pp. 655-663, 2003/02/01/ 2003, doi: https://doi.org/10.1016/S0927-0248(02)00149-6.

[145] M.-H. Wang and M.-J. Chen, "Two-Stage Fault Diagnosis Method Based on the Extension Theory for PV Power Systems," *International Journal of Photoenergy*, vol. 2012, p. 892690, 2012/06/28 2012, doi: 10.1155/2012/892690.

[146] A. Drews *et al.*, "Monitoring and remote failure detection of grid-connected PV systems based on satellite observations," *Solar Energy*, vol. 81, no. 4, pp. 548-564, 2007/04/01/ 2007, doi: https://doi.org/10.1016/j.solener.2006.06.019.
[147] A. Drews *et al.*, "Intelligent performance check of PV system operation based on satellite data," Germany, 2004-07-01 2004, Deutsche Gesellschaft fuer Sonnenenergie e.V. (DGS), Muenchen (Germany); PSE GmbH - Forschung, Entwicklung, Marketing, Freiburg (Germany).
[148] A. Ali *et al.*, "Review of Online and Soft Computing Maximum Power Point Tracking Techniques under Non-Uniform Solar Irradiation Conditions," *Energies*, vol. 13, no. 12, 2020, doi: 10.3390/en13123256.
[149] N. Onat, "Recent Developments in Maximum Power Point Tracking Technologies for Photovoltaic Systems," *International Journal of Photoenergy*, vol. 2010, p. 245316, 2010/12/20 2010, doi: 10.1155/2010/245316.
[150] Y. Zou, F. Yan, X. Wang, and J. Zhang, "An efficient fuzzy logic control algorithm for photovoltaic maximum power point tracking under partial shading condition," *Journal of the Franklin Institute*, vol. 357, no. 6, pp. 3135-3149, 2020/04/01/ 2020, doi: https://doi.org/10.1016/j.jfranklin.2019.07.015.
[151] T. Esram and P. L. Chapman, "Comparison of Photovoltaic Array Maximum Power Point Tracking Techniques," *IEEE Transactions on Energy Conversion*, vol. 22, no. 2, pp. 439-449, 2007, doi: 10.1109/TEC.2006.874230.
[152] N. A. Kamarzaman and C. W. Tan, "A comprehensive review of maximum power point tracking algorithms for photovoltaic systems," *Renewable and Sustainable Energy Reviews*, vol. 37, pp. 585-598, 2014/09/01/ 2014, doi: https://doi.org/10.1016/j.rser.2014.05.045.
[153] B. Al-kazemi and C. K. Mohan, "Training feedforward neural networks using multi-phase particle swarm optimization," in *Proceedings of the 9th International Conference on Neural Information Processing, 2002. ICONIP '02.*, 18-22 Nov. 2002 2002, vol. 5, pp. 2615-2619 vol.5, doi: 10.1109/ICONIP.2002.1201969.
[154] Syafaruddin, E. Karatepe, and T. Hiyama, "Artificial neural network-polar coordinated fuzzy controller based maximum power point tracking control under partially shaded conditions," *IET Renewable Power Generation*, vol. 3, no. 2, pp. 239-253. [Online]. Available: https://digital-library.theiet.org/content/journals/10.1049/iet-rpg_20080065
[155] R. Storn and K. Price, "Differential Evolution – A Simple and Efficient Heuristic for global Optimization over Continuous Spaces," *Journal of Global Optimization*, vol. 11, no. 4, pp. 341-359, 1997/12/01 1997, doi: 10.1023/A:1008202821328.
[156] H. Taheri, Z. Salam, K. Ishaque, and Syafaruddin, "A novel Maximum Power Point tracking control of photovoltaic system under partial and rapidly fluctuating shadow conditions using Differential Evolution," in *2010 IEEE Symposium on Industrial Electronics and Applications (ISIEA)*, 3-5 Oct. 2010 2010, pp. 82-87, doi: 10.1109/ISIEA.2010.5679492.
[157] M. B. Smida and A. Sakly, "Genetic based algorithm for maximum power point tracking (MPPT) for grid connected PV systems operating under partial shaded conditions," in *2015 7th International Conference on Modelling, Identification and Control (ICMIC)*, 18-20 Dec. 2015 2015, pp. 1-6, doi: 10.1109/ICMIC.2015.7409433.
[158] S. Daraban, D. Petreus, and C. Morel, "A novel MPPT (maximum power point tracking) algorithm based on a modified genetic algorithm specialized on

tracking the global maximum power point in photovoltaic systems affected by partial shading," *Energy*, vol. 74, pp. 374-388, 2014/09/01/ 2014, doi: https://doi.org/10.1016/j.energy.2014.07.001.

[159] R. Eberhart and J. Kennedy, "A new optimizer using particle swarm theory," in *MHS'95. Proceedings of the Sixth International Symposium on Micro Machine and Human Science*, 4-6 Oct. 1995 1995, pp. 39-43, doi: 10.1109/MHS.1995.494215.

[160] S. Motahhir, A. El Hammoumi, and A. El Ghzizal, "The most used MPPT algorithms: Review and the suitable low-cost embedded board for each algorithm," *Journal of Cleaner Production*, vol. 246, p. 118983, 2020/02/10/ 2020, doi: https://doi.org/10.1016/j.jclepro.2019.118983.

[161] S. Sengupta, S. Basak, and R. A. Peters, "Particle Swarm Optimization: A Survey of Historical and Recent Developments with Hybridization Perspectives," *Machine Learning and Knowledge Extraction*, vol. 1, no. 1, 2019, doi: 10.3390/make1010010.

[162] N. Femia, G. Petrone, G. Spagnuolo, and M. Vitelli, "Optimization of perturb and observe maximum power point tracking method," *IEEE Transactions on Power Electronics*, vol. 20, no. 4, pp. 963-973, 2005, doi: 10.1109/TPEL.2005.850975.

[163] D. P. Hohm and M. E. Ropp, "Comparative study of maximum power point tracking algorithms using an experimental, programmable, maximum power point tracking test bed," in *Conference Record of the Twenty-Eighth IEEE Photovoltaic Specialists Conference - 2000 (Cat. No.00CH37036)*, 15-22 Sept. 2000 2000, pp. 1699-1702, doi: 10.1109/PVSC.2000.916230.

[164] M. Kamran, M. Mudassar, M. R. Fazal, M. U. Asghar, M. Bilal, and R. Asghar, "Implementation of improved Perturb & Observe MPPT technique with confined search space for standalone photovoltaic system," *Journal of King Saud University - Engineering Sciences*, vol. 32, no. 7, pp. 432-441, 2020/11/01/ 2020, doi: https://doi.org/10.1016/j.jksues.2018.04.006.

[165] O. Wasynezuk, "Dynamic Behavior of a Class of Photovoltaic Power Systems," *IEEE Transactions on Power Apparatus and Systems*, vol. PAS-102, no. 9, pp. 3031-3037, 1983, doi: 10.1109/TPAS.1983.318109.

[166] V. Salas, E. Olías, A. Barrado, and A. Lázaro, "Review of the maximum power point tracking algorithms for stand-alone photovoltaic systems," *Solar Energy Materials and Solar Cells*, vol. 90, no. 11, pp. 1555-1578, 2006/07/06/ 2006, doi: https://doi.org/10.1016/j.solmat.2005.10.023.

[167] T. Shimizu, O. Hashimoto, and G. Kimura, "A novel high-performance utility-interactive photovoltaic inverter system," *IEEE Transactions on Power Electronics*, vol. 18, no. 2, pp. 704-711, 2003, doi: 10.1109/TPEL.2003.809375.

[168] X. Weidong and W. G. Dunford, "A modified adaptive hill climbing MPPT method for photovoltaic power systems," in *2004 IEEE 35th Annual Power Electronics Specialists Conference (IEEE Cat. No.04CH37551)*, 20-25 June 2004 2004, vol. 3, pp. 1957-1963 Vol.3, doi: 10.1109/PESC.2004.1355417.

[169] W. J. A. Teulings, J. C. Marpinard, A. Capel, and D. O. Sullivan, "A new maximum power point tracking system," in *Proceedings of IEEE Power Electronics Specialist Conference - PESC '93*, 20-24 June 1993 1993, pp. 833-838, doi: 10.1109/PESC.1993.472018.

[170] T. Esram, J. W. Kimball, P. T. Krein, P. L. Chapman, and P. Midya, "Dynamic maximum power point tracking of photovoltaic arrays using ripple correlation

control," *IEEE Transactions on Power Electronics*, vol. 21, no. 5, pp. 1282-1291, 2006, doi: 10.1109/TPEL.2006.880242.

[171] D. Casadei, G. Grandi, and C. Rossi, "Single-phase single-stage photovoltaic generation system based on a ripple correlation control maximum power point tracking," *IEEE Transactions on Energy Conversion*, vol. 21, no. 2, pp. 562-568, 2006, doi: 10.1109/TEC.2005.853784.

[172] I. Abdalla, J. Corda, and L. Zhang, "Multilevel DC-Link Inverter and Control Algorithm to Overcome the PV Partial Shading," *IEEE Transactions on Power Electronics*, vol. 28, no. 1, pp. 14-18, 2013, doi: 10.1109/TPEL.2012.2209460.

[173] C. Pan, M. Cheng, C. Lai, and P. Chen, "Current-Ripple-Free Module Integrated Converter With More Precise Maximum Power Tracking Control for PV Energy Harvesting," *IEEE Transactions on Industry Applications*, vol. 51, no. 1, pp. 271-278, 2015, doi: 10.1109/TIA.2014.2326076.

[174] C. Barth and R. C. N. Pilawa-Podgurski, "Dithering Digital Ripple Correlation Control for Photovoltaic Maximum Power Point Tracking," *IEEE Transactions on Power Electronics*, vol. 30, no. 8, pp. 4548-4559, 2015, doi: 10.1109/TPEL.2014.2357796.

[175] C. Moo and G. Wu, "Maximum Power Point Tracking With Ripple Current Orientation for Photovoltaic Applications," *IEEE Journal of Emerging and Selected Topics in Power Electronics*, vol. 2, no. 4, pp. 842-848, 2014, doi: 10.1109/JESTPE.2014.2328577.

[176] J. W. Kimball and P. T. Krein, "Discrete-Time Ripple Correlation Control for Maximum Power Point Tracking," *IEEE Transactions on Power Electronics*, vol. 23, no. 5, pp. 2353-2362, 2008, doi: 10.1109/TPEL.2008.2001913.

[177] R. Khanna, Q. Zhang, W. E. Stanchina, G. F. Reed, and Z. Mao, "Maximum Power Point Tracking Using Model Reference Adaptive Control," *IEEE Transactions on Power Electronics*, vol. 29, no. 3, pp. 1490-1499, 2014, doi: 10.1109/TPEL.2013.2263154.

[178] A. N. R. Ahmed, K. Nowaz, J. Tasnim, and N. Afroze, "A complete modeling and analysis of solar system (cell/module/array) based on MATLAB," in *2015 International Conference on Electrical & Electronic Engineering (ICEEE)*, 4-6 Nov. 2015 2015, pp. 149-152, doi: 10.1109/CEEE.2015.7428242.

[179] S. Pareek and R. Dahiya, "Output Power Maximization of Partially Shaded 4*4 PV Field by Altering its Topology," *Energy Procedia*, vol. 54, pp. 116-126, 2014/01/01/ 2014, doi: https://doi.org/10.1016/j.egypro.2014.07.254.

[180] P. Samantaray and S. Sasmita, "Performance of solar photovoltaic module under partial shading conditions," in *2016 10th International Conference on Intelligent Systems and Control (ISCO)*, 7-8 Jan. 2016 2016, pp. 1-4, doi: 10.1109/ISCO.2016.7726912.

[181] S. Vijayalekshmy, S. RamaIyer, and B. Beevi, "Analysis of solar photovoltaic array configurations under changing illumination conditions," in *2014 International Conference on Circuits, Power and Computing Technologies [ICCPCT-2014]*, 20-21 March 2014 2014, pp. 1032-1037, doi: 10.1109/ICCPCT.2014.7054973.

[182] S. Malathy and R. Ramaprabha, "Comprehensive analysis on the role of array size and configuration on energy yield of photovoltaic systems under shaded conditions," *Renewable and Sustainable Energy Reviews*, vol. 49, pp. 672-679, 2015/09/01/ 2015, doi: https://doi.org/10.1016/j.rser.2015.04.165.

[183] F. Belhachat and C. Larbes, "Modeling, analysis and comparison of solar photovoltaic array configurations under partial shading conditions," *Solar*

Energy, vol. 120, pp. 399-418, 2015/10/01/ 2015, doi: https://doi.org/10.1016/j.solener.2015.07.039.

[184] N. D. Kaushika and A. K. Rai, "An investigation of mismatch losses in solar photovoltaic cell networks," *Energy*, vol. 32, no. 5, pp. 755-759, 2007/05/01/ 2007, doi: https://doi.org/10.1016/j.energy.2006.06.017.

[185] S. Khatoon, Ibraheem, and M. F. Jalil, "Analysis of solar photovoltaic array under partial shading conditions for different array configrations," in *2014 Innovative Applications of Computational Intelligence on Power, Energy and Controls with their impact on Humanity (CIPECH)*, 28-29 Nov. 2014 2014, pp. 452-456, doi: 10.1109/CIPECH.2014.7019127.

[186] R. Candela, V. d. Dio, E. R. Sanseverino, and P. Romano, "Reconfiguration Techniques of Partial Shaded PV Systems for the Maximization of Electrical Energy Production," in *2007 International Conference on Clean Electrical Power*, 21-23 May 2007 2007, pp. 716-719, doi: 10.1109/ICCEP.2007.384290.

[187] M. Jazayeri, S. Uysal, and K. Jazayeri, "A comparative study on different photovoltaic array topologies under partial shading conditions," in *2014 IEEE PES T&D Conference and Exposition*, 14-17 April 2014 2014, pp. 1-5, doi: 10.1109/TDC.2014.6863384.

[188] V. D. Dio, D. L. Cascia, R. Miceli, and C. Rando, "A mathematical model to determine the electrical energy production in photovoltaic fields under mismatch effect," in *2009 International Conference on Clean Electrical Power*, 9-11 June 2009 2009, pp. 46-51, doi: 10.1109/ICCEP.2009.5212083.

[189] V. Gupta, M. Sharma, R. K. Pachauri, and K. N. Dinesh Babu, "Comprehensive review on effect of dust on solar photovoltaic system and mitigation techniques," *Solar Energy*, vol. 191, pp. 596-622, 2019/10/01/ 2019, doi: https://doi.org/10.1016/j.solener.2019.08.079.

[190] M. Z. S. El-Dein, M. Kazerani, and M. M. A. Salama, "Optimal total cross tied interconnection for photovoltaic arrays to reduce partial shading losses," in *2012 IEEE Power and Energy Society General Meeting*, 22-26 July 2012 2012, pp. 1-6, doi: 10.1109/PESGM.2012.6344845.

[191] R. D. d. O. Reiter, L. Michels, J. R. Pinheiro, R. A. Reiter, S. V. G. Oliveira, and A. Péres, "Comparative analysis of series and parallel photovoltaic arrays under partial shading conditions," in *2012 10th IEEE/IAS International Conference on Industry Applications*, 5-7 Nov. 2012 2012, pp. 1-5, doi: 10.1109/INDUSCON.2012.6452791.

[192] N. K. Gautam and N. D. Kaushika, "Reliability evaluation of solar photovoltaic arrays," *Solar Energy*, vol. 72, no. 2, pp. 129-141, 2002/02/01/ 2002, doi: https://doi.org/10.1016/S0038-092X(01)00085-8.

[193] N. K. Gautam and N. D. Kaushika, "An efficient algorithm to simulate the electrical performance of solar photovoltaic arrays," *Energy*, vol. 27, no. 4, pp. 347-361, 2002/04/01/ 2002, doi: https://doi.org/10.1016/S0360-5442(01)00089-5.

[194] D. Picault, B. Raison, S. Bacha, J. de la Casa, and J. Aguilera, "Forecasting photovoltaic array power production subject to mismatch losses," *Solar Energy*, vol. 84, no. 7, pp. 1301-1309, 2010/07/01/ 2010, doi: https://doi.org/10.1016/j.solener.2010.04.009.

[195] S. Hamdi, D. Saigaa, and M. Drif, "Modeling and simulation of photovoltaic array with different interconnection configurations under partial shading conditions for fill factor evaluation," in *2014 International Renewable and*

Sustainable Energy Conference (IRSEC), 17-19 Oct. 2014 2014, pp. 25-31, doi: 10.1109/IRSEC.2014.7059896.

[196] N. K. Gautam and N. D. Kaushika, "Network analysis of fault-tolerant solar photovoltaic arrays," *Solar Energy Materials and Solar Cells*, vol. 69, no. 1, pp. 25-42, 2001/08/01/ 2001, doi: https://doi.org/10.1016/S0927-0248(00)00356-1.

[197] S. Khatoon, Ibraheem, and M. F. Jalil, "Feasibility analysis of solar photovoltaic array configurations under partial shading conditions," in *2015 Annual IEEE India Conference (INDICON)*, 17-20 Dec. 2015 2015, pp. 1-6, doi: 10.1109/INDICON.2015.7443701.

[198] E. Karatepe, M. Boztepe, and M. Çolak, "Development of a suitable model for characterizing photovoltaic arrays with shaded solar cells," *Solar Energy*, vol. 81, no. 8, pp. 977-992, 2007/08/01/ 2007, doi: https://doi.org/10.1016/j.solener.2006.12.001.

[199] C. A. Ramos-Paja, J. D. Bastidas, A. J. Saavedra-Montes, F. Guinjoan-Gispert, and M. Goez, "Mathematical model of total cross-tied photovoltaic arrays in mismatching conditions," in *2012 IEEE 4th Colombian Workshop on Circuits and Systems (CWCAS)*, 1-2 Nov. 2012 2012, pp. 1-6, doi: 10.1109/CWCAS.2012.6404068.

[200] M. Balato, L. Costanzo, and M. Vitelli, "Series–Parallel PV array re-configuration: Maximization of the extraction of energy and much more," *Applied Energy*, vol. 159, pp. 145-160, 2015/12/01/ 2015, doi: https://doi.org/10.1016/j.apenergy.2015.08.073.

[201] S. Mohammadnejad, A. Khalafi, and S. M. Ahmadi, "Mathematical analysis of total-cross-tied photovoltaic array under partial shading condition and its comparison with other configurations," *Solar Energy*, vol. 133, pp. 501-511, 2016/08/01/ 2016, doi: https://doi.org/10.1016/j.solener.2016.03.058.

[202] R. Ramaprabha and B. L. Mathur, "A Comprehensive Review and Analysis of Solar Photovoltaic Array Configurations under Partial Shaded Conditions," *International Journal of Photoenergy*, vol. 2012, p. 120214, 2012/03/08 2012, doi: 10.1155/2012/120214.

[203] D. La Manna, V. Li Vigni, E. Riva Sanseverino, V. Di Dio, and P. Romano, "Reconfigurable electrical interconnection strategies for photovoltaic arrays: A review," *Renewable and Sustainable Energy Reviews*, vol. 33, pp. 412-426, 2014/05/01/ 2014, doi: https://doi.org/10.1016/j.rser.2014.01.070.

[204] L. F. L. Villa, D. Picault, B. Raison, S. Bacha, and A. Labonne, "Maximizing the Power Output of Partially Shaded Photovoltaic Plants Through Optimization of the Interconnections Among Its Modules," *IEEE Journal of Photovoltaics*, vol. 2, no. 2, pp. 154-163, 2012, doi: 10.1109/JPHOTOV.2012.2185040.

[205] J. Storey, P. R. Wilson, and D. Bagnall, "The Optimized-String Dynamic Photovoltaic Array," *IEEE Transactions on Power Electronics*, vol. 29, no. 4, pp. 1768-1776, 2014, doi: 10.1109/TPEL.2013.2265497.

[206] M. Fausto Pedro García, "A New Method for Maintenance Management Employing Principal Component Analysis," (in English), *Structural Durability & Health Monitoring*, vol. 6, no. 2, pp. 89-100, 2010

2020-05-02 2010, doi: http://dx.doi.org/10.3970/sdhm.2010.006.089.

[207] Á. H. Herraiz, A. P. Marugán, and F. P. G. Márquez, "Chapter 7 - A review on condition monitoring system for solar plants based on thermography," in *Non-*

Destructive Testing and Condition Monitoring Techniques for Renewable Energy Industrial Assets, M. Papaelias, F. P. G. Márquez, and A. Karyotakis Eds. Boston: Butterworth-Heinemann, 2020, pp. 103-118.

[208] E. R. Sanseverino *et al.*, "Dynamic programming and Munkres algorithm for optimal photovoltaic arrays reconfiguration," *Solar Energy*, vol. 122, pp. 347-358, 2015/12/01/ 2015, doi: https://doi.org/10.1016/j.solener.2015.09.016.

[209] N. Scarlat, J.-F. Dallemand, F. Monforti-Ferrario, M. Banja, and V. Motola, "Renewable energy policy framework and bioenergy contribution in the European Union – An overview from National Renewable Energy Action Plans and Progress Reports," *Renewable and Sustainable Energy Reviews*, vol. 51, pp. 969-985, 2015/11/01/ 2015, doi: https://doi.org/10.1016/j.rser.2015.06.062.

[210] Y. Hu, J. Zhang, P. Li, D. Yu, and L. Jiang, "Non-Uniform Aged Modules Reconfiguration for Large-Scale PV Array," *IEEE Transactions on Device and Materials Reliability*, vol. 17, no. 3, pp. 560-569, 2017, doi: 10.1109/TDMR.2017.2731850.

[211] J. Camarillo-Peñaranda, F. Ramírez-Quiroz, D. Gonzalez Montoya, F. Bolaños, and C. Ramos-Paja, *Reconfguration of photovoltaic arrays based on genetic algorithm*. 2015.

[212] D. Nguyen and B. Lehman, "An Adaptive Solar Photovoltaic Array Using Model-Based Reconfiguration Algorithm," *IEEE Transactions on Industrial Electronics*, vol. 55, no. 7, pp. 2644-2654, 2008, doi: 10.1109/TIE.2008.924169.

[213] S. Mekhilef, R. Saidur, and M. Kamalisarvestani, "Effect of dust, humidity and air velocity on efficiency of photovoltaic cells," *Renewable and Sustainable Energy Reviews*, vol. 16, no. 5, pp. 2920-2925, 2012/06/01/ 2012, doi: https://doi.org/10.1016/j.rser.2012.02.012.

[214] A. Tabanjat, M. Becherif, and D. Hissel, *Reconfiguration solution for shaded PV panels using switching control*. 2014.

[215] M. Manjunath, B. V. Reddy, and B. Lehman, "Performance improvement of dynamic PV array under partial shade conditions using M2 algorithm," *IET Renewable Power Generation*, vol. 13, no. 8, pp. 1239-1249, 2019, doi: 10.1049/iet-rpg.2018.5675.

[216] P. Udenze, Y. Hu, H. Wen, X. Ye, and K. Ni, "A Reconfiguration Method for Extracting Maximum Power from Non-Uniform Aging Solar Panels," *Energies*, vol. 11, no. 10, 2018, doi: 10.3390/en11102743.

[217] P. Guerriero and S. Daliento, "Toward a Hot Spot Free PV Module," *IEEE Journal of Photovoltaics*, vol. 9, no. 3, pp. 796-802, 2019, doi: 10.1109/JPHOTOV.2019.2894912.

[218] Y. Hu, J. Zhang, J. Wu, W. Cao, G. Y. Tian, and J. L. Kirtley, "Efficiency Improvement of Nonuniformly Aged PV Arrays," *IEEE Transactions on Power Electronics*, vol. 32, no. 2, pp. 1124-1137, 2017, doi: 10.1109/TPEL.2016.2544842.

[219] Y. Hu, W. Cao, J. Ma, S. J. Finney, and D. Li, "Identifying PV Module Mismatch Faults by a Thermography-Based Temperature Distribution Analysis," *IEEE Transactions on Device and Materials Reliability*, vol. 14, no. 4, pp. 951-960, 2014, doi: 10.1109/TDMR.2014.2348195.

[220] J. Liu, Y. Yao, S. Q. Xiao, and X. Gu, *Review of status developments of high-efficiency crystalline silicon solar cells*. 2018.

[221] G. Velasco-Quesada, F. Guinjoan-Gispert, R. Pique-Lopez, M. Roman-Lumbreras, and A. Conesa-Roca, "Electrical PV Array Reconfiguration Strategy for Energy Extraction Improvement in Grid-Connected PV Systems," *IEEE Transactions on Industrial Electronics*, vol. 56, no. 11, pp. 4319-4331, 2009, doi: 10.1109/TIE.2009.2024664.

[222] M. L. Orozco-Gutierrez, G. Spagnuolo, J. M. Ramirez-Scarpetta, G. Petrone, and C. A. Ramos-Paja, "Optimized Configuration of Mismatched Photovoltaic Arrays," *IEEE Journal of Photovoltaics*, vol. 6, no. 5, pp. 1210-1220, 2016, doi: 10.1109/JPHOTOV.2016.2581481.

[223] E. Romero-Cadaval, G. Spagnuolo, L. G. Franquelo, C. A. Ramos-Paja, T. Suntio, and W. M. Xiao, "Grid-Connected Photovoltaic Generation Plants: Components and Operation," *IEEE Industrial Electronics Magazine*, vol. 7, no. 3, pp. 6-20, 2013, doi: 10.1109/MIE.2013.2264540.

[224] J. D. Bastidas, E. Franco, G. Petrone, C. A. Ramos-Paja, and G. Spagnuolo, "A model of photovoltaic fields in mismatching conditions featuring an improved calculation speed," *Electric Power Systems Research*, vol. 96, pp. 81-90, 2013/03/01/ 2013, doi: https://doi.org/10.1016/j.epsr.2012.10.020.

[225] M. Alkahtani *et al.*, "Investigating Fourteen Countries to Maximum the Economy Benefit by Using Offline Reconfiguration for Medium Scale PV Array Arrangements," *Energies*, vol. 14, no. 1, 2021, doi: 10.3390/en14010059.

[226] T. N. Ngoc *et al.*, "A hierarchical architecture for increasing efficiency of large photovoltaic plants under non-homogeneous solar irradiation," *Solar Energy*, vol. 188, pp. 1306-1319, 2019/08/01/ 2019, doi: https://doi.org/10.1016/j.solener.2019.07.033.

[227] PowerFilm. "Electronic Component Solar Panels." PowerFilm, Inc. https://www.powerfilmsolar.com/products/electronic-component-solar-panels/classic-application-series/ (accessed 21-03, 2021).

[228] L. Cristaldi *et al.*, "Simplified method for evaluating the effects of dust and aging on photovoltaic panels," *Measurement*, vol. 54, pp. 207-214, 2014/08/01/ 2014, doi: https://doi.org/10.1016/j.measurement.2014.03.001.

[229] M. Sankar and R. Ramabadran, *Comprehensive analysis on the role of array size and configuration on energy yield of photovoltaic systems under shaded conditions*. 2015, pp. 672-679.

[230] C. R. Osterwald, A. Anderberg, S. Rummel, and L. Ottoson, "Degradation analysis of weathered crystalline-silicon PV modules," in *Conference Record of the Twenty-Ninth IEEE Photovoltaic Specialists Conference, 2002.*, 19-24 May 2002 2002, pp. 1392-1395, doi: 10.1109/PVSC.2002.1190869.

[231] A. Ndiaye, C. M. F. Kébé, P. A. Ndiaye, A. Charki, A. Kobi, and V. Sambou, "A Novel Method for Investigating Photovoltaic Module Degradation," *Energy Procedia*, vol. 36, pp. 1222-1231, 2013/01/01/ 2013, doi: https://doi.org/10.1016/j.egypro.2013.07.138.

[232] M. A. Munoz, M. C. Alonso-García, N. Vela, and F. Chenlo, "Early degradation of silicon PV modules and guaranty conditions," *Solar Energy*, vol. 85, no. 9, pp. 2264-2274, 2011/09/01/ 2011, doi: https://doi.org/10.1016/j.solener.2011.06.011.

[233] E. L. Meyer and E. E. v. Dyk, "Assessing the reliability and degradation of photovoltaic module performance parameters," *IEEE Transactions on Reliability*, vol. 53, no. 1, pp. 83-92, 2004, doi: 10.1109/TR.2004.824831.

[234] Y. Hu, W. Cao, J. Wu, B. Ji, and D. Holliday, "Thermography-Based Virtual MPPT Scheme for Improving PV Energy Efficiency Under Partial Shading

Conditions," *IEEE Transactions on Power Electronics,* vol. 29, no. 11, pp. 5667-5672, 2014, doi: 10.1109/TPEL.2014.2325062.

[235] R. A. Kumar, M. S. Suresh, and J. Nagaraju, "Measurement of AC parameters of gallium arsenide (GaAs/Ge) solar cell by impedance spectroscopy," *IEEE Transactions on Electron Devices,* vol. 48, no. 9, pp. 2177-2179, 2001, doi: 10.1109/16.944213.

[236] M. Mattei, G. Notton, C. Cristofari, M. Muselli, and P. Poggi, "Calculation of the polycrystalline PV module temperature using a simple method of energy balance," *Renewable Energy,* vol. 31, no. 4, pp. 553-567, 2006/04/01/ 2006, doi: https://doi.org/10.1016/j.renene.2005.03.010.

[237] J. P. Storey, P. R. Wilson, and D. Bagnall, "Improved Optimization Strategy for Irradiance Equalization in Dynamic Photovoltaic Arrays," *IEEE Transactions on Power Electronics,* vol. 28, no. 6, pp. 2946-2956, 2013, doi: 10.1109/TPEL.2012.2221481.

[238] Z. Wu, C. Zhang, M. Alkahtani, Y. Hu, and J. Zhang, "Cost Effective Offline Reconfiguration for Large-Scale Non-Uniformly Aging Photovoltaic Arrays Efficiency Enhancement," *IEEE Access,* vol. 8, pp. 80572-80581, 2020, doi: 10.1109/ACCESS.2020.2991089.

[239] Global Petrp Prices. "Electricity prices around the world." https://www.globalpetrolprices.com/electricity_prices/ (accessed 20 November, 2020).

[240] Salary Expert. "Electrician Salary." https://www.salaryexpert.com/salary/job/electrician/ (accessed 25 November, 2020).

[241] Lazard. "Levelized Cost of Energy and Levelized Cost of Storage – 2020." https://www.lazard.com/perspective/levelized-cost-of-energy-and-levelized-cost-of-storage-2020/ (accessed 25 November 2020).

[242] IRENA. "Renewable Power Generation Costs - 2019." https://www.irena.org/publications/2020/Jun/Renewable-Power-Costs-in-2019 (accessed 25 November 2020).

[243] S. Djordjevic, D. Parlevliet, and P. Jennings, "Detectable faults on recently installed solar modules in Western Australia," *Renewable Energy,* vol. 67, pp. 215-221, 2014/07/01/ 2014, doi: https://doi.org/10.1016/j.renene.2013.11.036.

[244] Z. Wang, N. Zhou, L. Gong, and M. Jiang, "Quantitative estimation of mismatch losses in photovoltaic arrays under partial shading conditions," *Optik,* vol. 203, p. 163950, 2020/02/01/ 2020, doi: https://doi.org/10.1016/j.ijleo.2019.163950.

[245] G. Nobile *et al.*, "Study on mismatch losses in large PV plants: data analysis of a case study and modeling approach," in *2020 International Symposium on Power Electronics, Electrical Drives, Automation and Motion (SPEEDAM)*, 24-26 June 2020 2020, pp. 858-864, doi: 10.1109/SPEEDAM48782.2020.9161767.